Tampere University

MIAO LI

Printed and Coated, Thin-Film Organic and Metal Oxide Diodes and Rectifier Circuits for RF Energy Harvesting

Tampere University Dissertations 575

Tampere University Dissertations 575

MIAO LI

Printed and Coated, Thin-Film Organic and Metal Oxide Diodes and Rectifier Circuits for RF Energy Harvesting

ACADEMIC DISSERTATION
To be presented, with the permission of
the Faculty of Information Technology and Communication Sciences
of Tampere University,
for public discussion in the auditorium SA203 S2
of the Sähkötalo Building, Korkeakoulunkatu 8, Tampere,
on 1 April 2022, at 12 o'clock.

ACADEMIC DISSERTATION
Tampere University, Faculty of Information Technology and Communication Sciences
Finland

Responsible supervisor and Custos	Professor Donald Lupo Tampere University Finland	
Supervisor	Professor Paul Berger, Docent Tampere University, Finland The Ohio State University, USA	
Pre-examiners	Associate Professor Radu Sporea University of Surrey UK	Dr. Edsger Smits Holst Centre TNO Netherlands
Opponent	Professor Henning Sirringhaus University of Cambridge UK	

The originality of this thesis has been checked using the Turnitin OriginalityCheck service.

Cover design: Roihu Inc.

ISBN 978-952-03-2343-1 (print)
ISBN 978-952-03-2344-8 (pdf)
ISSN 2489-9860 (print)
ISSN 2490-0028 (pdf)
http://urn.fi/URN:ISBN:978-952-03-2344-8

PunaMusta Oy – Yliopistopaino
Joensuu 2022

PREFACE

This work was carried out by the research group of Laboratory for Future Electronics in the Electrical Engineering Unit at Tampere Universities. The research was funded by the Academy of Finland (AoF) under project AUTOVOLT, and the Finnish Funding Agency for Technology and Innovation (Tekes, now Business Finland) under project PAUL. The research was also financially supported in part by the Austrian Research Foundation under project Self-PoSH and by Flextech Alliance. The financial support is gratefully acknowledged.

The work presented in this thesis would not have this form without the support of many people. I would like to take this opportunity to thank all those who contributed to the completion of this thesis. First of all, I would like to express my deepest gratitude to my supervisor, Prof. Donald Lupo for providing me the opportunity to enter the organic electronics field and for his continuous guidance and encouragement throughout my research years. I am also grateful to Prof. Paul Berger for his support and being a great mentor. I would like to thank my present and former colleagues in the Laboratory for Future Electronics for the great working atmosphere. Special thanks are reserved to Dr. Kaisa Lilja and Dr. Petri Heljo who laid the groundwork on rectifying diodes. I would like to thank Dr. Marika Janka, Anna Railanmaa, Sagar Bhalerao, Dr. Mika-Matti Laurila and Dr. Jari Keskinen, for fruitful and interesting discussions both in the research and in the general life, which makes this journey very special and enjoyable to me. I would like to extend my gratitude to all co- and main authors of the publications, especially the following: Dr. Suvi Lehtimäki, George Daniel at PARC, Prof. Bruce Kahn at Clemson University, Prof. Mats Fahlman at Linlöping university. I am also grateful to Prof. Matti Mäntysalo for his insight and help.

I would like to acknowledge the pre-examiners Prof. Radu Sporea and Dr. Edsger Smits for reviewing my thesis.

I wish to thank all my friends in Finland for the wonderful moments, gathering and parties, especially Vili, Ayat, Niloofer and Yuli.

Finally, I would like to express my gratitude to my parents for their endless love, support and encouragement. I especially want to thank my beloved partner Wenqian for always being there for me, and our daughter Liara for bringing me great joy.

Tampere, September 2021

Miao Li

ABSTRACT

The demands for autonomous energy solutions are increasing rapidly due to the explosive growth in the Internet of Things (IoT) ecosystem. The overall IoT connections have been estimated to reach 35 billion in 2020 and have been projected to reach over 80 billion by the end of 2024. Therefore, sustainable and diverse energy solutions incorporating remote charging are acute to power billions of devices in IoT and other ubiquitous electronics. Due to ease of implementation and availability, energy scavenging by harvesting power from radio frequency (RF) sources is a promising energy solution. A typical RF harvester comprises two functional units: an antenna to gather RF energy and a rectifier circuit to convert them to electric energy such as voltages to power up electronic devices. RF rectifying diodes, as the simplest rectifying components, are vital for such energy autonomy systems.

Emerging printing and coating techniques, with their low-cost and ease of fabrication, make solution-processed and printed electronics very attractive. It enables researchers to explore new ways of material processing to develop devices, circuits, and systems, which are difficult to achieve with traditional wafer-based manufacturing techniques. With the steady development in printing and coating methods, it is of great interest to develop solution-processed and printed, low-cost RF energy harvesters with unconventional semiconductor materials, such as organic polymers and metal oxides. Due to unique bonding and carrier transport mechanism, solution-processed organic and metal oxide diodes have dramatically different properties compared to their Si-based counterparts; their circuits have unique characteristics, and their optimization can differ strongly from conventional inorganic equivalents. Therefore, as one of the most fundamental active electronic components, solution-processed rectifying diodes are not only essential to low-cost RF energy harvesters but also an important steppingstone to understanding other solution-processed electronic devices.

The work presented in this thesis, including the publications therein, focuses on the development and analysis of solution-processed thin film organic and metal oxide diodes and their rectifier circuits for RF energy harvesting applications. The thesis discusses how to improve the properties of the diodes, especially their frequency response. The gravure printed organic diodes offer improved electrical

performance at 13.56 MHz whereas the solution-processed spin-coated indium oxide diodes operate up to and above 0.7 GHz. Furthermore, the thesis demonstrates fully printable RF energy harvesters based on printed diodes with working distance from a few cm to 4 meters at 13.56 MHz. The utilization in an autonomous energy harvesting and storage unit is presented as well. The unique properties of the printed diodes are investigated when integrated into harvester circuits. The results in this thesis demonstrate the capability of solution processed rectifying organic and metal oxide diodes utilized in RF energy harvesting systems for IoT applications.

CONTENTS

Preface
Abstract
List of figures
List of Tables
Abbreviations
List of publications
Contribution of the author

1 Introduction 15

2 Background 18
2.1 Printed organic rectifying diodes 18
2.1.1 Properties 19
2.1.2 Characteristics 21
2.2 Metal oxide rectifying diodes 25
2.3 Printed and solution-processed electronics 26
2.4 Applications and circuits 28
2.4.1 RF energy harvesting applications 29
2.4.2 RF energy harvester antennas 31
2.4.3 Rectifying circuit 34

3 Experimental 36
3.1 Materials 36
3.2 Device fabrication 38
3.2.1 Fabrication of PTAA diodes 38
3.2.2 Fabrication of indium oxide diodes 40
3.2.3 Fabrication of other components 41
3.3 Characterization Applications and circuits 42

4 Results and discussion 44
4.1 Diode interface and IV characteristics 44
4.2 Diode frequency performance 49
4.3 RF energy harvester 55
4.4 Research question discussion 60

5 Conclusions and open issues 61

Bibliography

List of Figures

Figure 1. Simplified equivalent circuit model for an organic diode.....25

Figure 2. The principle of the sheet-fed gravure printing process used in this thesis [24].....27

Figure 3. Applications of rectifying diodes.....29

Figure 4. Pictures of energy autonomous temperature sensor mounted inside a smart chocolate box [73].....30

Figure 5. Coils on smartphones and Qi charger (left), a 13.56 MHz RFID card (middle) and a loop antenna with a diameter of 2 meters operating at 1.75-30 MHz (right).....32

Figure 6. Circuit diagram of a 13.56 MHz loop antenna transaction.....32

Figure 7. Schematic of a halfwave rectifier (left) and a double half-wave rectifier (right).....35

Figure 8. Schematic layout of the PTAA diodes. 39

Figure 9. Microscopy images of the silver layer. High viscosity silver ink with visible holes(left) and low viscosity silver ink with less hole area (right).....40

Figure 10. A photo of Al/In_2O_3/Au diodes (left). FIB-SEM cross section image of the diode (right).....41

Figure 11. IV measurement set up (top left), small-signal impedance measurement setup (top right) frequency response measurement set up (bottom left) and a probe station for IV measurement set up (bottom right). 43

Figure 12. Printed Cu-PTAA-Ag diode current density – voltage (J (log)-V) characteristics.....45

Figure 13. A microscope image of the device, the gap between two electrodes is 60 μm. Linear I-V plot of Al electrodes on top of indium oxide at forward biasing from 0 to 5 V. 45

Figure 14. I (log)-V plot of indium oxide with various metal electrodes on top. 46

Figure 15. Al/In_2O_3/Al diode I (log)-V characteristics. 47

Figure 16. Al/In_2O_3/Au diode J (log)-V characteristics (left). Log-log plot of the diode J-V characteristics at forward biasing (right). 48

Figure 17. Rectified DC output at 13.56 MHz with an input AC of 10 V. 49

Figure 18. Measured DC output voltages of the diodes for 10 V AC input signal from a signal generator as a function of frequency. 50

Figure 19. Diode rectified DC output voltage and diode voltage loss vs. input AC voltage at 13.56 MHz....52

Figure 20. Diode output vs AC input of 20 Vpp at 13.56 MHz. No capacitor included. 53

Figure 21. Frequency response of the Al/In_2O_3/Au rectifier with a comprising to PTAA diode and Si-diode rectifier up to 50 MHz. 54

Figure 22. Frequency response of the Al/In_2O_3/Au rectifier up from 20 MHz to 1.2 GHz. The measured power of the power amplifier and its relative loss vs frequency....54

Figure 23. Schematic illustration of 13.56 MHZ RF harvester. 55

Figure 24. Schematic circuit diagram for the harvester operating at 13.56 Hz (left), for open circuit coupling AC voltage (middle) measurement, and for output DC voltage measurement (right). 57

Figure 25. Measured results of the rectennas DC output of the 5-turns loop (top), the 6-turns loop (bottom left) and the 7-turns loop (bottom right) vs. the capacitance, i.e., Cdiode for diode DC output and Cres for open circuit. The dashed curves with arbitrary amplitudes to represent the open-circuit characteristics of the loop antennas. 58

Figure 26. Measurement set up in office environments (top). Output DC voltage of 13.56 MHz printed harvesting systems (bottom). Input power of (1 W) from the signal generator is fed to the transmit antenna placed 1, 2, 3 and 4 meters away. Load resistance is 1 MΩ....59

List of Tables

Table 1. A summary of reported results for organic rectifying diodes 35

Table 2. Properties of printed PTAA diodes 50

Table 3. Properties of loop antennas 56

ABBREVIATIONS

AC	Alternating current
AFM	Atomic force microscopy
ASIC	Application specific integrated circuit
DC	Direct current
FIB	Focused ion beam
HF	High frequency
HOMO	Highest occupied molecular orbital
I(J)-V	Current(density)-voltage
IoT	Internet of things
IS	Impedance spectroscopy
ISM	Industrial, scientific and medical
LF	Low frequency
MIM	Metal-insulator-metal
NFC	Near field communication
TFT	Thin-film transistor
PET	Poly(ethylene terephthalate)
PCB	Printed circuit board
PTAA	Poly(triarylamine)
RF	Radio frequency
RFID	Radio frequency identification
SCLC	Space-charge limited current
SEM	Scanning electron microscopy
SMT	Surface-mount technology
TOF	Time-of-flight
UHF	Ultra-high frequency
XPS	X-ray photoelectron spectroscopy

LIST OF PUBLICATIONS

Publication I M. Li, P. S. Heljo, D. Lupo. Organic Diodes for RF Energy Harvesting. *Large-area, Organic and Printed Electronics Convention LOPE-C 2012 Proceedings*. ISBN 978-3-00-038122-5.

Publication II M. Li, P. S. Heljo, D. Lupo. Organic Rectifying Diode and Circuit for Wireless Power Harvesting at 13.56 MHz. *IEEE Transactions on Electron Devices*, 61(2014)6, pp. 2164-2169. doi: 10.1109/TED.2014.2318523.

Publication III S. Lehtimäki, M. Li, J. Salomaa, J. Pörhönen, A. Kalanti, S. Tuukkanen, D. Lupo. Performance of printable supercapacitors in an RF energy harvesting circuit. *International Journal of Electrical Power and Energy Systems*, 58(2014) pp. 42-46. doi: 10.1016/j.ijepes.2014.01.004.

Publication IV M. Li, G. Daniel, B. E. Kahn, L. H. Ohara, B. D. F. Casse, N. Pretorius, B. Krusor, P. Mei, G. L. Whiting, C. Tonkin, D. Lupo. All printed Large Area E-field Antenna Utilizing Printed Organic Rectifying Diodes for RF Energy Harvesting. *In 2018 IEEE 18th International Conference on Nanotechnology (IEEE-NANO)*. doi: 10.1109/NANO.2018.8626318.

Publication V M. Li, M. Honkanen, X.J. Liu, C. Rokaya, A. Schramm, M. Fahlman, P. R. Berger, D. Lupo. 0.7 GHz Solution-Processed Indium Oxide Rectifying Diodes, *IEEE Transactions on Electron Devices*, 67(2020)1, pp. 360-364. doi: 10.1109/TED.2019.2954167.

CONTRIBUTION OF THE AUTHOR

The publications included in this thesis are the result of collaboration with other researchers. The contribution of the author is as follows:

Publication I: The author planned the experiments, fabricated and characterized the rectifying diodes as well as the harvesters. The author analyzed the data and wrote the first version of the manuscript. Other co-authors revised and improved the manuscript.

Publication II: The author planned the experiments, fabricated the harvester circuit. The author performed the measurements, analyzed the data and wrote the first version of the manuscript. Other co-authors revised and improved the manuscript.

Publication III: The author's and Suvi Lehtimäki contributions to this work were nearly equal. The author designed, fabricated and characterized the printed harvester. Suvi Lehtimäki prepared the supercapacitors and the ASIC was provided by Aalto University. The author planned and performed the harvesting measurement together with S. Lehtimäki. The author wrote in the parts of the manuscript regarding the harvester. S. Lehtimäki wrote the rest parts. Other co-authors revised and improved the manuscript.

Publication IV: The author planned the experiments and fabricated the diodes. The large area antenna was designed and simulated at Palo Alto Research Center and printed at Clemson University. The author measured and analyzed the harvester data and wrote the first version of the manuscript. Other co-authors revised and improved the manuscript.

Publication V: The author planned the experiments, fabricated the diodes, and measured the diode characteristics and frequency performance. The XPS measurements and analysis were carried out by Xianjie Liu and the FIB-SEM images by Mari Honkanen. The author analyzed the data and wrote the first version of the manuscript. Other co-authors revised and improved the manuscript.

1 INTRODUCTION

Energy and power sources are fundamental to all electronic components and systems. For a conventional wireless or portable device, where direct power supply derived from power outlets by wiring is excluded, replaceable batteries become the primary power source. However, with the rise of emerging Internet of Things (IoT), wireless sensors and other ubiquitous small electronics, installing, maintaining and replacing batteries for billions of sensors and small electronic devices in the near future is by no means an elegant solution, and not sustainable. There is an urgent demand for new, sustainable energy supply solutions to overcome this bottleneck. Harvesting energy from ambient power sources like light, radio frequency (RF) radiation, motion or thermal energy holds a tremendous amount of promise to be an efficient energy solution [1]–[3]. The harnessed energy can either be used immediately to power devices, or it can be stored in batteries or other novel energy storage devices, such as supercapacitors, to enable an autonomous energy system. Among different energy harvesting methods, wireless RF energy harvesting from ambient or dedicated sources has massive appeal because of its simplicity and ease of implementation. An RF harvester typically comprises two functional units: an antenna to gather and channel RF energy and a rectifier circuit to convert the received RF signals to DC voltages. RF rectifying diodes, as the simplest rectifying components, are essential for such low-cost energy autonomous systems.

Printed and coated electronics has opened new opportunities in manufacturing of electronics. Solution-processed organic or inorganic materials utilizing various printing and coating methods enable fast, cost-effective and high-volume production. These solution-processed materials also offer advantages such as thin layers, large scale, flexibility and low-temperature processability, which allow structures and devices that were not feasible with conventional materials and fabrication methods. Based on these novel materials and deposition methods, many devices have been demonstrated, such as transistors, photovoltaics (PV)s, light-emitting diodes (LED)s and rectifying diodes [4]–[13]. As the simplest active electronic components, rectifying diodes are important building blocks for a better understanding of device physics and operations of other solution-processed devices

in which there is interaction between optical and electrical properties, such as PV devices and organic light-emitting diodes (OLED). Despite the advancements, there are several challenges in solution-processed materials, especially their electrical performance. A great effort has been made to enhance the electrical performance of these materials in the past years. Therefore, it is of enormous interest to investigate and demonstrate the possibility of harvesting RF energy on a cheap flexible plastic substate with simple, low-cost solution-processed organic or metal oxide diodes. With the rapidly expanding IoT market, there is massive potential for this approach.

The work presented in this thesis focuses on RF rectifying diodes utilizing solution-processed organic or metal oxide materials for energy harvesting applications. Compared with conventional Si-based rectifying diodes, these solution-processed, thin-film rectifying diodes have unique properties, characteristics, advantages and disadvantages. The specific objectives of this thesis are the following:

Research Question 1: Can solution-processed organic and metal oxide diodes offer sufficient electrical rectifying performance at 13.56 MHz or even higher frequencies? To address this question, the diode properties and frequency performance are investigated.

Research Question 2: Can RF energy harvesters based on solution-processed diodes be used to provide sufficient voltage to power load devices? To answer this question, the harvesting circuit analysis and the harvester demonstration are required.

The thesis outlines the work done in five peer-reviewed publications. In publication I, a fully printed RF energy harvester operating at 13.56 MHz comprising an inkjet-printed antenna with a capacitor and a gravure-printed organic rectifying diode is presented. Depending on the transmitting power and distance of the source antenna, this printed energy harvester can provide up to 3-5 DC voltage. Publication II further investigates the effect of these organic rectifying diodes on the performance of a rectenna circuit with an operating frequency of 13.56 MHz. The geometric capacitance of the diodes has a huge impact on the resonant frequency and the coupling AC voltage of the loop antenna. Based on the findings, a rectenna circuit with a double half-wave rectifier is designed. In publication III, we demonstrate an autonomous energy harvesting and storage system. The printed 13.56 MHz energy harvester with organic rectifying diodes is used to charge two supercapacitors connected in series up to approximately 1.8 V. The stored energy powers a voltage regulator application specific integrated circuit (ASIC) with a regulated output of 1.2 V for up to 10 hours. The charging voltages from the harvester to the supercapacitors are controlled by the distance between the source

antenna and harvesting antenna. Publication IV presents a fully printed RF energy harvester with a novel screen-printed large area antenna integrated with a printed organic rectifying diode for long-range harvesting up to a few meters at 13.56 MHz. In publication V, solution-processed indium oxide is utilized for rectifying diodes that dramatically extend into higher-speed application. The 3-dB cutoff frequency was found to be over 700 MHz.

This thesis is divided into five chapters. Chapter 2 discusses the fundamentals relevant to the work. The experimental methods and materials used are presented in Chapter 3. Chapter 4 outlines the main results of the included publications. Chapter 5 concludes the thesis with a summary of the contributions.

2 BACKGROUND

This chapter provides the essential background of solution-processed, thin film organic and metal oxide diodes. First, the fundamental properties and characteries of the p-type organic semiconductor rectifying diodes are presented. A brief overview of solution-processed n-type metal oxide is given. Next, various solution-processed deposition methods including printing and coating are discussed. In the end, the applications and the circuits for these diodes are described.

2.1 Printed organic rectifying diodes

Organic semiconductors, especially conjugated polymers, are intrinsically solution processable and printable at low temperatures, making them compatible with inexpensive, plastic film substrates, unlike inorganic semiconductors. These flexible and printed organic devices can be realized for various emerging applications such as the increasing demand for IoTs. In particular, printed rectifying diodes based on organic semiconductors fabricated at low temperatures have the potential to be used in such applications as a key enabling component of future pervasive wireless power systems.

An organic rectifying diode is a two-terminal electronic device that has low resistance to current flow in one direction and high resistance in the other direction. The structure of an organic high frequency rectifying diode can be realized by vertically sandwiching an organic semiconductor between two metal electrodes. Thus, the diode length for which carriers travel is determined by the semiconductor layer thickness in contrast to a thin-film transistor or a lateral diode, in which the diode length depends on the horizontal distance between two electrodes. This structure is distinct from conventional Si-based rectifying diodes, which are commonly based on p-n junctions or heavily doped semiconductors. Indeed, organic semiconductors and devices bear unique and attractive properties that distinguish

them from their conventional counterparts and add new value that is difficult to obtain from conventional electronics technology.

2.1.1 Properties

Organic semiconductors used as active layers in thin film diodes can be divided into two major classes, small molecules and conjugated polymers [14], [15]. In general, small molecules can form well-ordered films of high purity to offer high charge carrier mobilities. However, they normally require extra effort of handling and deposition, e.g., through thermal sublimation in vacuum condition. Conjugated polymers, especially amorphous polymers, on the other hand, can be more easily processed due to their excellent solubility and therefore are more suitable for mass production through coating and printing.

Polymer semiconductors consist of σ-bonded backbone with satellite π-conjugated bonds that are held together by weak van der Waals interactions. The π-conjugated structure, meaning alternating single and double carbon bonds, is essential to achieve charge carrier mobility [16], [17]. To improve solubility, flexible side chains are added to the polymer backbone, which inevitably causes disorder and impurities [17]. As a result, carriers in polymers are easily localized or trapped due to these defects and disorder, which leads to lower mobilities in the range of 10^{-3} to 1 cm^2/Vs. Since the bonding of polymer semiconductors differs from the strong covalent bonding in inorganic semiconductors such as silicon, the carrier transport mechanism in polymer semiconductors is fundamentally different from the band transport model used for conventional inorganic crystalline semiconductors. Instead, the motion of the carriers in polymers has been described by hopping transport, where charge carriers hop from one site to another by thermally activated lattice vibrations or tunneling [14], [18], [19].

In addition to carrier mobility μ, the carrier density n has a huge effect on conductivity σ of the organic semiconductors, defined by $\sigma=qn\mu$, where q is the electronic charge unit. Undoped organic semiconductors have low intrinsic carrier density, though it can be enhanced by chemical doping and carrier injection from metal contacts. However, unlike in inorganic semiconductors where the doping normally just increases carrier density and does not interfere with the band structure, molecular doping in organic semiconductors (with weak Van der Waals interactions) affects the physical arrangement of the molecules, hence the electrical properties of the film such as mobility and charge distribution. Although different dopants have

been developed to enhance conductivity in organic materials [20]–[22], the lack of fundamental physical understanding of the transport and band mechanisms in doped organic semiconductors makes organic doping very challenging. As a result, conjugated polymers are often referred to as "electron transporting" or "hole transporting," as a manifestation of their lack of intrinsic carrier concentration.

Most solution-processed organic rectifying diodes have a single active layer sandwiched between two metal electrodes to achieve high speed operation. For this reason, the Schottky diode model has been commonly used to describe the energy alignment at the metal-organic semiconductor interface [23]–[27]. In the Schottky model, when the metal and the semiconductor are brought into contact, the charges flow over the interface until the Fermi levels on both sides aligned to establish thermal equilibrium. This creates a thin depletion region at the anode (for n-type) or the cathode (p-type) and semiconductor interface which manifests as a Schottky barrier where all mobile charges have diffused away. The depletion region W_d is given by

$$W_d = \sqrt{\frac{2\varepsilon_0\varepsilon_r(V_{bi}-V)}{qN}}, \tag{1}$$

where ε_0 is the permittivity of vacuum, ε_r is the permittivity of the semiconductor, V_{bi} is the build-in potential, equal to the total potential difference across the semiconductor, V is the applied voltage and N is the density of charge carriers [28]. On the other end of the diode, an Ohmic contact is formed between the heavily doped semiconductor and the other metal electrode, where the highly concentrated dopant-induced carriers bend the bands such that any potential barrier becomes quantum mechanically thin so carriers can easily tunnel through the interface. Thus, the Ohmic contacts exhibit negligible contact resistance and have a negligible voltage loss [26]. However, polymer organic semiconductors usually have low charge carrier mobility in the order of 10^{-3} cm^2/Vs and exhibit low density of charge carriers [29]–[33]. Consequently, the depletion region W_d calculated from Equation (1) can be several μm, which exceeds the whole semiconductor thickness. This indicates that the entire semiconductor layer of the diode is fully depleted and independent of applied voltage. Therefore, the Schottky barrier model cannot be directly applied. In addition, since doping is complex and often inapplicable for polymer semiconductors, the Ohmic contacts in polymers are normally realized by carrier injection directly from the metal electrodes. Due to these properties, the organic polymer diodes are fit more suitably with the metal-insulator-metal (MIM) diode

model, wherein a thin dielectric is sandwiched between two metal electrodes with dissimilar work functions [29], [30]. In practice, the Ohmic injection contact for p-type organic semiconductors is achieved by selecting a metal with a higher work function than the highest occupied molecular orbital (HOMO) level of the polymer. This metal, as an anode, injects charge carriers into the fully depleted semiconductors under forward bias. On the other hand, non-Ohmic contacts, or sometimes referred as rectifying contacts, for p-type organic semiconductors are realized by having a lower work function metal electrode compared to the HOMO level of the semiconductor. This energy difference between this cathode metal and the semiconductor creates a rectifying barrier which blocks carriers to move under reverse bias. The difference in work function of the two metal electrodes becomes the built-in voltage V_{bi} across the semiconductor. However, since the interface chemistry and energetics will change as the materials are brought into contact, forming an ideal Ohmic contact and non-Ohmic contact for an organic semiconductor becomes complicated and hard to predict [34]–[37]. Key interfaces in the active region, formed by the printing process, are paramount to diode performance, thus they are a barometer of the printing efficacy. The energy diagram and interfaces of p-type organic diode were investigated in detail in previous works by Kaisa Lilja [23] and Petri Heljo [24].

2.1.2 Characteristics

DC current (density) -voltage ((I(J)-V) measurement and AC impedance spectroscopy (IS) are commonly used for organic diodes characterization. The I(J)-V characteristics represent the most important DC properties of the diode including rectification ratio, charge transport mechanisms, diode contact properties, etc. Several analytical models for DC I(J)-V characteristic of organic diodes have been reported in the literature [38]–[41]. The general approach is to partially fit electrical characteristics in different voltage regimes. For MIM diodes the current characteristics can be divided into three regimes, reverse current region ($V<0$), diffusion and contact limited current region ($0<V<V_{bi}$) and space charge limited current (SCLC) region ($V>V_{bi}$), where the built-in voltage V_{bi} is defined as work function difference of the metal electrodes [42].

For p-type organic diodes, under reverse bias, the injection barrier between the work function of the cathode metal and the HOMO level of the semiconductor is large enough to prevent significant current flowing. As a result, the current level, also

called reverse leakage current, is typically low. In forward bias, when the applied voltage is below the built-in voltage, the resulting electric field within the semiconductor is opposite to the applied voltage, pointing toward the anode. This causes a small negative drift current. However, the current is dominated by diffusion of holes towards the cathode due to the hole density gradient. The combined diffusion-drift current in this voltage region is positive. In the past, the Shockley diode equation which was developed for p-n junction diodes has been applied. However, it is flawed to apply the recombination-current-based Shockley model to describe the single carrier diffusion-limited current in the MIM diodes. Later, De Bruyn *et al.* proposed a model to calculate the I(J)-V characteristics of hole-only MIM organic diodes below SCLC modified from the Schottky's model of diffusion current at MS interfaces with no band bending at both contact interfaces [42], in which the current density is given by

$$J=\frac{q\mu N_v(\varphi_b-V)\left(e^{\frac{qV}{kT}}-1\right)}{L\left(e^{\frac{q\varphi_b}{kT}}-e^{\frac{qV}{kT}}\right)}, \tag{2}$$

where N_v is the hole density at the Ohmic contact, φ_b is the barrier height at the rectifying contact, and L is the thickness of the semiconductor. A similar equation was derived for organic light-emitting diodes earlier by Nguyen *et al.* [43]. In MIM diodes, there is no band bending at the Schottky contact induced by dopants. On the other hand, the single carrier diffusion from the anode into the semiconductor forms an accumulation region close to the anode and causes band bending at the Ohmic contact [42]. This band bending reduces the built-in voltage and has an impact on the diffusion current. As a result, the calculation of the current below the V_{bi} region becomes more complicated. When the applied voltage is larger than the built-in voltage, the resulting electric field turns positive, and the drift current starts to dominate. This is the well-known SCLC, described by the expression of Mott and Gurney [44]

$$J=\frac{9\varepsilon_r\varepsilon_0\mu(V-V_{bi})^2}{8L^3}. \tag{3}$$

In addition, some basic parameters such as mobility, equilibrium carrier concentration and work function difference between the two contracts can be extracted from the DC I(J)V-characteristics.

Impedance spectroscopy (IS) is another useful technique to study the carrier transport mechanism and interface effects in organic diodes [45], [46]. IS records the linear electrical response of the device of interest to small signals at certain DC biasing. The measured spectra can be electrically interpreted with a proper equivalent circuit model, which normally includes a chain of resistor-capacitor (RC) networks to represent individual interfaces and layers. However, it should be pointed out the small signal model obtained by IS at certain DC biases is not adequate to represent the nonlinear behavior of organic diodes with large AC input signals [47]. The intrinsically nonlinear nature of the rectification cannot be described by the conventional linear small signal approach.

The primary application of the diodes is high frequency rectification of incoming AC singles to DC voltages in rectifier circuits. Therefore, it is of great interest to analyze the frequency response of the diodes used in a rectifier circuit. However, since organic diodes essentially operate in a different way than Si-based diodes, and the physics of the frequency response of organic rectifying diodes are not completely understood, the nonlinear large signal analysis model for organic diodes is thus far not available. In fact, the nonlinear nature of the rectification increases the complexity of frequency operation analysis drastically. Nonetheless, several approaches to analyze the diode frequency response have been reported. As the diodes are unipolar, *i.e.*, the charge carriers are either holes or electrons only, and the transport of carriers is along the transverse direction in the vertical structure, the carrier transit time or so-called time-of-flight (TOF) time t_T to move between two electrodes is given by

$$t_T = \frac{L^2}{\mu(V_{in}-V_{bi})}, \tag{4}$$

where V_{in} is the applied bias on the diode and V_{bi} is the diode build-in voltage. Here, the semiconductor is assumed to be trap-free. Equation (4) provides an oversimplified way to estimate the maximum operation frequency of the diode, as f_{max} is reciprocal of time, denoted by $1/t_T$. Steudel *et al.* [47] proposed a different formula where the maximum theoretical frequency of the diode is determined by charging and discharging rate between the load capacitor and resistor in a half-wave rectifier circuit. Although this approach offers a more realistic upper frequency limitation compared to the one obtained from the TOF, it involves some ambiguous assumptions such as no leakage current in reverse bias. Since this complicates the calculation but still does not deliver fully reliable results, this analysis is also not ideal.

Moreover, pure numerical approaches involving solving a set of continuity, drift diffusion and Poisson equation under Schottky boundary conditions have been reported to calculate the frequency response of the diode [48], [49], but the computational time is excessive, especially in the high frequency regime.

In practice, an effective route to analyze the rectifier circuit operation is to employ an equivalent circuit model. The most simplified model of vertical MIM diodes, without including the contact effects of the diode, consists of a single RC network as shown in Fig 1, where R represents the resistance of the semiconductor layer and C_{diode} is the bulk capacitance. For MIM diodes with a fully depleted semiconductor layer, the bulk capacitance of the diodes is the same as the geometric capacitance given in Equation (5) which remains reasonably constant over different bias voltages and frequencies [30].

$$C_{diode} = \frac{\varepsilon_r \varepsilon_0 A}{L}, \tag{5}$$

where A is the cross-section area of the diode. The bulk resistance, on the other hand, appears to be both frequency and voltage dependent. Altazin *et al.* [49] later proposed an improved model in which the equivalent resistor was replaced by a voltage dependent conductance, with an expanded time dependent function based on TOF to properly capture the frequency performance of devices. Though the resistance which represents the nonlinear operation of the diodes is still complex, the model (Figure 1) was found sufficient to explain the diode performance in the rectifier application.

For rectifying diodes operating at higher frequencies, both the geometric and electric properties play a huge role. The layer thickness, as the dominant factor in Equation (4), dictates the cutoff frequency. The carrier mobility determines how fast the carriers travel between two electrodes where the carrier density affects the injection current.

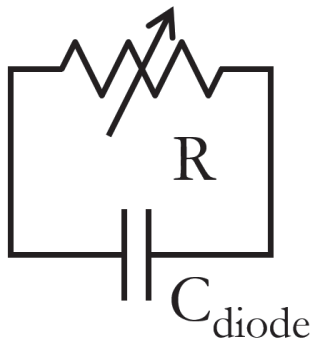

Figure 1. Simplified equivalent circuit model for an organic diode.

2.2 Metal oxide rectifying diodes

Solution-based organic diodes offer flexibility and low temperature processing, but have a low operating frequency range, typically limited to tens of MHz due to relatively poor carrier mobility and density. Transparent metal oxide semiconductors, with a number of great properties such as large band gap, wide optical transparency, high carrier mobility and moderate temperature deposition process, have gained special attention in recent years and established as one of the most promising technologies for leading next generation electronics [50]–[54]. The most prevalent amorphous metal oxide semiconductors involve indium (In), tin (Sn), zinc (Zn), and gallium (Ga) as starting elements. Due to great interest, the deposition methods of these thin films have been studied and innovated. A variety of deposition techniques have been reported such as spin-coating, electron beam evaporation, RF sputtering, pulsed laser deposition, atomic layer deposition, and various printing depositions [50]–[54]. Metal oxide semiconductors devices are mostly reported in the context of thin-film transistors (TFT)s, although in recent years, metal oxide diodes have attracted attention for rectifying applications. Among them, vacuum processed RF sputtered In-Ga-Zn-O (IGZO) diodes have demonstrated frequency performance up to and above 1 GHz [55]–[57]. Despite such excellent results, the properties of IGZO rely heavily on the oxygen/argon ratio during the sputtering process, which makes them not compatible with cost-effective mass production. To move a step forward to low-cost deposition, solution-processed metal oxide diodes have been recently reported with promising results [58], [59]. One outstanding material that has

been extensively investigated is indium oxide. This is due to its simplicity of solution formulation and high electrical performance including large electron mobility, high charge carrier concentration and wide band gap compared to other metal oxide semiconducting materials [60].

Metal oxide semiconductors are valence compounds between metal (M) ns and oxygen (O) 2p orbitals with a high degree of ion bonding. In general, the M orbitals are highly dispersive while the O orbitals are more localized. This leads to a better electron transport in comparison to hole transport [61]. Therefore, typical metal oxide semiconductors such as indium oxide is an intrinsic n-type semiconductor. Similar to polymer organic semiconductors, when undoped indium oxide is sandwiched between two metal electrodes, a MIM diode structure is formed. The characteristics of the solution-processed metal oxide rectifying diodes follow the MIM diode model, as presented in section 2.1.

2.3 Printed and solution-processed electronics

Advances in the properties of organic semiconductors as well as metal oxide semiconductors, such as solution processability and ambient stability, offer possibilities in cost effective printed electronics. Printed electronics has been associated with various names in scientific publications depending on the context such as organic, flexible and plastic electronics, large area or low-cost electronics. Regardless of the name, the core of this new technology is solution-based processes. A wide range of large area deposition and patterning techniques can be used for solution-processed devices. For clarification, printing techniques are defined as patternable solution processes while coating techniques are non-patternable solution processes. In this work, spin coating, gravure printing, screen printing and inkjet printing techniques were utilized for the fabrication of various layers and devices.

Spin-coating is arguably the simplest and most common coating technique to spread uniform thin films on flat substrates. Thus, it is a facile tool for rapid prototyping of novel structures. In the spin-coating process, a solution is first dispensed onto the surface of a substrate, which then rotates at high speed (hundreds to thousands of rotations-per-minute (rpm)) until the excess solution spins off. The remaining solvent, which is usually volatile, evaporates during deposition due to diffusion. With an additional drying or annealing process, the resulting thickness of the thin film from spin coating ranges from a few nm to a few μm determined by the spin speed, concentration, and viscosity of the solution. The major advantages

of spin-coating over other methods are its simplicity, high consistency, and low cost. However, spin-coating is difficult to scale up, therefore is not compatible for large area manufacturing [62]. Alternatively, slot die coating, as a large area solution-based coating process, is a widely used approach for non-patterned high-speed roll-to-roll deposition of uniform thin films [63], [64].

Printing techniques, especially the ones adapted from the graphic arts industry, enable roll-to-roll or high-speed sheet-to-sheet mass printing processes. The common mass printing methods includes gravure, flexographic, offset and screen printing etc. In addition, non-contact printing methods, especially inkjet printing, have become widespread in functional printing due to the digital nature of the process. In general, each printing process has specific strengths, weaknesses and areas of applicability.

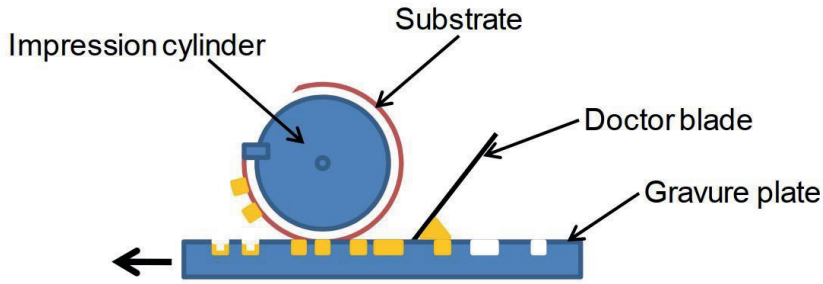

Figure 2. The principle of the sheet-fed gravure printing process used in this thesis [24].

Gravure printing is a method in which the pattern to be printed is engraved as a discrete arrangement of cavities, called cells, into a printing cylinder or plate, which is traditionally made of metal. For a sheet-fed gravure printing process, as shown in Figure 2, the engraved cells are filled with ink by a doctor blade. The ink on the plate is then transferred to a substrate rolled over the impression cylinder when the substrate is brought into contact with the plate. A similar principle is used in a roll fed gravure printing, in which the gravure cylinder with engraved cells is dipped in an ink bath and the excess ink is removed with a doctor blade; the ink is then transferred from the cells to a substate by pressure. Due to the simplicity of the gravure printing process, the inks interact only with a limited number of components, which ensures reliability. The thickness of the films is controlled through the engraved cell depths and densities. With the help of laser engraving and modern microfabrication techniques, gravure printing offers high resolution of few μm [65]. The excellent printing quality and high consistency of gravure printing

makes it a promising printing process in printing electronics for a variety of applications including solar cells, transistors, rectifying diodes, and light-emitting diodes [5], [8], [9], [11]. However, the gravure plates in general are expensive, which makes flexographic printing with relatively low-cost rubber plate favorable for short runs. In contrast to gravure printing, in which the ink resides inside the engraved cells, the ink on the flexography plates is transferred onto the embossed ridges of the pattern. In flexography printing, the anilox roll is first inked. The ink is transferred to the embossed area of the elastic printing plate. The printing roll then contacts the surface of the film and transfers the patterned image. Because of the soft printing plate, flexography printing has been facing challenges to accommodate highly aggressive solvents, which are often required for solution-processed materials. In recent years, there has been progress in viability of flexography printing for organic devices [6]. Other mass printing methods such as offset printing and screen printing have also been used in printed electronics for various applications [4], [12]. Offset printing offers excellent printing resolution and registration but has a high-cost ink printing unit. Screen printing, well-known through its use in printed circuit board (PCB), is suitable for depositing large area, thick films at low cost.

Inkjet printing is one of the most utilized non-contact direct printing techniques. In this method, the ink is formed into small droplets and then ejected onto the substrate guided by a digital layout. Owning to its simple principle, excellent ink compatibility as well as digital, additive and contactless deposition process, inkjet printing has become an attractive fabrication technique with a variety of applications in printed electronics [7], [10], [13]. One shortcoming of the inkjet printing is the low throughput compared to the above mass printing methods such as gravure printing. But this is being improved through the use of multiple printheads in parallel as demonstrated in Publication I.

2.4 Applications and circuits

Rectifying Schottky diodes are indispensable components of an RF-to-DC rectifying system. The most prominent application of rectifying diodes is energy harvesting in radio frequency identification (RFID), near field communication systems (NFC) and for wireless sensors in IoT applications. Figure 3 summarizes key applications for rectifying Schottky diodes. The performance of solution-processed devices cannot compete with conventional electronics. Nonetheless, the development of solution-processed electronic components leads to great opportunities for the realization of

low-cost and flexible thin-film devices. These thin-film devices can be easily incorporated into simple circuits to provide necessary functionalities to, for example, various smart objects of IoT at low cost.

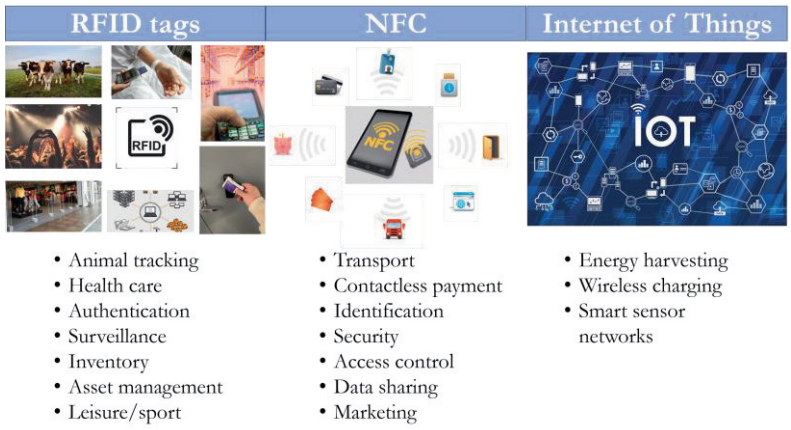

Figure 3. Applications of rectifying diodes.

2.4.1 RF energy harvesting applications

RF energy harvesting is the concept of scavenging the electromagnetic waves and converting them to electrical energy (*i.e.*, into voltages and currents) to power up electronic devices. A rectifier acts upon an AC signal such that one half of the cycle is clipped, or attenuated, leaving the opposite side of the waveform intact. Normally an electromagnetic wave has an average DC value of zero, as the two halves cancel each other. But with a rectifier, the remaining intact half leads to a small DC voltage induced by the rf energy received. Thus, RF energy harvesting systems, or in short RF harvesters, comprise a minimum of two functional units: an antenna to gather RF energy and a rectifying circuit to convert the received RF signals to DC voltages. An impedance matching network between the antenna and the rectifier, and a power management unit integrated after the rectifier can be incorporated to maximize the harvested energy. The RF harvesters can be classified into two types based on the source of the RF power, either from a dedicated RF source or from the ambient RF energy provided by common wireless devices like phones, Wi-Fi equipment, etc. The former RF harvesters are often called wireless power transfer harvesters, while the latter are referred as ambient RF energy harvesters. The choice of the RF harvester application depends on the operating frequency. Low-frequency (LF) RF harvesters

mainly suit the Qi standard developed by wireless power consortium (WPC) [66] and work at 80-300 kHz. High frequency (HF) harvesters operate at the 13.56 MHz ISM (Industrial, Scientific and Medical) and NFC band, and ultra-high frequencies (UHF) systems refer to frequencies beyond 450MHz. The large corresponding wavelengths at low frequencies such as the Qi and 13.56MHz prevent sufficient ambient RF energy scavenging; the ambient energy is already very low at these low frequencies. Therefore, dedicated RF sources, for instance wireless charger and RFID readers, are commonly employed to provide direct transmitting power. At these frequencies, printed RF harvesters usually utilize small inductive loop antennas together with rectifying diodes featuring either polymer- or metal oxide- based printable semiconducting materials [67]–[69]. In general, these printed small inductive loop antennas, also known as inductive couplers or coils, are the size of credit cards and operate in the magnetic near field, typically under few tens of centimeters. On the other hand, at UHF or higher frequencies, a hybrid RF harvester combining printed antennas with a rectifying circuit based on discrete surface-mount technology (SMT) components [70]–[72] and an integrated circuit (IC) is widely used for scavenging ambient RF radiation at GSM (Global System for Mobile Communications), Wi-Fi band, etc. There have been reports of vacuum processed organic diodes and solution-processed inorganic diodes rectifying at close to 1 GHz but the power loss on these novel devices due to non-ideal semiconductor and contact properties set a severe challenge to harness ambient RF energy with an average power density in the order of 60 W/m^2 in the low GHz range.

Figure 4. Pictures of energy autonomous temperature sensor mounted inside a smart chocolate box [73].

Figure 4 shows an example application of the printed RF harvester in a flexible energy autonomous temperature sensor system integrated into a smart chocolate

box. As one of the energy sources, the printed 13.56 MHz RF harvester (Publication I) was used to charge the supercapacitors. The stored energy ran the temperature sensor and display for at least 6 hours [73].

2.4.2 RF energy harvester antennas

The basic RF energy harvester that operates at or below 13.56 MHz utilizes a rectenna circuit which is composed of a small loop antenna and a rectifying circuit. The loop antenna gathers the RF energy through inductive-coupling, and the rectifying circuit converts the coupled AC signals to DC voltages. Since these small loops operate at radio frequencies, they are usually called "small loop antennas", however, they should not be mistaken as the traditional small loop antennas for real-world far field radio wave communications. Specifically, these small loops, which are essentially inductors, interact with the near field magnetic induction rather than the far field radiation, therefore they are not radio loop antennas that carry RF currents as electromagnetic waves. Strictly speaking, they are not real antennas, as typical antenna parameters such as the radiation pattern and the antenna gain are not applicable. The utilization of these loops is because of the restraints put by the operation frequency and the commonly established antenna size. At the operation frequency of 13.56 MHz, the corresponding wavelength is 22 meters long. This means to get high radiation efficiency a loop antenna or a dipole antenna would have to be about 11 meters, *i.e.*, half wavelength, in perimeter length. In practice, NFC and 13.56 MHz RFID devices that accommodate these antennas commonly have a size of a smart phone or a credit card to fit easily into a pocket. As antennas are squeezed into an area about 0.5% or less of one wavelength, nearly no radiation will be generated based on antenna theory [74]. As a result, the small inductive loops are better suited to offer contactless energy transfer than a real antenna at LF and HF range. Consequently, inductively coupled small loops are exclusively used in NFC and 13.56 MHz RFID applications [75]–[77]. Figure 5 shows loop antennas in a commercial smartphone and RFID cards compared to a loop antenna for radio wave communications.

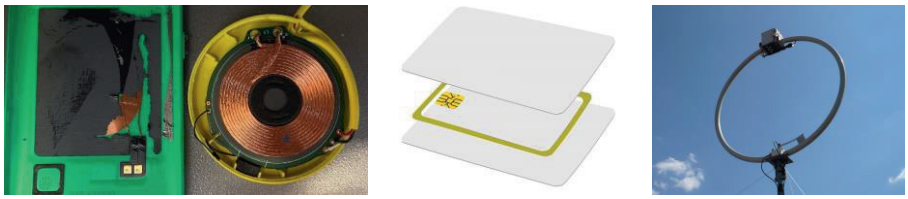

Figure 5. Coils on smartphones and Qi charger (left), a 13.56 MHz RFID card (middle) and a loop antenna with a diameter of 2 meters operating at 1.75-30 MHz (right).

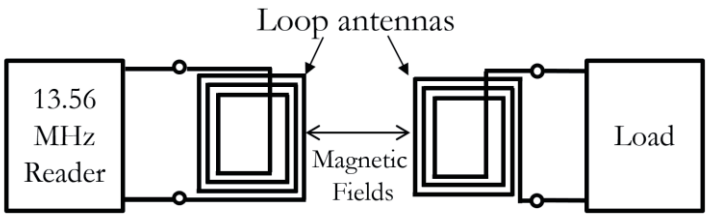

Figure 6. Circuit diagram of a 13.56 MHz loop antenna transaction.

A circuit diagram of the 13.56 MHz loop antenna system is shown in Figure 6. The 13.56 MHz reader antenna excites current in the loop which is an inductor. This induces a magnetic field, and when the pair of loops is closely placed an electric current is further induced in the paired of loops through inductive coupling. This induced current can be used to power or communicate to the load. For inductively-coupled loops, the induced voltage on the antenna coil can be estimated based on Lenz's law as the induced voltages equals to the time rate of change of the magnetic flux [78], *i.e.*,

$$V=-N\frac{d\Psi}{dt}, \tag{6}$$

where N is number of turns of the loop antenna and Ψ is magnetic flux through each turn. The magnetic flux can be described in terms of mutual inductance and induced current, and the equation becomes

$$V=-M\frac{di}{dt}, \tag{7}$$

where i is the induced current and M is total mutual inductance that depends on both loop geometry and the distance between the two antennas. The inductances of the planar antennas can be estimated with theoretical equation as

$$L=L_0+M_+-M_-, \tag{8}$$

where L is the total inductance, L_0 is the sum of the self-inductance of all straight segments, M_+ is the sum of the positive mutual inductances, and M_- is the sum of the negative mutual ones [79]. Expanding the loop area and number of turns enhances the mutual inductance but also leads to a higher resistance due to the increased length of the loop. This results in a bigger voltage loss in the loop, which will lower the quality factor (Q) as well as shift the resonant frequency. This effect is weaker for loops using highly conductive materials such as copper conductor coils and Cu on PCBs, compared to printed loop antenna. However, for printed loops the high resistance of the loop will affect the Q factor and frequency as shown in Equation (9.b).

To obtain maximum performance such as reading range, coupling voltage amplitude, etc., the rectenna circuit needs to be tuned to the 13.56 MHz operating frequency. This resonant frequency is determined by the inductance and capacitance of the rectenna circuit and can be affected by the loop resistance as given in Equation (9.a) and (9.b)

$$f_{res}=\frac{1}{2\pi\sqrt{LC}}, \tag{9.a}$$

$$f_{res}=\frac{1}{2\pi}\sqrt{\frac{1}{LC}-\left(\frac{R}{L}\right)^2}. \tag{9.b}$$

Traditionally, a solid-state capacitor will be added to the loop antenna to tune the targeted LC product, resulting in the desired resonant frequency. In general, for loop antennas with a size of a credit card, a few μH to few tens μH can be achieved by increasing the loop turns. This means extra tuning capacitance of tens of nF and tens of pF is required for the loops to resonate at Qi frequency and 13.56 MHz, respectively.

Due to the nature of inductive coupling with a magnetic field near the loop antenna, the operation range of small loops is limited to few cm at Qi frequency and few tens of cm at 13.56 MHz. To address this bottleneck, printed large area E-field

antenna with an enhance long range operation is considered. Since the wavelength of the 13.56 MHz signal is 22 m, therefore even for a short dipole with a total length less than a half wavelength of 11m at 13.56 MHz can be deemed impractical. Thus, a novel design for an E-field dipole antenna to reduce the antenna size to a reasonable area is needed, as presented in Publication IV. Nevertheless, the printed E-field antenna at 13.56 MHz requires large areas and the printing is particularly well suited to such large area devices.

2.4.3 Rectifying circuit

Organic rectifying circuit design has generally been adopted directly from established solid-state inorganic rectifier topologies, such as half-wave, full-wave, double half-wave rectifiers, charge pumps and other voltage multipliers. For many years, the half-wave rectifier, which utilizes a rectifying diode in series with a filtering capacitor, has been used extensively for its simplicity. In addition, it offers the most straightforward insight on the frequency performance of a diode. The organic diode half-wave rectifiers have been demonstrated in literature using a variety type of semiconductors, such as P3HT [80], Poly(triarylamine) PTAA, pentacene [47], [69], [81] and C_{60} [82] and their performance is summarized in Table 1. For high performance organic semiconductors such as vacuum deposited pentacene, or C_{60}, operating frequencies toward GHz were reported, however, their performance deteriorated quickly when exposed to air. On the other hand, half-wave rectifiers based on solution-processed diodes have targeted primarily 13.56 MHz due to their inherent electric properties and lower mobilities, but they offered good stability under ambient conditions. Table 1 clearly indicates that the voltage loss on the organic diodes is significantly larger than the built-in (or threshold) voltage of the diode as of that Si-based diodes. Besides the built-in voltage, low carrier mobility and carrier concertation as well as non-ideal Ohmic contact resistance contribute to voltage drop on the polymer diodes.

Table 1. A summary of reported results for organic rectifying diodes

Frequency, MHz	Input AC p-p Voltage, V	Rectified DC Voltage, V	Semiconductor	Fabrication	Reference
13.56	20	4	P3HT	Spin coating	[80]
13.56	20	5	PTAA	Printing	[Publication I]
13.56	20	4	PQT-12	Spin coating	[83]
13.56	20	4.5	C_{16}IDT-BT	Spin coating	[84]
50	36	8	Pentacence	Vacuum processing	[69]
869	30	4.5	Pentacence	Vacuum processing	[81]
700	4	1	C_{60}	Vacuum processing	[82]

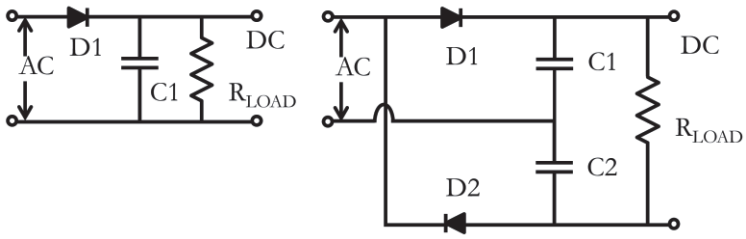

Figure 7. Schematic of a halfwave rectifier (left) and a double half-wave rectifier (right).

For devices or applications where a higher DC voltage is required, the double half-wave rectifier and charge pump approach have been considered. Full-wave and double half-wave rectifiers using organic diodes have been reported [69], [85] and in Publication II. Printed organic charge pumps as voltage tripler and quadrupler operating at 13.56 MHz have also been demonstrated [11], [67], [84], [86]–[88] where the output voltage exceeds the input AC amplitude. Despite the enhanced output, a higher voltage multiplier demands not only more diodes but also capacitors. This inevitably raises the difficulty for a monolithic circuit integration. Thus, the choice of rectifier circuit to a specified application requires consideration of the properties of the diodes such as the relatively high voltage loss with increased frequency and the complexity of the circuit in terms of fabrication and integration process. In this work, the half-wave and the double half-wave rectifier configurations (Figure 7) are utilized.

3 EXPERIMENTAL

The sample preparation, fabrication and characterizations are described in this chapter. The basic operation and some optimization of PTAA diodes have been carried out in previous work [23], [24]. One focus of the work reported in this thesis is to further improve the fabrication process for thinner diodes to reach higher cut-off frequencies. In addition, some other related experiments and improvements such as doping are present. In order to be compatible with low-cost mass production, in this work all materials and devices were air-stable without encapsulation, and all fabrication and measurements were carried out at ambient air conditions. The only exception was the use of a vacuum evaporator, which is integrated into a nitrogen glovebox, for metal contact depositions of the indium contacts. However, the devices were taken back into ambient air immediately after the evaporation since the nitrogen environment was not required.

3.1 Materials

PTAA is an amorphous p-type organic semiconductor with a modest carrier mobility of 10^{-3} -10^{-2} cm^2/Vs [89]. Despite its low charge carrier mobility and concentration, PTAA semiconductor possesses certain properties that make it well suitable for printing; it can be handled in air with an excellent stability [90], it has a good solubility in non-chlorine-based solvents like tetralin, xylene and toluene, it requires no high temperature annealing process, and it is fully amorphous, which enables high quality film formation and high reproducibility during printing. The PTAA used in this work was purchased from Merck and later from Sigma-Aldrich in both powder and solution form. Other four noncommercial PTAA materials with different substituents and molecular weights were investigated. These alternative PTAA materials either did not wet the Poly(ethylene terephthalate) (PET) substrates well or showed worse electrical performance compared to that of commercial PTAA materials. This is probably due to a smaller molecular weight and a lower carrier mobility because of more trap states as a result of impurities remaining from the chemical synthesis process.

To increase the carrier mobility as well as the carrier concentration of PTAA semiconductor, some blending and doping experiments were conducted. First, solution-processed 6,13-Bis(triisopropylsilylethynyl)pentacene (TIPS-pentacene) has been tested as an additive for polymeric semiconductor PTAA. Such blends have shown good performance in organic TFT applications [91]. It has been reported that TIPS-Pentacene-PTAA blends show phase segregation of the semiconductor layer, forming a polymer-TIPS-pentacene interface with improved crystalline order in the active layer in a lateral direction, which enhanced the electrical performance in TFTs [92]. This can lead to improved field-effect mobility in lateral conduction devices such as TFTs. However, the blends with TIPS-Pentacene have a negligible effect on the vertical diodes. Although the TIPS-Pentacene layer increased the carrier concentration at layer interfaces, it did not change the carrier mobility within the PTAA layer. Hence, the vertical diode performance remained the same, as confirmed by the experimental results (not shown here).

Next, Tris (4-bromophenyl) aluminum hexachloroantimonate (TBPAH), and hexafluorotetracyanonaphthoquinodimethane (F6TCNNQ) have been tested as p-type dopants for organic semiconductor. TBPAH and F6TCNNQ (or F4TCNNQ) have been reported to improve the hole injection layer in OLEDs [93] and to increase the conductivity of polymer semiconductors [22]. Compared to the undoped PTAA diode, the forward current and the reverse current of low % TBPAH doped PTAA diode were raised 2 times and 100 times, respectively, whereas F6TQNN doped PTAA diodes had a significant increase in reverse current, while the forward current remained the same or even a little worse than in the undoped diode. For both dopants, the diode frequency response showed no significant improvement. With a higher doping level, the diode started to become short-circuited and the yield dropped. The TBPAH dopant can bring extra carriers to fill the traps in PTAA and thus improve the mobility, but might also shift the HOMO/Fermi level of the semiconductor and cause unwanted energetic mismatching. Considering the extreme toxicity of dichloro-ethane that is required for dissolving the TBPAH, the doping approach was discontinued. On the other hand, the absorption spectrum showed no interaction between F6TCNNQ and PTAA to enable charge dissociation, which is essential to increase the conductivity of the samples. The lack of interaction in the doped films could be due to doping concentration below the threshold concentration to enter the crystalline phase [22]. Indeed, these doping tests of PTAA revealed that the doping mechanism of organic semiconductor is complicated and not well understood, and in many aspects even problematic. The interaction between each dopant and organic semiconductor has a

distinct and subtle chemical basis, which leads to a case-based research approach. Most of the reported doping in organic diodes aimed to create a doped buffer layer between the ohmic contact and the semiconductor. Although this can increase the injection current of the diode as observed from TBPAH doped PTAA diodes, the frequency response of the diode, which depends on the carrier mobility, remains unimproved. Due to the problems with performance, the doped PTAA material diodes were not used in any of the applications.

Solution-processed metal oxides are promising materials as an alternative to organic materials for high-speed diodes, as they exhibit higher carrier mobility. Indium oxide is a n-type undoped semiconductor with a high carrier mobility and a wide bandgap 3.6-3.75 eV [94]. The reported theoretical carrier mobility of solution process indium oxides in thin film transistors is as high as 3.5 cm^2/Vs [95]. The air-stability of solution-processed indium oxide is excellent as well.

3.2 Device fabrication

3.2.1 Fabrication of PTAA diodes

The PTAA diodes in Publication I-IV were assembled on evaporation deposited Cu on PET substrates (Melinex ST506, DuPont Teijin Films). The 50 nm (or 100nm) Cu layer was patterned (Fig.3.1) through a shadow mask as the bottom cathode electrode. The Cu pattern includes 4 repeated units with 5 different widths, *i.e.*, 0.1, 0.2, 0.3, 0.4, 0.5 mm. A total of 20 devices can be fabricated on a single substrate, as shown in Figure 8. The PTAA semiconductor ink and the PM-460A silver paste from Acheson were successively deposited using a sheet-fed automatic gravure printing press, Labratester Automatic from Norbert Schläfli Maschinen. Both layers were cured for 5 minutes at 115 ^oC in air. The PTAA layer thickness is controlled by the ink formulation and the printing parameters. The ink should have a proper viscosity and surface energy, which can be realized by choosing the suitable solvent, a mixed solvent or by adding extra additives. A diluted ink normally leads to a thinner layer under the same printing settings, but the curing of the PTAA should be effective in a predictable way to ensure layer uniformity. Due to the engraved cell structure for transferring the inks, thickness control in the gravure printing process is not very accurate. The layer thickness fluctuations are estimated in the order of tens of nm in a gravure printed layer. In addition, the edges of gravure cells are always

rough which causes small area variations in a printed layer. Therefore, differences between two printed diodes will always occur. As mentioned before, these limitations set by the gravure printing method can be overcome by using advanced engraving methods for high resolution gravure cell structures. However, the cost of such plates goes up, resulting in a more expensive manufacturing process. In this work, two different gravure plates were employed: one has a cup density of 100 cups/cm and a cup depth of 30 μm and the other one has a cup density of 40 cups/cm and a cup depth of 80 μm. The plate with a higher cup density and a lower cup depth can yield significant thinner and smoother layers compared to the other plate, therefore it is mainly used to print thin PTAA layers. On the hand, the high viscosity Ag flake ink is printed with the low density and great depth plate to achieve a thick electrode layer.

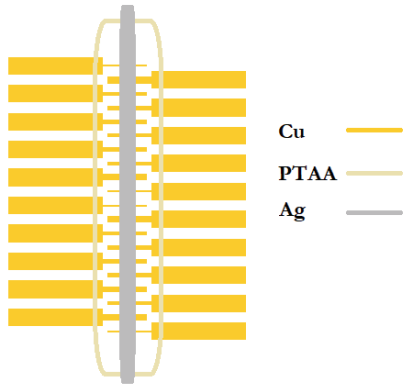

Figure 8. Schematic layout of the PTAA diodes.

All printing processes are required to have the ability to deposit a uniform, pinhole free, layer which translates to high yield with a desired film thickness. In general, a thinner layer requires that the PTAA must be deposited from a diluted solution. Thus, several formulation approaches with tetralin, xylene, toluene and anisole were tested to modify solution viscosity with a high yield. The most promising formulation was the mixture of a low viscosity (thin film) and a high viscosity (high yield) solvent, for example toluene/tetralin or O-xylene/tetralin (4:1 in weight). With 6% by weight PTAA in the mixed solutions, the printed PTAA film thickness was around 300 nm and the yield was excellent, i.e., 19 or 20 out of 20.

The properties of the Ag flake paste are crucial in forming the Ohmic contact to the PTAA layer. Based on the reported work function of Ag at 4.3 eV and the HOMO level of PTAA of 5.1 eV, a Schottky contact should be expected. However, Kelvin probe measurements showed that Ag flake ink was heavily oxidized and had

an effective work function of 5.2 eV [23]. This leads to formation of an Ohmic contact between the Ag electrode and the PTAA. The viscosity of the Ag ink was adjusted with extra solvents to suit the gravure printing method. With a high viscosity Ag ink, the resulting layer showed visible holes with diameters of 50-150 μm; while a further diluted Ag ink with a low viscosity diminished the hole areas and yielded a smoother layer, as shown in Figure 9. Interestingly, the diodes with a rough Ag layer provide better I-V and rectifying output. The smaller amount of solvent used leads to a better curing, which affects the Ag oxidation level hence the work function of Ag layer. In addition, when printed on top of the cured polymer PTAA layer, the rougher Ag flake layer can press into the soft PTAA layer causing a reduction in the effective PTAA layer thickness and thus enhance the diode frequency response. However, the high local electric field due to the Ag penetration in an ultra-thin PTAA layer can cause current spikes to DC voltages and short circuits to low frequencies AC signals for the diode. This phenomenon was studied in [24].

The roughness and distortion due to curing of the PET substrate set limitations on how thin a PTAA layer can be printed as well. The PET substrate exhibits occasional high peak spikes of tens nm that could happen in the diode area. The 115 ^{o}C curing temperature and the cool back process will cause distortion to the film, including bending, shrinking, and expanding of the film. These effects should be considered during the fabrication of diodes with very thin layers.

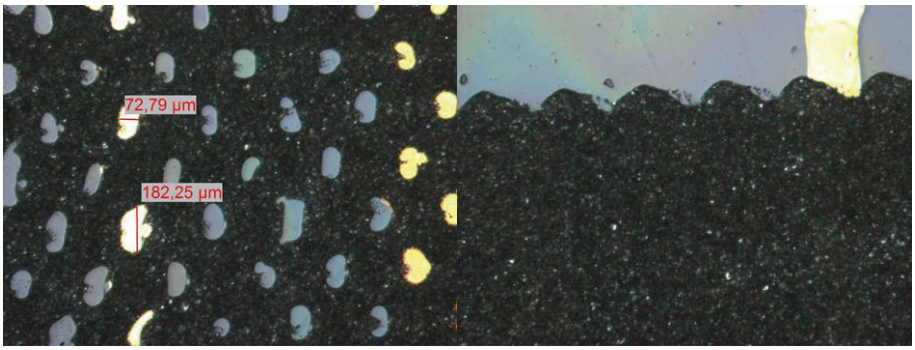

Figure 9. Microscopy images of the silver layer. High viscosity silver ink with visible holes(left) and low viscosity silver ink with less hole area (right).

3.2.2 Fabrication of indium oxide diodes

The indium oxide diodes in Publication I were fabricated on SiO_2 coated Si wafers. A 25 nm thick patterned Al electrode was first evaporated on the wafer through a

mask, followed by three iterative layers of spin coated indium oxide precursor to prevent short circuits in the diode structure by increasing the aggregate diode active thickness. The precursor, with a molar concentration 0.2 mol/L, was made by mixing indium nitrate hydrate with 2-methoxyethanol (both from Sigma Aldrich). This precursor formula was first published by VTT (Technical Research Centre of Finland) [96]. The first two layers were cured at 300 °C in an oven under atmosphere for 5 minutes and the last layer was cured for 30 minutes at the same temperature. Finally, a 100 nm patterned Au electrode was evaporated. To improve the wetting of the indium oxide precursor, the Al electrode was subjected to ultraviolet (UV)-ozone treatment for 15 minutes immediately before the deposition of indium oxides. The cross section of the diode was studied by focused ion beam-scanning electron microscope (FIB-SEM) image as shown in Figure 10. Pt and Carbon layers were deposited as protection layers for the FIB milling process. Different layers were defined by energy-dispersive X-ray spectroscopy (EDS). The SiO_2 layer was determined to be around 100 nm. The layer thickness of three-layer indium oxide film was around 200 nm.

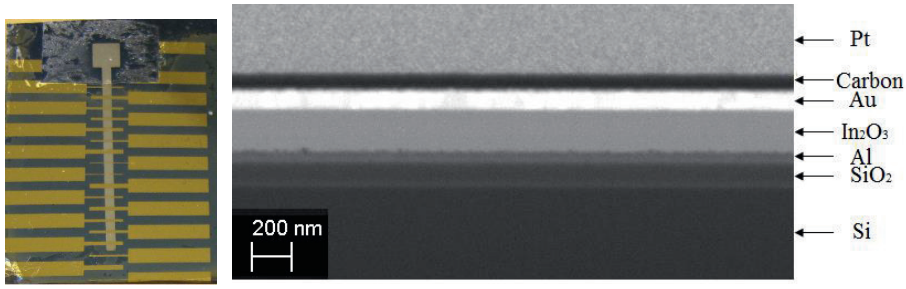

Figure 10. A photo of Al/In_2O_3/Au diodes (left). FIB-SEM cross section image of the diode (right).

3.2.3 Fabrication of other components

Besides the rectifier diodes, the filtering capacitors in the rectifier circuits and the antennas can be fully printed as well. In Publication I, the loop antenna and the bottom Ag electrodes for the capacitor were printed with an iTi MDS 2.0 inkjet printer using a Spectra S-class printhead with 128 nozzles for higher speed large area deposition. The dielectric and top Ag layers for the antenna bridge and the capacitor were printed using a Dimatix materials printer DMP-2831 with a low cost 16 nozzles printhead for fast and accurate small pattern printing. Harima NPS-JL silver NanoPaste ink and SunTronic Jettalbe insulator U5388 were used as the conductive

ink and the dielectric ink, respectively. The Ag ink was sintered at 150 °C for 1 hour. The dielectric ink was cured by exposure to UV-light (PSD-UV from Novascan Technologies) for 30 sec, and then oven sintered at 150 °C for 30 mins. A PET film Melinex ST506 from DuPont Teijin Films was used as the substrate.

In Publication IV, the antennas were screen printed on a Graficaindia Flextonica Nano Print Plus flat-bed press using Novacentrix (PChem) ink, PSI-219. The ink was cured two times using a DragonAir drying tunnel at 140 °C with a dwell time of 90 seconds. The final thickness of the printed antennas was about 5 μm. The sheet resistance was about 30 mΩ/square. The printing work was done in Clemson University.

3.3 Characterization Applications and circuits

The I(J)-V measurements of the PTAA diodes were carried out either using a Keithley 236 source-measure unit or a Zahner Zennium potentiostat. The I(J)-V characteristics of the indium oxide diodes were determined using a Keysight B1500A semiconductor analyzer connected to a probe station. The small-signal properties of the diodes were measured by a HP network analyzer 8752A. The diode geometric capacitance value was drawn from this measurement. According to Equation (5) the PTAA layer thickness is then calculated on the basis of the measured geometric capacitance using a relative permittivity of 3. The measurement setup is shown in Figure 11.

The basic diode frequency responses up to 50 MHz were evaluated in a half-wave rectifier configuration; the rectified DC output voltage of the rectifier as a function of frequency was measured. In these measurements, the amplitude of the input AC signal was 10 V, provided by a Keithley 3390 50 MHz arbitrary waveform generator. In publication V, a Hewlett Packard ESG-DS300A 250 kHz to 3000 MHz digital signal generator was used to provide input signal for frequencies beyond 50 MHz. The power of the input signal was further boosted with a ZHL-2-12 high dynamic range amplifier 10 MHz to 1.2 G Hz from Mini-circuits. The rectifier DC output was measured with a Tektronix DPO4104 digital phosphor oscilloscope. The filtering capacitor in the half-wave rectifier was a 47 nF discrete capacitor. The 1 MΩ internal load of the oscilloscope was used as the load resistor.

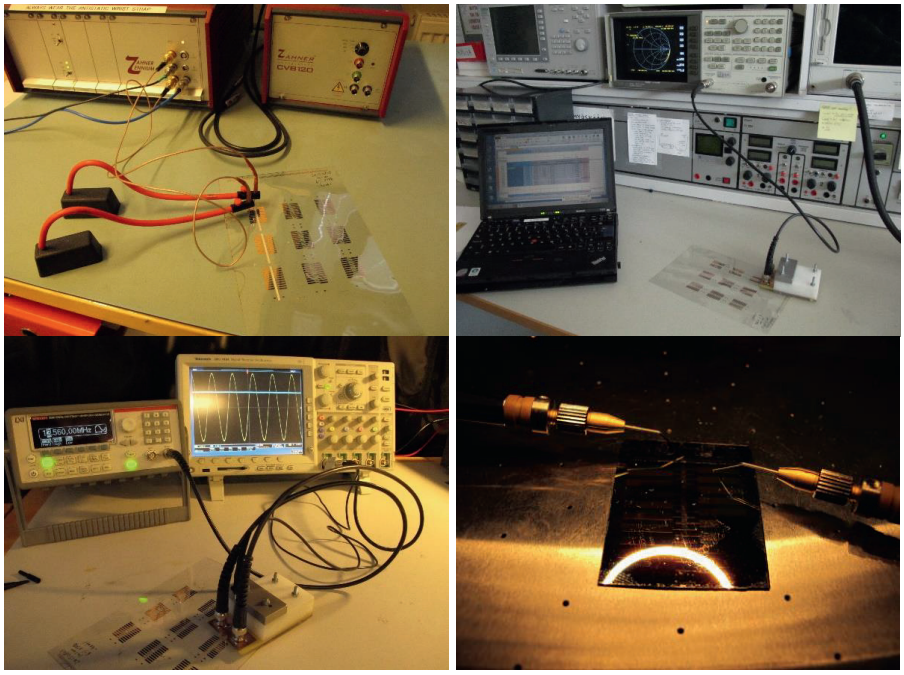

Figure 11. IV measurement set up (top left), small-signal impedance measurement setup (top right) frequency response measurement set up (bottom left) and a probe station for IV measurement set up (bottom right).

When integrated into a rectenna circuit, the performance of the harvester was measured. For the 13.56 MHz harvesters with loop antennas, an i-scan HF long range reader ID ISC.LR200 from OBID was as the AC power source. The input AC coupling voltage and DC rectified output voltage of the harvester was measured using a Tek P6139A 10X voltage probe from Tektronix.

In addition, the indium oxide diodes were studied by SEM and X-ray photoelectron spectroscopy (XPS). The method and results can be found in Publication V.

4 RESULTS AND DISCUSSION

This chapter is divided into three sections that outline the main results of the publications. The first section presents the diode interface and IV characteristics. The second section concentrates on the diode frequency performance, and the last section focuses on the performance of RF energy harvesters incorporating solution-processed diodes.

4.1 Diode interface and IV characteristics

As discussed in Chapter 2, for MIM diodes the MS interface consists of one injecting Ohmic contact and one rectifying contact, determined by the energy difference between the metal work function and the energy level of the semiconductor. The HOMO level of the PTAA semiconductor has been reported at 5.1 eV [97]. Therefore, the anode electrode needs to have a work function higher than 5.1 eV to form an Ohmic contact while the cathode electrode with a lower work function than 5.1 eV is needed. Thus, gravure printed Ag with a work function of 5.2 eV and evaporated Cu with a work function of 4.8 eV metal electrodes were chosen as the Ohmic injecting anode contact and rectifying cathode contact, respectively. Kaisa Lilja [23] has investigated the effect of the diode cathode interface on PTAA diode characteristics in detail. In addition, the formation of the Ohmic contact at the anode with a highly oxidized printed Ag layer with an increased work function is explained by Lilja *et al.* [46]. Heljo [24] has further studied the effect of silver oxide interfacial layer through anodization on the diode performance. Therefore, a detailed I-V analysis of PTAA diodes will not be given here. The as-fabricated Cu-PTAA-Ag diodes have a forward current density of 0.03 A/cm^2 at 5 V and a reverse leakage current density of 0.02 mA/cm^2 at -5 V. The resulting rectification ratio is about 1.5×10^3 as shown in Figure 12.

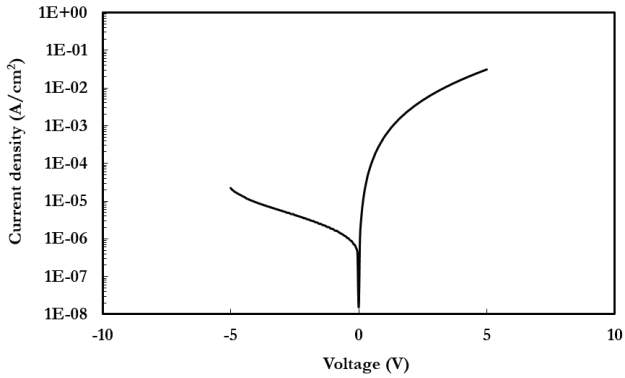

Figure 12. Printed Cu-PTAA-Ag diode current density – voltage (J (log)-V) characteristics.

Solution-processed indium oxide rectifying diodes, on the other hand, have not been thoroughly investigated. Therefore, preliminary tests have been conducted to determine the suitable Ohmic and non-Ohmic contacts for indium oxide in Publication V. The reported work function of indium oxide around 4.3-5 eV [98], [99] is used. Therefore, for n-type indium oxide semiconductor, two different metal electrodes with a lower work function and a higher work functions than the work function of indium oxide are required for the formation of the Ohmic contact and the rectifying contact, respectively. Candidate metal electrodes such as Ag (4.64 eV), Al (4.2 eV), Au (5.47 eV), Cu (5.1 eV) and Cr (4.5 eV) and Pd (5.6 eV) with work functions as given in [100], have been fabricated to observe the contact effects.

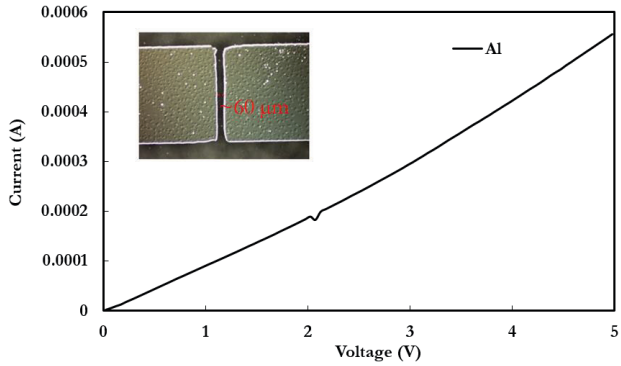

Figure 13. A microscope image of the device, the gap between two electrodes is 60 µm. Linear I-V plot of Al electrodes on top of indium oxide at forward biasing from 0 to 5 V.

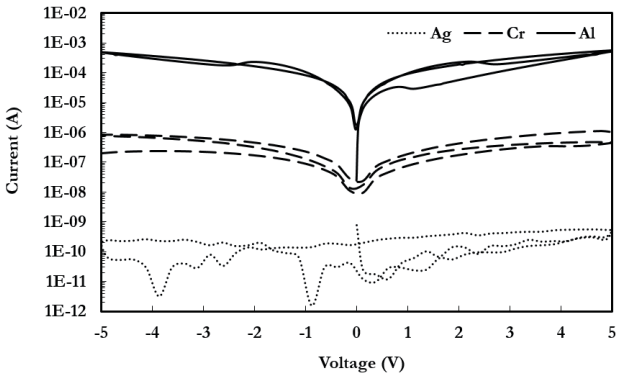

Figure 14. I (log)-V plot of indium oxide with various metal electrodes on top.

The test devices include a spin coated indium oxide layer and a top metal layer with a lateral gap structure fabricated on a glass substrate as shown in Figure 13. The I-V characteristics were measured to briefly determine each candidate's contact characteristic, Ohmic or non-Ohmic behavior.

Among the low work function metal electrodes including Ag, Cr, Al as shown in Figure 14, Al contacts exhibited linear I-V (Figure 13) characteristics with minimum hysteresis indicating the formation of reasonable Ohmic contacts. We attempted to measure contact resistance of indium oxide and Al using the transfer length (TLM) method, however, as the minimum gap on steel shadow mask was limited to 60 μm, the TLM results were not accurate. For Cr and Ag as well as Cu (current level not shown here), initial results showed significant lower current levels likely due to high contact resistance at the metal-semiconductor interface from the work function mismatch, therefore these metals were not considered further as Ohmic contacts. On the other hand, high work function metals Pd and Au both showed non-Ohmic contact behavior when fabricated into the metal-indium oxide diode structure. Pd with a slightly higher work function than Au was the primary cathode candidate, however, Pd showed a severe chemical reaction to the indium precursor. Thus, Au with better wetting properties for indium oxide has been chosen as the rectifying contact for the diodes. Therefore, the preliminary tests indicated that Al and Au were suitable anode and cathode, respectively, for the solution-processed indium oxide diodes in this work. This approach to find suitable metal electrodes seems straightforward in principle as the work functions can be measured individually beforehand. However, interfacial layers due to oxygen migration or electron accumulation will be created during and after the deposition and curing in ambient air of each layers, making the formation of contacts intricate and process variant [94],

[101], [102]. Combining the subtle change of properties of the indium oxide during solution process, the semiconductor energy level and the interfaces to two electrodes can be unexpected. This can be seen from the rectifying behavior with a symmetric Al-In_2O_3-Al structure fabricated on glass. The measured I-V characteristics of the diodes are shown in Figure 15. It is suspected that the evaporated bottom Al electrodes forms a thin aluminum oxide layer in ambient air conditions before the deposition of the indium oxide precursor atop. This native oxide interlayer changes the contact properties between the bottom Al and the indium oxide, which resultes in modest rectification, i.e., different current levels for forward/reverse voltages. The forward current of the diodes is smaller than the reverse current, which indicates that the bottom electrodes acted as the anode and the top electrodes acted as the cathode. This result differs from literature reports for molecular-beam epitaxy (MBE)-grown indium oxide layers [94], [102], where the formation of Schottky contacts is difficult at the surface due to electron accumulation. On the contrary, in solution-processed indium oxide diodes, the bottom contacts are advantageous for the formation of Ohmic contacts while the top contacts are better for non-Ohmic contacts. A similar behavior has been observed with Au electrodes, in other words, Au as non-Ohmic contacts are better fabricated on top of indium oxide. These findings demonstrate that metal/metal oxide contacts are complicated for solution-processed indium oxide.

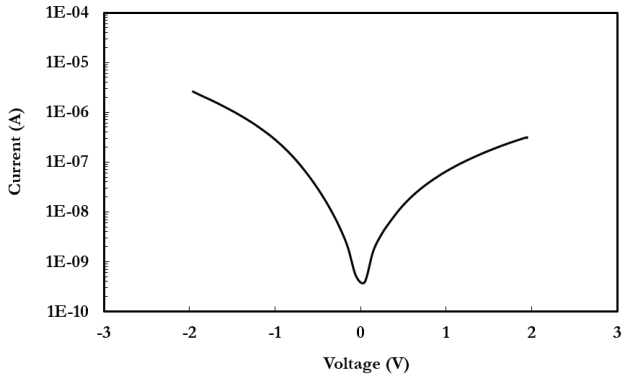

Figure 15. Al/In_2O_3/Al diode I (log)-V characteristics.

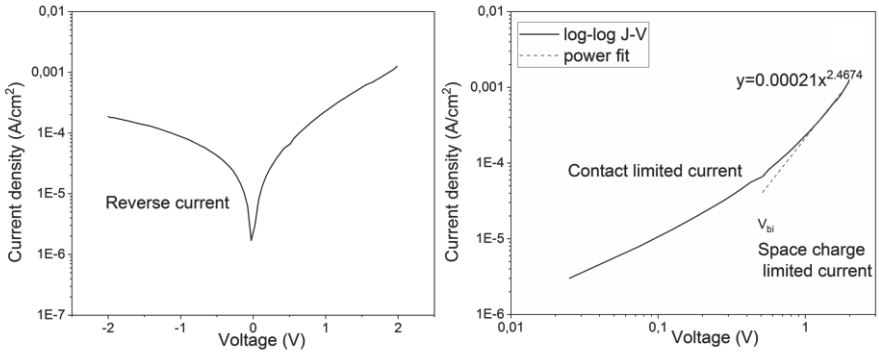

Figure 16. Al/In_2O_3/Au diode J (log)-V characteristics (left). Log-log plot of the diode J-V characteristics at forward biasing (right).

J-V characteristics of the Al/In_2O_3/Au diodes are shown in Figure 16. The diodes demonstrate robust rectifying behavior. As explained in Chapter 2, the current characteristics of MIM diodes can be divided into three regimes, namely reverse current region, diffusion and contact limited current region and SCLC region. V_{bi} can be determined based on the log-log plot of J-V characteristics of the diode when it enters the SCLC region, which was about 0.52 V. In reverse bias, the current level is normally low due to the junction barrier. The diffusion and contact limited current can be determined by assuming an ideal Ohmic contact at the anode and using a conventional thermionic emission model. However, the ideality factor in this model, which is based on recombination of charge carriers at junctions, is usually inapplicable to MIM diodes. In fact, the value of bulk resistance and the ideality factor of the indium oxide diode is calculated to be 1.76 MΩ and 8.93, respectively, when using Cheung's function [103]. The significantly high ideality factor witnessed here assures that the contacts do not fit well to a classic Schottky contact model. At voltages higher than the V_{bi} of the diode, the current is no longer diffusion and injection limited and follows SCLC, assuming that the semiconductor is trap-free. As shown in Equation (3), SCLC is proportional to the square of the applied voltage, i.e., ($I \alpha V^2$). However, due to the non-ideal interfaces and trap states within the indium oxide semiconductor the proportion becomes the form of $I \propto V^m$, where $m>2$ [104]. The value extracted here was around 2.47, as shown in Figure 16. XPS analysis of O1s spectra showed that a corresponding peak originated from oxygen defects in the indium oxide. The vacancy states of the oxygen have a huge effect on electrical performance of the device [105], [106], and therefore affect the J-V

characteristics of the diodes and contribute to imperfections, e.g., m>2 in SCLC regions.

4.2 Diode frequency performance

As discussed in Chapter 2, the high frequency performance of the diodes depends heavily on the diode properties, especially the diode thickness as shown in Equation (4). In 2009, Lilja *et al.* first reported gravure printed PTAA rectifying diode with a PTAA layer thickness of 500 nm operating up to 10 MHz [107]. Later, in 2013, Heljo *et al.* published printed PTAA diodes operating at 13.56 MHz with a half-wave rectifier output of 3.5 V to 10 V AC input. The PTAA layer thickness was reduced to 360 nm [30]. As a continuum, the printed PTAA diodes with a thinner layer thickness were fabricated to improve cutoff frequency was reported in Publication I and II. Through printing optimization, including ink formulation and printing settings, the diode layer thickness was successfully reduced to 300 nm with the same printing yield as thicker diodes.

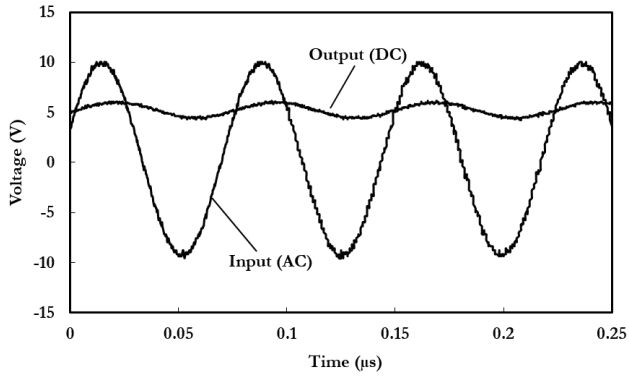

Figure 17. Rectified DC output at 13.56 MHz with an input AC of 10 V.

With the reduced 300 nm PTAA layers, the obtained DC output at 13.56 MHz was increased from 3.5 V to 5 V, as shown in Figure 17. In publication II, the diode with different thickness and diode area presented in Table 2 were fabricated to investigate their performance in a half-wave rectifier circuit. As shown in Figure 18, at 13.56 MHz, A-series diodes with an approximate thickness of 500 nm were able to yield 0.6-0.7 V DC output voltages, whereas B-series diodes with an average thickness of 300 nm could provide DC voltages above 4 V. These results correspond well with

the theory that the frequency performance of organic diodes is dominant by the semiconductor thickness. In addition, diodes with larger active area provide more current, thus resulting in higher output DC voltages especially in low frequency region. However, at high frequencies the geometric capacitance of the diode as shown in Table 2 will shunt the circuit and lower the output DC voltage. In the B-series diodes for example, at low frequencies the diodes with larger area, hence more generated current, yield higher DC output voltages; however, at frequencies exceeding 18 MHz the voltage loss due to the diode capacitance surpassed the voltage gain from higher current so that the diodes with smaller active area offered higher DC output voltages.

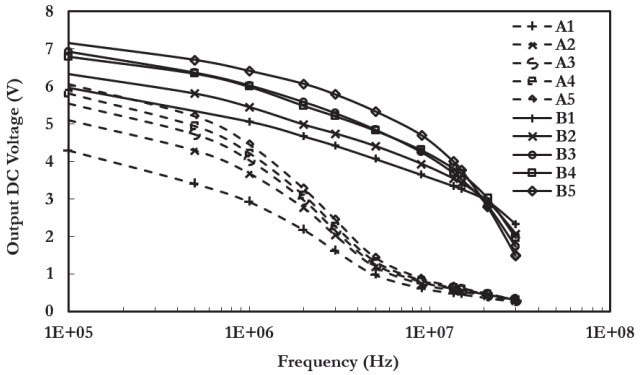

Figure 18. Measured DC output voltages of the diodes for 10 V AC input signal from a signal generator as a function of frequency.

Table 2. Properties of printed PTAA diodes

Diode	Properties				
	Area (cm^2)	C_{diode} (pF)		Area (cm^2)	C_{diode} (pF)
A series, average thickness 500 nm			B series, average thickness 300 nm		
A1	0.002	15.16	B1	0.002	23.83
A2	0.004	23.09	B2	0.004	38.85
A3	0.006	30.97	B3	0.006	52.69
A4	0.008	39.73	B4	0.008	66.00
A5	0.01	47.07	B5	0.01	91.07

Reducing the diode thickness has a huge effect on the forward and reverse leakage current of the diodes. The reported current density of 1200 nm PTAA diodes is around 0.3×10^{-3} A/cm^2 at 5 V and 0.3×10^{-8} A/cm^2 at -5 V [23], while the diodes

with a 300 nm PTAA layer have an improved forward current density of 0.3×10^{-1} A/cm^2 at 5 V and an enormous increase of reverse leakage current density of 0.2×10^{-4} A/cm^2 at -5 V, respectively. The resulting DC rectification ratio at 5 V makes a strong drop from 100000 to 1500 between thick and thin diodes. However, the actual frequency behavior of the diodes in a rectifier circuit shows the opposite results where thin diodes offer far better performance than thick diodes. In practice, a DC rectification ratio of 100 is sufficient for the diodes to convert the AC input voltages to high DC voltages in a rectifier [49]. Furthermore, it can be observed that the thinner diodes possess the smaller voltage drops over the diodes, hence higher V_{DC} over the entire frequency range. This leads to the interesting finding that the DC rectification ratio is not the dominant factor determining diode frequency performance. Indeed, as given in Equation (4), the TOF formula suggests that the built-in voltage V_T plays a more direct role than the absolute forward and reverse current levels of the diodes. Furthermore, as the semiconductor layer becomes thinner, the interfacial effects and traps play a more significant role, which makes the SCLC trap-free model less viable. Therefore, it is unwise to improve the parameters of rectifying diodes based solely on the DC I-V characteristics.

As discussed in Chapter 2, the PTAA diode can be modelled as an RC network. The impedance value obtained from a vector network analyzer is the diode small-signal impedance, which has a typical resistance value of few kΩ and a capacitance value of tens of pF. This capacitance value comes from the geometric capacitance of the diode and has been demonstrated to be independent of the voltage and the frequency [30], while the resistance is both voltage- and frequency- dependent. In publication IV, the model of the diode is further studied. Diodes with four different active areas from 0.004 to 0.01 cm^2 were analyzed. Firstly, the rectified DC output of a half-wave rectifier at 13.56 MHz with a single printed PTAA diode and a filtering capacitance of 47 nF was measured as a function of input AC voltage. As shown by the size of error bars in Figure 19 at 13.56 MHz, the rectifier voltage outputs are very similar, despite the variation of active area. With an input AC signal of 10 V_{PP} (peak to peak), the average DC output of all diodes was about 1.18 V. As the input root mean squares (rms) voltage of 10 V_{pp} was 3.54 V, the resulting voltage loss across the diode was found to be 2.36 V. When input voltages increased to 16 and 20 V_{pp}, the corresponding voltage losses were about 2.83 and 3.01 V, respectively. Therefore, in contrast to Si-based diodes, the voltage losses across PTAA diodes are not constant but increase with the input AC voltages. Since the capacitance of the diode remains the same, the increment voltage loss in diode is likely owing to the nonlinear voltage-dependent resistance of the diode. Next, to evaluate this

resistance, the output voltage of the diodes with AC input voltages of 20 Vpp at 13.56 MHz was measured, but without the presence of the 47 nF filtering capacitor, as shown in Figure 20. During the positive cycles, the outputs of the diodes were around 5.68 to 6.68 V for small and large area diodes. While in the negative cycles, the outputs were reduced to -0.54 and -3.376 V. The equivalent impedance of diodes for both positive and negative cycles can be calculated from the rms input and the rms voltage of diode output as shown in equation below

$$\frac{V_{rms.out}}{Z_{load}} = \frac{V_{rms.in} - V_{rms.out}}{Z_{diode}}. \tag{10}$$

Here, both the load and diode impedance were assumed to be purely resistive to simplify the calculation. The resistance of the organic diode is then determined to be in the range of hundreds of kΩ and few MΩ for positive and negative cycles, respectively, for an AC input of 20 V_{pp} at 13.56 MHz. These obtained values ignore the reactance; though not accurate, they indicate that the printed PTAA diode has a significantly large forward resistance and a relatively small reverse resistance compared to Si-based diodes. The resistance in the diode model changes with input amplitude as well as frequencies. Due to its non-linear behavior, the numerical analysis becomes complex.

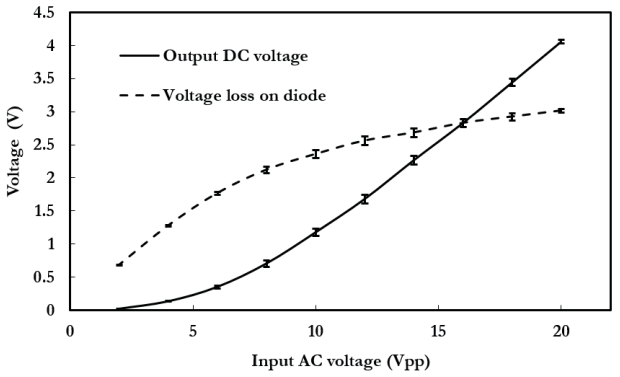

Figure 19. Diode rectified DC output voltage and diode voltage loss vs. input AC voltage at 13.56 MHz

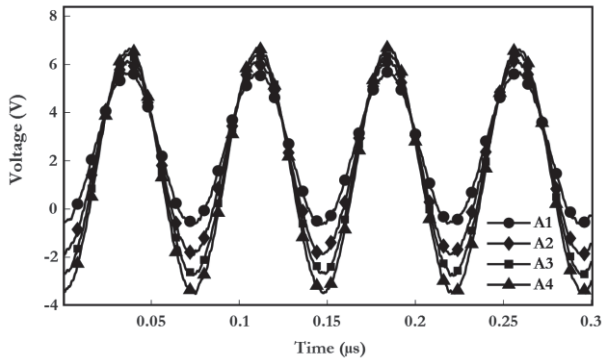

Figure 20. Diode output vs AC input of 20 Vpp at 13.56 MHz. No capacitor included.

The printed PTAA diodes enable low temperature roll-to-roll compatible printing process and offer very stable performance under ambient conditions. However, the low carrier mobility of the PTAA material, which is in the range of 10^{-3}-10^{-2} cm^2/Vs, puts a limitation on its high frequency operation. To reach the minimum frequency of 13.56 MHz, the low mobility can be simply compensated by using diodes with a thinner layer to increase the ratio of μ/L^2, as demonstrated. Such thin layers, in the order of hundreds of nm, have approached the limit of the achievable layer thickness of gravure printing with the gravure cell volume used in this thesis. It became challenging to fabricate uniformity pin-hole free ultra-thin layers on non-flat flexible substrates. Therefore, a new semiconductor material with a high carrier mobility is desired for UHF applications. Publication V presents the solution-processed indium oxide diode with a structure of Al-In_2O_3-Au. The XPS analysis of Al-In_2O_3 indicates that a pinhole-free, homogenous coverage of indium oxide layer on top of Al. The layer thickness of the indium oxide was around 200 nm determined by SEM image. As shown in Figure 21, the rectifier with the indium oxide diode exhibited similar rectified DC output at low frequencies to that of the PTAA rectifier. However, whereas the rectified DC output of the PTAA diode rectifier started to decrease rapidly with increased frequency, the output of the indium oxide diode rectifier remained constant and only dropped slightly beyond 35 MHz. This voltage drop, which is also present in the comparative commercial Si-based diode rectifiers, was caused by the parasitic reactance within the measurement set-up. Compared to commercial Si-based rectifiers, the indium oxide diode rectifiers had a bigger voltage loss due to high contact resistances and to trap states in the semiconductor, as witnessed from the J-V and XPS results.

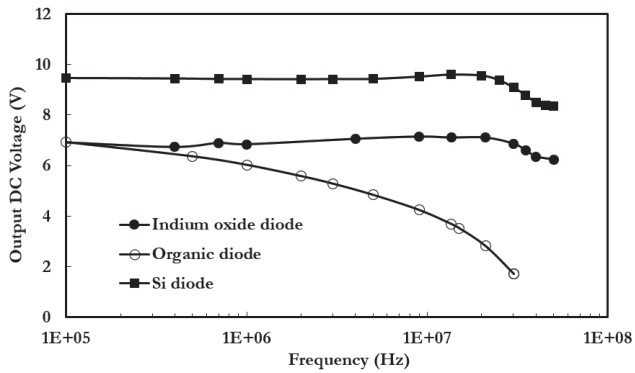

Figure 21. Frequency response of the Al/In_2O_3/Au rectifier with a comprising to PTAA diode and Si-diode rectifier up to 50 MHz.

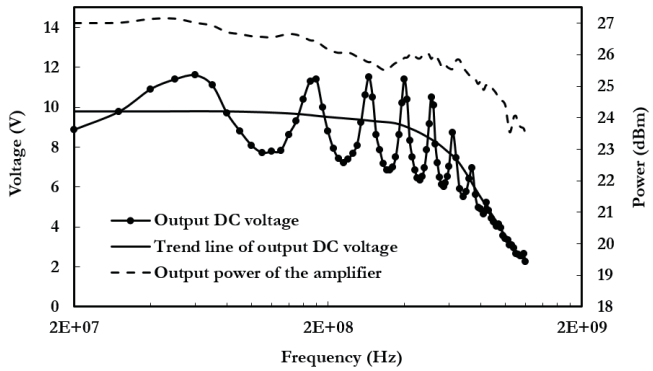

Figure 22. Frequency response of the Al/In_2O_3/Au rectifier up from 20 MHz to 1.2 GHz. The measured power of the power amplifier and its relative loss vs frequency.

To investigate the frequency performance beyond 50 MHz and to find the cutoff frequency of the indium diode rectifier, a 3 GHz RF signal generator together with a power amplifier were used to replace the standard signal generator as the power source. No additional impedance matching circuits were included. The waveform of the output DC voltage indicated that there were standing waves between the diode and the power amplifier causing by impedance mismatching. The solid line functioned as a trend line of the measured data to help interpret the data due to the standing waves. The filtering capacitor and load impedance was the same as that of previous 50MHz measurement. The actual output power of the amplifier started at 27 dBm at 10 MHz and slowly dropped to below 24 dBm at GHz range. As shown in Figure 22, the cutoff frequency of the indium oxide diodes was determined to be around 700 MHz, where the output DC voltage dropped from 10 to 7 V. This

estimated cutoff frequency is much lower than the exact frequency value of the rectifier, since the feeding power of the amplifier drops as frequency increased.

4.3 RF energy harvester

In publication I, a fully printed RF energy harvester circuit that uses one inkjet-printed antenna and capacitor, and a roll-to-roll compatibly printed PTAA diode with an operating frequency of 13.56 MHz was fabricated and measured. The harvester is of the size of a credit card 75×42 mm^2, defined by the antenna area as shown in Figure 23. The antenna had a length of 1445 mm and a total resistance of 240 Ω. The chosen antenna structure has eight turns, 1 mm line width and 0.3 mm gap between lines to enhance the coupling AC voltage at 13.56 MHz. The capacitor area was 1.3 cm^2. The diode was fabricated separately and integrated onto the antenna substrate using sliver flake ink.

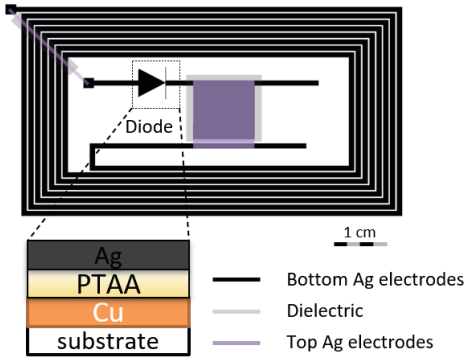

Figure 23. Schematic illustration of 13.56 MHZ RF harvester.

Due to the low 0.4 nF capacitance of the printed capacitor and the reverse leakage current of the printed diode, the DC output wave form had a slight ripple from impedance mismatches, as shown in Figure 17. However, the result clearly demonstrates that a DC output of 3-5 V of the fully printed harvester can be provided by either changing the transmitting power (2-3.5 W) and the distance (6.4 to 10.4 cm) from the source antenna.

Table 3. Properties of loop antennas

	Analytical Inductance (μH)	Measured Inductance (μH)	Tuning Capacitance (pF)
5 turns	2.70	2.96	46.5
6 turns	3.45	3.89	35.4
7 turns	4.31	4.97	26.7

To further evaluate the performance of the RF harvester, in Publication II the basic principles of the rectenna circuits were explored and the effect of PTAA diodes on the rectenna circuit was demonstrated. The loop antennas properties are given in Table 3. When evaluated separately, as discussed in Chapter 2, the thinner film diodes and the loop antennas with more loop turns were found to offer superior performance. However, when brought together into the rectenna circuit, the interaction between them affects the performance significantly. Due to the low resistance of the loop antennas fabricated on PCBs, they have a high Q factor of 300 to 400 and a narrow bandwidth. This makes these loop antennas highly sensitive to the tuning circuit. As shown in Figure 24, once the diodes were connected to the loop antennas, the total capacitance seen from the loop antenna was the sum of the tuning capacitor C_{res}, the diode geometric capacitance C_{diode} (Figure 1), and the filter capacitor C_{filter}. Since in conventional rectifiers C_{filter}, in the nF range, is decades larger than the diode capacitance in the pF range, the total capacitance becomes approximately the sum of C_{res} and C_{diode}. To resonate at 13.56 MHz, a tuning capacitor in the range of tens of pF is needed for a loop antenna with an inductance of a few μH. For Si-based high frequency diodes the total diode capacitance is typically around 1 pF at MHz range. Therefore, it has negligible effect on the total tuning capacitance and resonant frequency, i.e., when $C_{res} \gg C_{diode}$, $C_{res}+C_{diode} \approx C_{res}$. In the case of organic diodes with large geometric capacitances, as presented in Table 2, which are same as the required tunning capacitance values as presented in Table 3, they can effectively function as the tuning capacitor and thus cause dramatic changes in the resonant frequencies. To confirm this, the DC output of diodes with different geometric capacitance used as the tunning capacitance were plotted against the antenna tunning curve using real solid-state tunning capacitors C_{res} as dash curves in Figure 25. The measurement set up are shown in Figure 24. The variations in output DC voltages of diodes are a reflection of the coupling AC voltages of the antennas. It can be seen that the output DC voltages of different diodes on each antenna follow the shape of the open circuit coupling AC voltages (dash curves). Therefore, the geometric capacitance of the PTAA didoes can be used directly as the

tunning capacitor. The analysis of the interaction between the loop antennas and the organic diodes provided useful information on circuit design and development. Once the inductance of the loop antenna was determined, the required tuning capacitance can be realized by selecting the suitable organic diodes. Based on the findings, a double half-wave rectifying circuit was designed to be integrated with the 5-turns loop antennas. This configuration delivered approximately twice the DC output voltage of that half-wave rectifier. In addition, the ripples from each half-wave rectifier are in the opposite directions and cancel each other out. The desired tuning capacitance for the 5-turns loop antenna is 46.5 pF. This requires the combined capacitance of two diodes in the double half-wave rectifier to meet this value. Therefore, two diodes with capacitance of 23.83 pF were chosen. The measured output DC voltage of the harvester was 11 V to a 1 MΩ load. The reader antenna was placed 16.8 cm form the loop antenna with the transmitting power of 2 W. These results demonstrate the importance of circuit analysis in organic electronics.

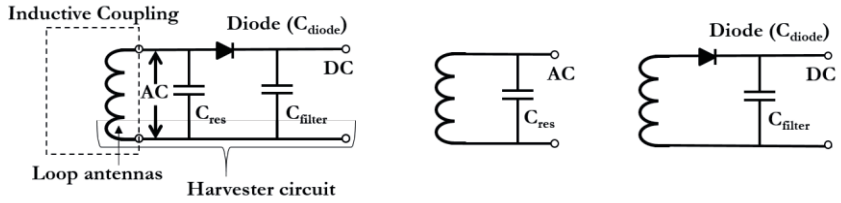

Figure 24. Schematic circuit diagram for the harvester operating at 13.56 Hz (left), for open circuit coupling AC voltage (middle) measurement, and for output DC voltage measurement (right).

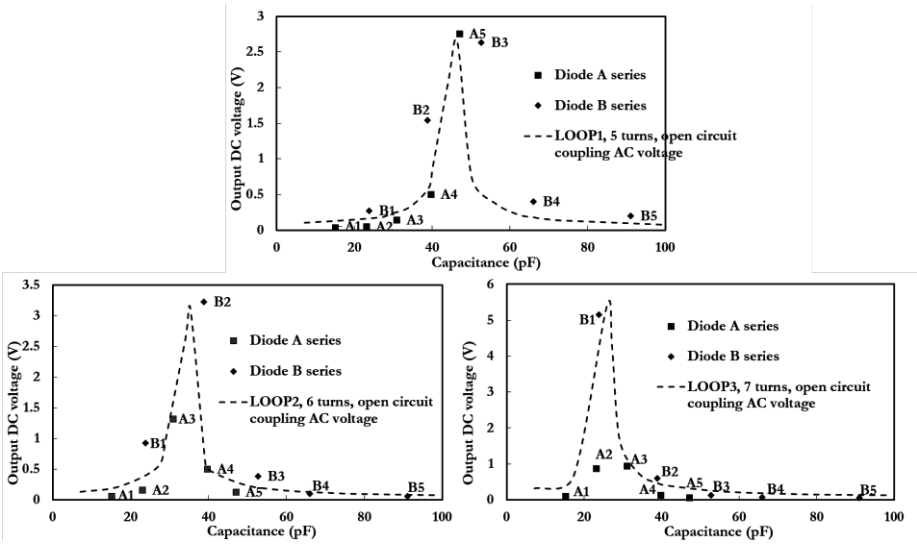

Figure 25. Measured results of the rectennas DC output of the 5-turns loop (top), the 6-turns loop (bottom left) and the 7-turns loop (bottom right) vs. the capacitance, i.e., C_{diode} for diode DC output and C_{res} for open circuit. The dashed curves with arbitrary amplitudes to represent the open-circuit characteristics of the loop antennas.

Next in Publication III, the printed RF energy harvester operating at 13.56 MHz, as reported in Publication I, was demonstrated in an autonomous energy harvesting and storage system. The printed harvester utilizing PTAA diodes was connected to printed supercapacitors and a voltage regulator ASIC [108]. This harvesting and storage system provides up to 10 hours of steady DC output when the RF input is absent. Integration of large-area, printed components and Si-based high-performance devices can be a smart route to meet high functionality demands with flexibility and relatively low cost; it can also be a steppingstone towards fully printed systems.

As the previously reported PTAA harvesters utilized credit card size inductive loops to gather RF energy, their operation range was in few tens of cm. This short-range operation puts a limitation on the applicability of these energy harvester. By increasing the operation range from centimeters to a few meters, it could enable advanced applications to power IoT sensors and devices. In Publication IV, a large screen-printed antenna which is capable of operating at a range of a few meters without significant performance drops was used to replace the small size loop antenna in the harvester. The printed PTAA diodes were effectively incorporated into the large area antenna to tune the resonant frequency and rectify the input AC signal simultaneously. To boost the DC output voltage, a double half-wave rectifier

was used. Due to the smaller ripples in the double half-wave rectifier, two filtering capacitors of 1.5 nF were used. This capacitance can be printed as previously demonstrated in Publication I. The 13.56 MHz harvesting antenna was placed 1, 2, 3 and 4 m from the transmit antenna in typical office environments as shown in Figure 26.

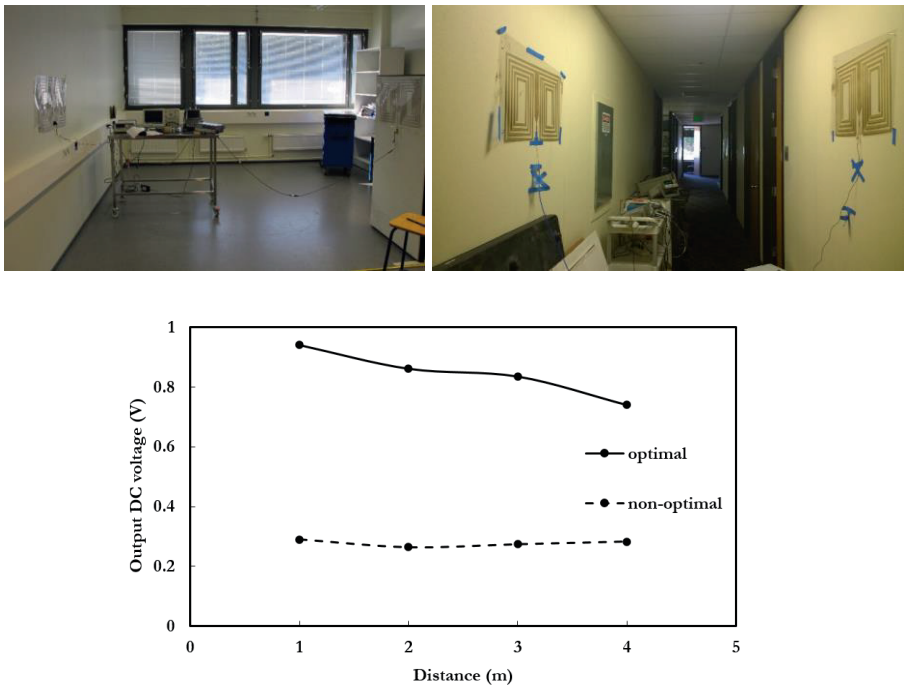

Figure 26. Measurement set up in office environments (top). Output DC voltage of 13.56 MHz printed harvesting systems (bottom). Input power of (1 W) from the signal generator is fed to the transmit antenna placed 1, 2, 3 and 4 meters away. Load resistance is 1 MΩ.

It can be seen from Figure 26 that over 800 mV DC output from the harvester was obtained using two diodes with proper capacitance of 28 pF from each diode. The output DC voltage declined slightly with distance in this case. On the other hand, the harvester with non-optimal diodes with capacitance of 45 pF from each diode yielded significantly lower output DC voltage below 300 mV. This result reconfirms that the unique capacitance properties of organic PTAA diodes have a huge effect on the performance of the harvester. More importantly, the result clearly shows that the operating range of this fully printable large area antenna harvesting system is in the range of a few meters with reasonable DC output voltages to enable low-power IoT sensors.

4.4 Research question discussion

The research problem of this dissertation was divided into two major research questions as described in Chapter 1. These research questions and the answers together with the article contributions are summarized here.

Research Question 1: Can the solution-processed organic and metal oxide diodes offer a decent electrical rectifying performance at 13.56 MHz or even higher frequencies?

To improve the frequency performance of the solution-processed diodes, the semiconductor layer properties including carrier mobility and layer thickness play a crucial role. Publication I and II discussed the thinner layer diode approach to enhance their frequency performance of printed PTAA diodes. In Publication V, the solution-processed spin-coated indium oxide diodes have reached above 0.7 GHz. The significant leap in operating frequency between the organic and metal-oxide diodes is owing to both the increased carrier mobility and reduced layer thickness of the indium oxide layer in the diodes. In addition, the indium diodes in Publication V appear to be the first one showing efficient rectification at close to UHF frequencies using solution-processed semiconductors and fabricating at ambient air conditions.

Research Question 2: Can the RF energy harvesters based on solution-processed diodes be used to provide voltage to load devices?

Publication I, III and IV demonstrated the capability of solution processed rectifying organic and metal oxide diodes utilized in RF harvesting systems at 13.56 MHz. In publication I, a fully printed RF energy harvester operating at 13.56 MHz comprising an inkjet-printed antenna with an inkjet-printed capacitor and a gravure-printed organic rectifying diode is presented. Depending on the transmitting power and distance of the source antenna, this printed energy harvester can provide up to 3-5 DC voltage. In publication III, we demonstrate an autonomous energy harvesting and storage system. The printed 13.56 MHz energy harvester with organic rectifying diodes is used to charge two supercapacitors connected in series up to approximately 1.8 V. The stored energy powers a voltage regulator ASIC with a regulated output of 1.2 V for up to 10 hours. Publication IV presents a fully printed RF energy harvester with a novel screen-printed large area antenna incorporated with a printed organic rectifying diode rectifier for long-range harvesting up to 4 meters at 13.56 MHz.

5 CONCLUSIONS AND OPEN ISSUES

Billions of devices for the IoT and other ubiquitous electronics have been integrated into every aspect of the modern world and play a significant role in people's life. There is a growing demand for an autonomous energy solution to address the myriad of charging elements. This need has brought out various energy harvesting solutions, including RF energy, into the center of attention in both academic and business fields. The emerging printed and, in a broad scope, solution-processed fabrication methods, with their low manufacturing temperature and no need for vacuum processes, offer an exciting path to large-area, high-volume, flexible, and ultra-low-cost electronics. Thus, a substantial amount of effort is put into investigating the capability of solution-processed and printed, low-cost RF energy harvester with unconventional semiconductor materials, such as organic polymers and metal oxides.

This dissertation, including the publication part, presents the development and analysis of solution-processed thin film organic and metal oxide diodes and their rectifier circuits for RF energy harvesting application. Rectifying diodes are extremely important active devices in an energy harvesting system. Solution-processed diodes based on a single active layer represent a very simple structure which is readily fabricated by printing or coating technologies. Especially in a vertical sandwich structure, the diode channel length, which is exactly the same as the thickness of the printed active layer between two electrodes, can be directly determined by the printing process. By adjusting the printed layer thickness and area, the properties of the diode vary dramatically, resulting in distinct performance changes.

Solution-processed organic and metal oxide diodes have dramatically different properties compared to their Si-based counterparts. The characterization of solution-processed diodes can be divided into two major categories: DC I(J)-V and AC frequency response. While a large amount of research was devoted to the improvement of the DC diode I-V performance, i.e. high forward current, low reverse current and high rectification ratio, through contact modifications and doping, there is no clear association between the DC current rectification and the diode frequency response. This can be clearly seen from the frequency data of the

indium oxide diodes, with much lower DC rectification than most reported diodes but an exceptional frequency response performance. It is found that the maximum operation frequency of the diode is governed by the carrier mobility and the thickness of the semiconductor. Despite the low carrier mobility in amorphous organic polymers, with a reduced layer thickness it is still feasible to achieve a prominent RF energy harvesting band at 13.56 MHz. The gravure printed organic diode in a half-wave rectifier, with a 10 V AC input and 1 MΩ output, achieved a DC output voltage of 5 V at 13.56 MHz, where the organic polymer thickness was around 300nm. This is a solid advancement for air-stable amorphous organic diodes.

Solution-processed rectifying diodes and their circuits have unique characteristics and their optimization can differ strongly from conventional inorganic equivalents. For efficient development of organic rectifying circuits, the diode was fit into an equivalent RC parallel model for device and circuit analysis. The capacitance of the diodes has a major impact on the resonant frequency and the coupling AC voltage of the loop antenna, and consequently the output DC voltage of the circuit. Specially, this unique high capacitance of solution-processed diodes enables effective frequency tuning and imaginary impedance matching to (two distinct) antennas simultaneously at 13.56 MHz. Based on the circuit analysis, an optimal rectenna circuit with a double half-wave rectifier was designed and measured. These results highlight the importance of circuit analysis which currently are often overlooked in organic electronics.

The thesis demonstrated a fully printed RF energy harvester with an inkjet printed small loop antenna and a half-wave organic diode rectifier operating at 13.56 MHz and its utilization in an autonomous energy harvesting and storage system. The RF energy was provided by a commercial 13.56 MHz RFID reader, the printed RF harvester charged a supercapacitor storage unit for about 20 minutes and this energy was able to run a low power ASIC regulator for over 10 hours. The result was promising; however, the harvester operating range was limited to cm range due to the usage of common small loop antennas. For this reason, an interesting long-range printable RF energy harvesting scheme was proposed. Two identical screen-printed large area antennas were used as a transmitter and a harvester. A double half-wave organic diode rectifier was incorporated onto the harvester. With an input power of 1W feeding to the transmit antenna, an approximately 800 mV DC output from the harvester was obtained 4 meters away from the source. The results demonstrate the possibility of fully printed organic diode RF energy harvester for long range operation at 13.56 MHz.

Due to the limitation put by the carrier mobility, it has become obvious that solution-processed amorphous polymers have difficulty to reach UHF RF band. Solution-processed metal oxides are another candidate material for high-speed diodes. With its inherently high carrier mobility, we successfully demonstrated a solution-processed indium oxide rectifying diode operating up to and above 0.7 GHz. Metal oxides require a higher processing temperature, for instance 300 ^{o}C in this work, compared to the organic material used in this work, which can be processed at a little over 100 ^{o}C. This limits the compatibility of solution-processed metal oxide diodes with most common flexible substates such as PET, but reaches a level compatible with polyimide. Although the present metal oxide diodes were fabricated on rigid substates, it is a steppingstone to the realization of fully printed, flexible devices.

Thanks to the rise of ubiquitous, wearable, and flexible electronics and IoT, the demand for new and diverse energy solutions is acute. The results in this thesis demonstrate the capability of solution-processed rectifying organic and metal oxide diodes utilized in RF energy harvesting systems. Owing to the low conductivity and carrier mobilities, the resulting low operation frequency, low current density and high voltage loss of solution-processed diodes place a significant limitation to replace of convention electronics. However, it is the author's belief that low-cost solution-processed devices with excellent air-stability and flexibility make them perfect to fit to the IoT devices and applications in near future.

Future research could focus on at least two major areas. First, to reach ultra-high frequency range it is important to discover and examine new air-stable solution-processed materials with better carrier mobilities and conductivities. The research should concentrate on the simplest diode structure including an anode, a semiconductor, and a cathode. An additional injection or interfacial layer may improve the DC properties of the diodes, but it can have unwanted effect at ultra-high frequencies, e.g., towards GHz range. Therefore, it is vital to secure the electrode materials for the anode and the cathode with optimal work functions. Note that solution-based processes can alter the work function of the metal electrodes and deposition processes can affect the key interfaces in the active region which in turn determine the diode performance. Second, for 13.56 MHz RF energy harvesters, a major challenge is to reduce the voltage loss on the diodes. This can be done by examining the possibility of doping and the injection layer to increase the conductivities.

BIBLIOGRAPHY

[1] R. Want, K. I. Farkas, and C. Narayanaswami, "Energy harvesting and conservation," *IEEE Pervasive Comput.*, vol. 4, no. 1, pp. 14–17, 2005, doi: 10.1109/MPRV.2005.12.

[2] I. John A. Stankovic, Life Fellow, "Research Directions for the Internet of Things," *Ieee Internet Things J.*, vol. 1, no. 1, pp. 3–9, 2014.

[3] H. Jayakumar, K. Lee, W. S. Lee, A. Raha, Y. Kim, and V. Raghunathan, "Powering the Internet of Things," *Proc. Int. Symp. Low Power Electron. Des.*, vol. 2015-Octob, pp. 375–380, 2015, doi: 10.1145/2627369.2631644.

[4] M. Koutake and Y. Katayama, "Reverse offset printing and specialized inks for organic TFTs," *2014 Int. Conf. Electron. Packag. ICEP 2014*, pp. 279–282, 2014, doi: 10.1109/ICEP.2014.6826701.

[5] G. Grau and V. Subramanian, "Fully High-Speed Gravure Printed, Low-Variability, High-Performance Organic Polymer Transistors with Sub-5 V Operation," *Adv. Electron. Mater.*, vol. 2, no. 4, pp. 1–8, 2016, doi: 10.1002/aelm.201500328.

[6] T. Cosnahan, A. A. R. Watt, and H. E. Assender, "Flexography Printing for Organic Thin Film Transistors," *Mater. Today Proc.*, vol. 5, no. 8, pp. 16051–16057, 2018, doi: 10.1016/j.matpr.2018.05.050.

[7] S. Chung, K. Cho, and T. Lee, "Recent Progress in Inkjet-Printed Thin-Film Transistors," *Adv. Sci.*, vol. 6, no. 6, 2019, doi: 10.1002/advs.201801445.

[8] Y. Y. Kim *et al.*, "Roll-to-roll gravure-printed flexible perovskite solar cells using eco-friendly antisolvent bathing with wide processing window," *Nat. Commun.*, vol. 11, no. 1, pp. 1–11, 2020, doi: 10.1038/s41467-020-18940-5.

[9] A. Kim, H. Lee, C. Ryu, S. M. Cho, and H. Chae, "Nanoscale thickness

and roughness control of gravure printed MEH-PPV layer by solvent printing for organic light emitting diode," *J. Nanosci. Nanotechnol.*, vol. 10, no. 5, pp. 3326–3330, 2010, doi: 10.1166/jnn.2010.2283.

[10] C. Feng *et al.*, "Highly efficient inkjet printed flexible organic light-emitting diodes with hybrid hole injection layer," *Org. Electron.*, vol. 85, no. May, p. 105822, 2020, doi: 10.1016/j.orgel.2020.105822.

[11] H. Park, H. Kang, Y. Lee, Y. Park, J. Noh, and G. Cho, "Fully roll-to-roll gravure printed rectenna on plastic foils for wireless power transmission at 13.56MHz," *Nanotechnology*, vol. 23, no. 34, 2012, doi: 10.1088/0957-4484/23/34/344006.

[12] R. Valmiro, H. Kitaguti, and S. E. Barbin, "A silk-screen printed RFID tag antenna," *2015 Asia-Pacific Microw. Conf. Proceedings, APMC*, vol. 3, pp. 9–11, 2015, doi: 10.1109/APMC.2015.7413586.

[13] C. Martínez-Domingo, S. Conti, L. Terés, H. L. Gomes, and E. Ramon, "Novel flexible inkjet-printed Metal-Insulator-Semiconductor organic diode employing silver electrodes," *Org. Electron.*, vol. 62, no. August, pp. 335–341, 2018, doi: 10.1016/j.orgel.2018.08.011.

[14] M. Pope and C. E. Swenberg, *Electronic processes in organic crystals and polymers / Martin Pope, Charles E. Swenberg.*, 2nd ed. New York: Oxford University Press, 1999.

[15] R. Farchioni and G. Grosso, *Organic Electronic Materials: Conjugted Polymers and Low Molecular Weight Electronic Solids*. Berlin: Springer, 2001.

[16] D. Gamota, P. Brazis, K. Kalyanasundaram, and J. Zhang, *Printed Organic and Molecular Electronics*. Springer US, 2004.

[17] W. Brütting, *Physics of Organic Semiconductor*. WILEY-VCH Verlag GmbH & Co. KGaA, Weinheim, 2005.

[18] K. D. Meisel *et al.*, "Charge-carrier mobilities in disordered semiconducting polymers: Effects of carrier density and electric field," *Phys. Status Solidi C Conf.*, vol. 3, no. 2, pp. 267–270, 2006, doi: 10.1002/pssc.200562718.

[19] H. Bässler and A. Köhler, "Charge transport in organic semiconductors,"

Top. Curr. Chem., vol. 312, pp. 1–65, 2012, doi: 10.1007/128_2011_218.

[20] D. B. Romero, M. Schaer, L. Zuppiroli, B. Cesar, and B. François, "Effects of doping in polymer light-emitting diodes," *Appl. Phys. Lett.*, vol. 67, p. 1659, 1995, doi: 10.1063/1.115048.

[21] B. Lüssem, M. Riede, and K. Leo, *Doping of organic semiconductors*, vol. 210, no. 1. 2013.

[22] D. T. Duong, C. Wang, E. Antono, M. F. Toney, and A. Salleo, "The chemical and structural origin of efficient p-type doping in P3HT," *Org. Electron.*, vol. 14, no. 5, pp. 1330–1336, 2013, doi: 10.1016/j.orgel.2013.02.028.

[23] K. Lilja, "Performance, Interfacial Properties and Applications of Printed Organic Diodes," Tampere University of Technology, 2011.

[24] P. Heljo, "Organic Diodes for High Frequency and Logic Applications," Tampere University of Technology, 2014.

[25] W. Schottky, "Halbleitertheorie der Sperrschicht," *Naturwissenschaften*, vol. 26, no. 52, p. 843, 1938, doi: 10.1007/BF01774216.

[26] W. Mönch, *Electronic properties of semiconductor interfaces*, vol. 7, no. 6. 2004.

[27] B. G. Streetman, *Solid State Electronic Devices*. Prentice Hall, 1995.

[28] S. M. Sze and K. K. Ng, *Physics and Properties of Semiconductors-A Review*. John Wiley & Sons, Ltd, 2006.

[29] C. H. Kim, O. Yaghmazadeh, D. Tondelier, Y. Bin Jeong, Y. Bonnassieux, and G. Horowitz, "Capacitive behavior of pentacene-based diodes: Quasistatic dielectric constant and dielectric strength," *J. Appl. Phys.*, vol. 109, no. 8, 2011, doi: 10.1063/1.3574661.

[30] P. Heljo, K. E. Lilja, H. S. Majumdar, and D. Lupo, "High rectifier output voltages with printed organic charge pump circuit," *Org. Electron.*, vol. 15, no. 1, pp. 306–310, 2014, doi: 10.1016/j.orgel.2013.11.024.

[31] A. J. Campbell, D. D. C. Bradley, and D. G. Lidzey, "Space-charge limited conduction with traps in poly(phenylene vinylene) light emitting diodes,"

J. Appl. Phys., vol. 82, no. 12, pp. 6326–6342, 1997, doi: 10.1063/1.366523.

[32] T. H. Richardson, *Functional Organic and Polymeric Materials*. 2000.

[33] D. Braga, M. Campione, A. Borghesi, and G. Horowitz, "Organic metal-semiconductor field-effect transistor (OMESFET) fabricated on a rubrene single crystal," *Adv. Mater.*, vol. 22, no. 3, pp. 424–428, 2010, doi: 10.1002/adma.200902124.

[34] H. Ishii, K. Sugiyama, E. Ito, and K. Seki, "Energy level alignment and interfacial electronic structures at organic/metal and organic/organic interfaces," *Adv. Mater.*, vol. 11, no. 8, pp. 605–625, 1999, doi: 10.1002/(SICI)1521-4095(199906)11:8<605::AID-ADMA605>3.0.CO;2-Q.

[35] Y. Shen, A. R. Hosseini, M. H. Wong, and G. G. Malliaras, "How to make ohmic contacts to organic semiconductors," *ChemPhysChem*, vol. 5, no. 1, pp. 16–25, 2004, doi: 10.1002/cphc.200300942.

[36] S. Braun, W. R. Salaneck, and M. Fahlman, "Energy-level alignment at organic/metal and organic/organic interfaces," *Adv. Mater.*, vol. 21, no. 14–15, pp. 1450–1472, 2009, doi: 10.1002/adma.200802893.

[37] S. Duhm, "5 - Interface energetics in organic electronic devices," in *Organic Flexible Electronics*, P. Cosseddu and M. Caironi, Eds. Woodhead Publishing, 2021, pp. 143–164.

[38] C. Hyun Kim, O. Yaghmazadeh, Y. Bonnassieux, and G. Horowitz, "Modeling the low-voltage regime of organic diodes: Origin of the ideality factor," *J. Appl. Phys.*, vol. 110, no. 9, 2011, doi: 10.1063/1.3660221.

[39] A. Haldi, A. Sharma, W. J. Potscavage, and B. Kippelen, "Equivalent circuit model for organic single-layer diodes," *J. Appl. Phys.*, vol. 104, no. 6, 2008, doi: 10.1063/1.2980324.

[40] P. S. Davids, I. H. Campbell, and D. L. Smith, "Device model for single carrier organic diodes," *J. Appl. Phys.*, vol. 82, no. 12, pp. 6319–6325, 1997, doi: 10.1063/1.366522.

[41] P. Kumar, S. C. Jain, V. Kumar, A. Misra, S. Chand, and M. N. Kamalasanan, "Current-voltage characteristics of an organic diode:

Revisited," *Synth. Met.*, vol. 157, no. 22–23, pp. 905–909, 2007, doi: 10.1016/j.synthmet.2007.08.021.

[42] P. De Bruyn, A. H. P. Van Rest, G. A. H. Wetzelaer, D. M. De Leeuw, and P. W. M. Blom, "Diffusion-limited current in organic metal-insulator-metal diodes," *Phys. Rev. Lett.*, vol. 111, no. 18, 2013, doi: 10.1103/PhysRevLett.111.186801.

[43] P. H. Nguyen, S. Scheinert, S. Berleb, W. Brüiting, and G. Paasch, "The influence of deep traps on transient current-voltage characteristics of organic light-emitting diodes," *Organic Electronics*, vol. 2, no. 3–4. pp. 105–120, 2001, doi: 10.1016/S1566-1199(01)00017-9.

[44] A. Rose, "Space-charge-limited currents in solids," *Phys. Rev.*, vol. 97, no. 6, pp. 1538–1544, 1955, doi: 10.1103/PhysRev.97.1538.

[45] A. Takshi and J. D. Madden, "Large apparent inductance in organic Schottky diodes at low frequency," *J. Appl. Phys.*, vol. 99, no. 8, pp. 3–8, 2006, doi: 10.1063/1.2189208.

[46] K. E. Lilja *et al.*, "Effect of dielectric barrier on rectification, injection and transport properties of printed organic diodes," *J. Phys. D. Appl. Phys.*, vol. 44, no. 29, 2011, doi: 10.1088/0022-3727/44/29/295301.

[47] S. Steudel *et al.*, "50 MHz rectifier based on an organic diode," *Nat. Mater.*, vol. 4, no. 8, pp. 597–600, 2005, doi: 10.1038/nmat1434.

[48] S. Scheinert and G. Paasch, "Fabrication and analysis of polymer field-effect transistors," *Phys. Status Solidi Appl. Res.*, vol. 201, no. 6, pp. 1263–1301, 2004, doi: 10.1002/pssa.200404335.

[49] S. Altazin *et al.*, "Physics of the frequency response of rectifying organic Schottky diodes," *J. Appl. Phys.*, vol. 115, no. 6, 2014, doi: 10.1063/1.4865739.

[50] J. E. Medvedeva, D. B. Buchholz, and R. P. H. Chang, "Recent Advances in Understanding the Structure and Properties of Amorphous Oxide Semiconductors," *Adv. Electron. Mater.*, vol. 3, no. 9, 2017, doi: 10.1002/aelm.201700082.

[51] M. G. Kim, M. G. Kanatzidis, A. Facchetti, and T. J. Marks, "Low-

temperature fabrication of high-performance metal oxide thin-film electronics via combustion processing," *Nat. Mater.*, vol. 10, no. 5, pp. 382–388, 2011, doi: 10.1038/nmat3011.

[52] E. Fortunato, P. Barquinha, and R. Martins, "Oxide semiconductor thin-film transistors: A review of recent advances," *Adv. Mater.*, vol. 24, no. 22, pp. 2945–2986, 2012, doi: 10.1002/adma.201103228.

[53] J. S. Park, W. J. Maeng, H. S. Kim, and J. S. Park, "Review of recent developments in amorphous oxide semiconductor thin-film transistor devices," *Thin Solid Films*, vol. 520, no. 6, pp. 1679–1693, 2012, doi: 10.1016/j.tsf.2011.07.018.

[54] N. Tiwari, A. Nirmal, M. R. Kulkarni, R. A. John, and N. Mathews, "Enabling high performance n-type metal oxide semiconductors at low temperatures for thin film transistors," *Inorg. Chem. Front.*, vol. 7, no. 9, pp. 1822–1844, 2020, doi: 10.1039/d0qi00038h.

[55] Q. Xin, L. Yan, Y. Luo, and A. Song, "Study of breakdown voltage of indium-gallium-zinc-oxide-based Schottky diode," *Appl. Phys. Lett.*, vol. 106, no. 11, 2015, doi: 10.1063/1.4916030.

[56] A. Chasin *et al.*, "UHF IGZO Schottky diode," *Tech. Dig. - Int. Electron Devices Meet. IEDM*, pp. 287–290, 2012, doi: 10.1109/IEDM.2012.6479030.

[57] J. Zhang, Y. Li, B. Zhang, H. Wang, Q. Xin, and A. Song, "Flexible indium-gallium-zinc-oxide Schottky diode operating beyond 2.45 GHz," *Nature Communications*, vol. 6. 2015, doi: 10.1038/ncomms8561.

[58] R. K. Gupta and F. Yakuphanoglu, "Analysis of device parameters of Al/In2O3/p-Si Schottky diode," *Microelectron. Eng.*, vol. 105, pp. 13–17, 2013, doi: 10.1016/j.mee.2012.12.026.

[59] J. Semple *et al.*, "Radio Frequency Coplanar ZnO Schottky Nanodiodes Processed from Solution on Plastic Substrates," *Small*, vol. 12, no. 15, pp. 1993–2000, 2016, doi: 10.1002/smll.201503110.

[60] A. Kyndiah *et al.*, "A Multifunctional Interlayer for Solution Processed High Performance Indium Oxide Transistors," *Sci. Rep.*, vol. 8, no. 1, pp. 1–7, 2018, doi: 10.1038/s41598-018-29220-0.

[61] H. He, "2 - Metal oxide semiconductors and conductors," in *Solution Processed Metal Oxide Thin Films for Electronic Applications*, Z. Cui and G. Korotcenkov, Eds. Elsevier, 2020, pp. 7–30.

[62] Z. Cui and L. Liao, "6 - Coating and printing processes," in *Solution Processed Metal Oxide Thin Films for Electronic Applications*, Z. Cui and G. Korotcenkov, Eds. Elsevier, 2020, pp. 83–97.

[63] OE-A, "OE-A Roadmap for Organic and Printed Electronics: White paper," 2017.

[64] C. Amruth *et al.*, "Slot-die coating of double polymer layers for the fabrication of organic light emitting diodes," *Micromachines*, vol. 10, no. 1, 2019, doi: 10.3390/mi10010053.

[65] G. Grau, R. Kitsomboonloha, and V. Subramanian, "Fabrication of a high-resolution roll for gravure printing of 2μm features," *Org. Field-Effect Transistors XIV; Org. Sensors Bioelectron. VIII*, vol. 9568, p. 95680M, 2015, doi: 10.1117/12.2187280.

[66] "https://www.wirelesspowerconsortium.com/." .

[67] H. Kang *et al.*, "Fully Roll-to-Roll Gravure Printable Tags for Smart Packaging," *Sci. Rep.*, vol. 4, no. 5387, pp. 2–8, 2014, doi: 10.1038/srep05387.

[68] Y. Jung, H. Park, J. Park, J. Noh, Y. Choi, and M. Jung, "Fully printed flexible and disposable wireless cyclic voltammetry tag," *Sci. Rep.*, vol. 5, no. 8105, pp. 1–6, 2015, doi: 10.1038/srep08105.

[69] K. Myny, S. Steudel, P. Vicca, J. Genoe, and P. Heremans, "An integrated double half-wave organic Schottky diode rectifier on foil operating at 13.56 MHz," *Appl. Phys. Lett.*, vol. 93, no. 093305, 2008, doi: https://doi.org/10.1063/1.2978348.

[70] R. Vyas and V. Lakafosis, "A Battery-less , Wireless Mote for Scavenging Wireless Power at UHF (470-570 MHz) Frequencies," in *2011 IEEE International Symposium on Antennas and Propagation (APSURSI)*, 2011, pp. 1069–1072, doi: doi: 10.1109/APS.2011.5996465.

[71] J. Kimionis, A. Georgiadist, M. Isakov, H. J. Qi, and M. M. Tentzeris,

"3D/Inkjet-printed Origami Antennas for Multi-direction RF Harvesting," in *2015 IEEE MTT-S International Microwave Symposium*, 2015, pp. 1–4, doi: 10.1109/MWSYM.2015.7166878.

[72] S. Kim, R. Vyas, A. Georgiadis, A. Collado, and M. M. Tentzeris, "Inkjet-printed RF Energy Harvesting and Wireless Power Trasmission Devices on Paper Substrate," in *2013 European Microwave Conference*, 2013, pp. 983–986.

[73] "https://www.youtube.com/watch?v=y7I98_3ZK6Y." .

[74] C. A. Balanis, *Antenna Theory: Analysis and Design*, 3rd editio. Newyork, Wiley, 2005.

[75] V. Coskun, K. Ok, and B. Ozdenizci, *Near Field Communication (NFC): From Theory to Practice*. Wiley Telecom, 2012.

[76] S. S. Basat, K. Lim, J. Laskar, and M. M. Tentzeris, "Design and modeling of embedded 13.56 MHz RFID antennas," *IEEE Antennas Propag. Soc. AP-S Int. Symp.*, vol. 4 B, pp. 64–67, 2005, doi: 10.1109/APS.2005.1552740.

[77] J. Nummela, L. Ukkonen, L. Sydänheimo, and M. Kivikoski, "13,56 MHz RFID antenna for cell phone integrated reader," *IEEE Antennas Propag. Soc. AP-S Int. Symp.*, pp. 1088–1091, 2007, doi: 10.1109/APS.2007.4395687.

[78] B. Grob, *Basic Electronics*, First Metr. McGraw-Hill, 1987.

[79] J. E. Müller, U. Ablassmeier, J. Schelle, W. Kellner, and H. Kniepkamp, "Design of planar rectangular microelectronic inductors," *Integr. Circuits Wirel. Commun.*, vol. II, pp. 581–584, 1998, doi: 10.1109/9780470544952.ch8.

[80] C. Y. Lin, C. H. Chou, T. S. Hu, and J. Hou, "Flexible wireless power-transmission system fabricated by 13.56 MHz polymer rectifier," 2008, doi: 10.1109/FEDC.2008.4483870.

[81] S. Steudel, K. Myny, P. Vicca, D. Cheyns, J. Genoe, and P. Heremans, "Ultra-high frequency rectification using organic diodes," *Tech. Dig. - Int. Electron Devices Meet. IEDM*, pp. 2–5, 2008, doi:

10.1109/IEDM.2008.4796622.

[82] D. Im, H. Moon, M. Shin, J. Kim, and S. Yoo, "Towards gigahertz operation: Ultrafast low turn-on organic diodes and rectifiers based on C60 and tungsten oxide," *Adv. Mater.*, vol. 23, no. 5, pp. 644–648, 2011, doi: 10.1002/adma.201002246.

[83] C. Y. Lin *et al.*, "High-frequency polymer diode rectifiers for flexible wireless power-transmission sheets," *Org. Electron.*, vol. 12, no. 11, pp. 1777–1782, 2011, doi: 10.1016/j.orgel.2011.07.006.

[84] S. G. Higgins, T. Agostinelli, S. Markham, R. Whiteman, and H. Sirringhaus, "Organic Diode Rectifiers Based on a High-Performance Conjugated Polymer for a Near-Field Energy-Harvesting Circuit.," *Adv. Mater.*, vol. 29, no. 46, Dec. 2017, doi: 10.1002/adma.201703782.

[85] P. S. Heljo, M. Li, K. E. Lilja, H. S. Majumdar, and D. Lupo, "Printed half-wave and full-wave rectifier circuits based on organic diodes," *IEEE Trans. Electron Devices*, vol. 60, no. 2, pp. 870–874, 2013, doi: 10.1109/TED.2012.2233741.

[86] P. Heljo, K. Lilja, S. Tuukkanen, and D. Lupo, "Charge Pump Circuit Using Printed Organic Diodes and Capacitors," in *LOPE-C; Large-area, Organic & Printed Electronics Convention*, 2011, pp. 53–55.

[87] S. Mutlu, I. Haydaroglu, and A. O. Sevim, "Realization of polymer charge pump circuits using polymer semiconductors," *Org. Electron.*, vol. 12, no. 2, pp. 312–321, 2011, doi: 10.1016/j.orgel.2010.11.006.

[88] M. Jung *et al.*, "All-Printed and roll-to-roll-printable 13.56-MHz-operated 1-bit RF tag on plastic foils," *IEEE Trans. Electron Devices*, vol. 57, no. 3, pp. 571–580, 2010, doi: 10.1109/TED.2009.2039541.

[89] "https://www.sigmaaldrich.com/catalog/product/aldrich/702471?lang=fi&region=FI." .

[90] W. Zhang *et al.*, "Systematic improvement in charge carrier mobility of air stable triarylamine copolymers," *J. Am. Chem. Soc.*, vol. 131, no. 31, pp. 10814–10815, 2009, doi: 10.1021/ja9034818.

[91] D. K. Hwang *et al.*, "Systematic reliability study of top-gate p- and n-channel organic field-effect transistors," *ACS Appl. Mater. Interfaces*, vol. 6, no. 5, pp. 3378–3386, 2014, doi: 10.1021/am405424k.

[92] D. Bharti and S. P. Tiwari, "Phase separation induced high mobility and electrical stability in organic field-effect transistors," *Synth. Met.*, vol. 221, pp. 186–191, 2016, doi: 10.1016/j.synthmet.2016.09.002.

[93] L. Xiao *et al.*, "Highly efficient electron-transporting/injecting and thermally stable naphthyridines for organic electrophosphorescent devices," *Adv. Funct. Mater.*, vol. 23, no. 10, pp. 1323–1330, 2013, doi: 10.1002/adfm.201202194.

[94] O. Bierwagen, "Indium oxide-a transparent, wide-band gap semiconductor for (opto)electronic applications," *Semicond. Sci. Technol.*, vol. 30, no. 2, p. 24001, Jan. 2015, doi: 10.1088/0268-1242/30/2/024001.

[95] S. R. Bhalerao *et al.*, "0.6V threshold voltage thin film transistors with solution processable indium oxide (In2O3) Channel and Anodized High-κ Al2O3 Dielectric," *IEEE Electron Device Lett.*, vol. 40, no. 7, pp. 1112–1115, 2019, doi: 10.1109/LED.2019.2918492.

[96] J. Leppäniemi, O. H. Huttunen, H. Majumdar, and A. Alastalo, "Flexography-Printed In2O3 Semiconductor Layers for High-Mobility Thin-Film Transistors on Flexible Plastic Substrate," *Adv. Mater.*, vol. 27, no. 44, pp. 7168–7175, 2015, doi: 10.1002/adma.201502569.

[97] B. S. Schols, S. Verlaak, C. Rolin, D. Cheyns, J. Genoe, and P. Heremans, "An Organic Light-Emitting Diode with Field-Effect Electron Transport," *Adv. Fuctional Mater.*, vol. 18, no. 1, pp. 136–144, 2008, doi: 10.1002/adfm.200700769.

[98] C. Miao, C. Chen, Q. Dai, L. Xu, and H. Song, "Dysprosium , Holmium and Erbium ions doped Indium Oxide nanotubes as photoanodes for dye sensitized solar cells and improved device performance," *J. Colloid Interface Sci.*, vol. 440, no. 3, pp. 162–167, 2015, doi: 10.1016/j.jcis.2014.10.055.

[99] A. Klein and K. Christoph, "Transparent Conducting Oxides for Photovoltaics: Manipulation of Fermi Level, Work Function and Energy Band Alignment," *Materials (Basel).*, vol. 3, pp. 4892–4914, 2010, doi: 10.3390/ma3114892.

[100] J. Hölzl, F. K. Schulte, and H. Wagner, Eds., *Solid Surface Physics*, vol. 85. Berlin, Heidelberg: Springer Berlin Heidelberg, 1979.

[101] M. Bachhav *et al.*, "Interpreting the Presence of an Additional Oxide Layer in Analysis of Metal Oxides-Metal Interfaces in Atom Probe Tomography," *J. Phys. Chem. C*, vol. 123, no. 2, pp. 1313–1319, 2019, doi: 10.1021/acs.jpcc.8b10895.

[102] O. Bierwagen and J. S. Speck, "High electron mobility In2O3(001) and (111) thin films with nondegenerate electron concentration," *Appl. Phys. Lett.*, vol. 97, no. 7, pp. 1–4, 2010, doi: 10.1063/1.3480416.

[103] S. K. Cheung and N. W. Cheung, "Extraction of Schottky diode parameters from forward current-voltage characteristics," *Appl. Phys. Lett.*, vol. 49, no. 2, pp. 85–87, 1986, doi: 10.1063/1.97359.

[104] M. A. Lampert, "Simplified theory of space-charge-limited currents in an insulator with traps," *Phys. Rev.*, vol. 103, no. 6, pp. 1648–1656, 1956, doi: 10.1103/PhysRev.103.1648.

[105] J. Gan *et al.*, "Oxygen vacancies promoting photoelectrochemical performance of in 2 O 3 nanocubes," *Sci. Rep.*, vol. 3, pp. 1–7, 2013, doi: 10.1038/srep01021.

[106] T. B. Daunis *et al.*, "Solution-processed oxide thin film transistors on shape memory polymer enabled by photochemical self-patterning," *J. Mater. Res.*, vol. 33, no. 17, pp. 2454–2462, 2018, doi: 10.1557/jmr.2018.296.

[107] K. E. Lilja, T. G. Bäcklund, D. Lupo, T. Hassinen, and T. Joutsenoja, "Gravure printed organic rectifying diodes operating at high frequencies," *Org. Electron.*, vol. 10, no. 5, pp. 1011–1014, 2009, doi: 10.1016/j.orgel.2009.04.008.

[108] A. Kalanti, M. Yücetas, J. Salomaa, L. Aaltonen, and K. Halonen, "Charge-pump based frequency regulator for precision supply generation," *ISCAS 2010 - 2010 IEEE Int. Symp. Circuits Syst. Nano-Bio Circuit Fabr. Syst.*, vol. 2, no. 2, pp. 4077–4080, 2010, doi: 10.1109/ISCAS.2010.5537622.

PUBLICATION I

Organic Diodes for RF Energy Harvesting

M. Li, P. S. Heljo, D. Lupo

Large-area, Organic and Printed Electronics Convention LOPE-C 2012 Proceedings
ISBN 978-3-00-038122-5.

PUBLICATION II

Organic Rectifying Diode and Circuit for Wireless Power Harvesting at 13.56 MHz

M. Li, P. S. Heljo, D. Lupo

IEEE Transactions on Electron Devices, 61(2014)6, pp. 2164-2169
doi: 10.1109/TED.2014.2318523

Organic Rectifying Diode and Circuit for Wireless Power Harvesting at 13.56 MHz

Miao Li, Petri S. Heljo, Donald Lupo

***Abstract*—Organic rectifying diodes and their circuits have unique characteristics and their optimization can differ strongly from conventional inorganic equivalents. In this paper, we investigate the effect of organic diodes on the performance of a rectenna circuit consisting of a loop antenna and a rectifying circuit with an operating frequency of 13.56 MHz. The geometric capacitance of the diodes has a major impact on the resonant frequency and the coupling ac voltage of the loop antenna, and consequently the output dc voltage of the circuit. Therefore, appropriate design considerations that take the special properties of organic devices into account should apply to organic diodes and circuits.**

***Index Terms*—Organic semiconductor, rectifying diodes, half-wave rectifier, double half-wave rectifier**

I. Introduction

ORGANIC rectifying devices and circuits continue to gain ground with their applications in radio frequency identification (RFID) tags as well as various wireless power systems [1]-[4]. Organic rectifying devices can be printable, flexible and stable in ambient environment [4]-[8]. These are the main advantages that have pointed to the possibility to fabricate low-cost circuitry consisting of numerous organic components. For recently reported printable organic rectifying diodes, their primary operating frequencies have reached MHz range [4], [8]. However, for the devices to be useful, they need to be integrated into circuits.

Organic rectifying circuit design has generally been adopted directly from established solid-state inorganic rectifier topologies. For many years, the half-wave (HW) rectifier, which utilizes an organic rectifying diode and a filtering capacitor, has been used extensively for its simplicity [2], [4], [5] and [9]. Because of low conductivity and low charge carrier mobility in organic semiconductors the voltage loss in organic rectifying diodes is high and the resulting output voltage of organic HW rectifiers is limited. With the need to obtain higher output voltage for use in applications like RFID and power transmission, more sophisticated organic rectifying circuits have been fabricated in recent years. For example, an integrated double half-wave rectifier based on Al-Pentacene-Au diodes has been demonstrated at 13.56 MHz as a part of an RFID tag, with the dc output voltage of about double of a HW rectifier [3]. In addition, several printable organic charge pump circuits for boosting dc output voltage at 13.56MHz have been published [7], [8] and [10]. However, the effect of the unique characteristics of the organic devices on wireless circuit operation has not been studied consistently.

Regardless of the type of rectifying circuit being used, the characteristics of organic rectifying diodes have an effect on the circuit functionality and performance. Therefore, device and circuit analysis is essential for efficient development of organic rectifying circuits, which currently are often overlooked in organic electronics. Previously, we reported that because of the high voltage drop on organic diodes the organic full-wave rectifier provided significantly lower output power and lower output voltage compared to the HW rectifier [6]. Here, we demonstrate the effect of organic diodes on the performance of rectenna circuits in wireless powering applications, with an operating frequency at 13.56MHz. The basic principles of rectenna circuits which are comprised of loop antennas and rectifiers based on organic diodes are explored. The properties of the circuits, such as resonant frequency and coupling voltage, are measured and evaluated in relation to the characteristics of organic diodes including their capacitance. The analysis of the results yields valuable design guidelines for utilizing organic diodes in RF harvesting rectifying circuits, and shows that basing circuit design on the results from a signal generator is not an adequate approach. Based on the findings, a rectenna circuit with a double half-wave rectifier is designed.

II. Methods and Experimental Details

The basic rectenna circuit that operates at 13.56 MHz is composed of a loop antenna and a rectifying circuit. The loop antenna gathers the RF energy through inductive-coupling, and the rectifying circuit converts the coupled ac signals to dc voltages (Fig. 1(a)). To obtain maximum performance (reading range, coupling voltage amplitude, etc) the rectenna circuit must be tuned to the 13.56 MHz operating frequency. The tuning of the rectenna, however, becomes more complicated when organic diodes are involved.

In order to perform consistent characterizations, two sets of organic diodes with different semiconductor layer thickness were fabricated. Both series consisted of five diodes with different active area defined by the cross sectional area of Cu and Ag electrodes (Table 1). The organic diodes were fabricated on a PET substrate (Melinex ST560 from Dupont Teijin Film), where the 50nm Cu cathode was evaporated and patterned. The semiconductor (poly(triarylamine)) PTAA and the top Ag anode were successively gravure printed. The process is described in more details in [4]. Here, PTAA is

Manuscript received January 27, 2014. This work was supported by Academy of Finland.

The authors are with the Department of Electronics, Tampere University of Technology, Tampere, Finland (phone: +358-50-3008273; e-mail: miao.li@tut.fi).

chosen for its excellent stability in ambient air [11]. All characterization and measurements were conducted at ambient conditions with no encapsulation.

Three loop antennas with different numbers of turns but otherwise identical parameters were prepared on credit card size printed circuit boards (PCB). In this work, the conventional PCB was chosen over printing methods for practical considerations, especially given the amount of organic diodes and antennas to be measured and analyzed. The printed organic diodes and the loop antennas were connected using customized probes. The 1.5nF filtering capacitor of the rectifier circuit was mounted on the probe.

The AC power was provided by a 13.56 MHz commercial reader antenna (i-scan HF long range reader ID ISC.LR200 from OBID). All voltages were measured by the oscilloscope (Tektronix DPO4104) through a 10X voltage probe (Tek P6139A from Tektronix).

A. *Organic Diode Model and Characterization*

Dc current-voltage (J-V) measurement and ac impedance spectroscopy (IS) are commonly used for organic diodes characterization. Several analytical models for dc J-V characteristic of organic diodes have been reported in the literatures [12]-[15]. The general approach is to partially fit electrical characteristics in different voltage regimes. In the low voltage regime, based on thermionic or Schottky emission, carrier injections from the electrode into the organic semiconductor determines the current. In the high voltage regime, space-charge limited current dominates the device.

On the other hand, impedance spectroscopy has been used to study the carrier transport mechanism and interface effects in organic diodes [16], [17]. IS records linear electrical response of the device of interest to small-signals at certain dc biasing. The measured spectra can be electrically interpreted with a proper equivalent circuit model which normally includes a chain of resistor-capacitor (RC) networks to represent individual interfaces and layers. However, the small signal model obtained by IS at certain dc biases are not adequate to represent the nonlinear behaviors of organic diodes with large ac input signals [9], such as 10 V in most organic rectifier circuits.

For the diodes used in this work the thickness of the depletion region is the entire thickness of the semiconductor and the metal-insulator-metal (MIM) diode model without voltage controlled depletion region should be applied [8]. In other words, the bulk capacitance of the diodes remains reasonably constant over different bias voltages and frequencies [8], [17]. Thus, without including the contact effects the diodes used in this work could be considered as a lossy capacitor with a voltage dependent resistance, as shown in Fig. 1 (b). Though the voltage dependent resistance was not determined in this work due to its nonlinear nature, the model introduced here was found sufficient to explain the diode performance in 13.56 MHz rectifier application, as shown in the results and discussion section. The capacitive properties of the diodes were measured by vector network analyzer (VNA) in reflection mode without bias voltage (HP network analyzer

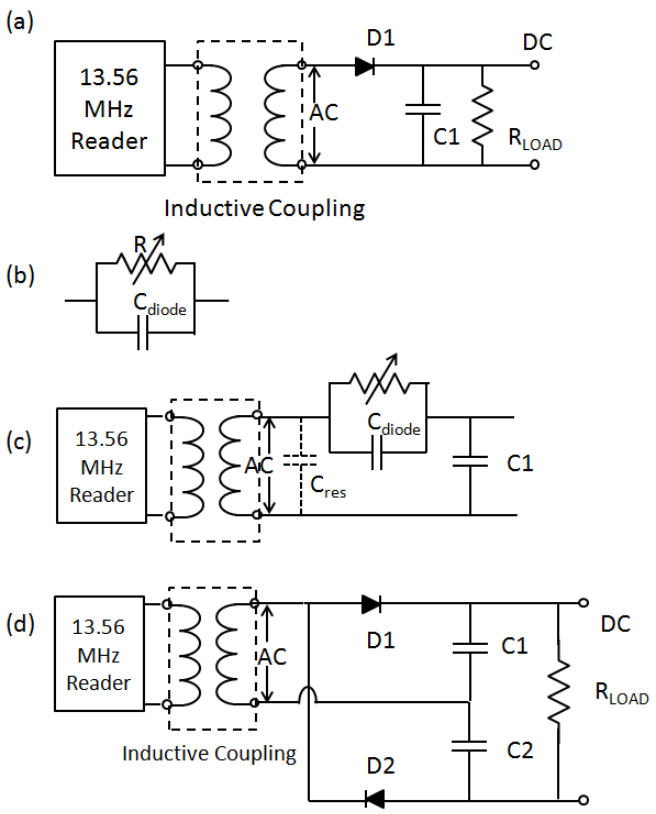

Fig.1. (a) Schematic circuit diagram for the rectenna operating at 13.56 MHz. (b) Equivalent circuit for an organic diode without contact effects, where R represents the voltage-dependent resistance and C_{diode} describes the diode geometric capacitance. (c) Schematic circuit diagram of the rectenna with diode equivalent circuit; C_{res} was not present in the real circuit (d) Schematic circuit diagram of the rectenna circuit with a double half-wave rectifier.

8752A). The measured real and imaginary impedance at 13.56 MHz were fit into the RC circuit (Fig. 1 (b)). Some of the properties of printed organic diodes are summarized in Table I. The presented thickness is the PTAA layer thickness which is calculated on the basis of the measured geometric capacitance C_{diode} and using a relative permittivity of 3. The current-voltage properties of the diodes used in this study were similar to those reported in [8], so the J-V curves are not shown. The forward current density of A-series and B-series diodes at 5 V was 0.02 A/cm^2 and 0.03 A/cm^2, respectively. The reverse leakage current density at -5 V was approximately 0.03 mA/cm^2 for both series. The resulting rectification ratio was about 10^3 for both series.

B. *Loop Antenna Characterization*

For 13.56 MHz loop antennas, a few μH of inductance is typically used. The loop antenna (72 mm ×42 mm) with 5, 6 and 7 turns were fabricated. The line width of loop antenna is 1 mm, the gap between lines is 0.3 mm and the line thickness is 47 μm. The inductances of the loop antenna were first estimated using theoretical equations and measured later (see Table 2). The total inductance (in μH) of an N-turn planar spiral inductor coil can be calculated as [18]

$$L = L_0 + M_+ - M_- \quad (1)$$

TABLE I.
PROPERTIES OF PRINTED ORGANIC DIODES

Diode	Properties	
	Area (cm^2)	C_{diode} (pF)
A series, average thickness 500 nm		
A1	0.002	15.16
A2	0.004	23.09
A3	0.006	30.97
A4	0.008	39.73
A5	0.01	47.07
B series, average thickness 300 nm		
B1	0.002	23.83
B2	0.004	38.85
B3	0.006	52.69
B4	0.008	66.00
B5	0.01	91.07

TABLE II.
PROPERTIES OF LOOP ANTENNAS

	Properties		
	Analytical Inductance [µH]	Measured Inductance [µH]	Tuning Capacitance [pF]
5 turns	2.70	2.96	46.5
6 turns	3.45	3.89	35.4
7 turns	4.31	4.97	26.7

where L is the total inductance, L_0 is the sum of the self-inductance of all straight segments, M_+ is the sum of the positive mutual inductances, and M_- is the sum of the negative mutual ones. The calculation details can be found in [18].

III. RESULTS AND DISCUSSION

The printed organic diodes and the loop antennas were initially examined separately, in an attempt to find the optimal characteristics of each device. Printed organic diodes with PTAA as the semiconducting material have been demonstrated to have excellent performance at frequencies around or exceeding 13.56 MHz [4], [5] and [8]. For example, we have reported a half-wave rectifier with a dc output voltage of 5 V at 13.56 MHz for an ac coupling input with amplitude of 10 V [4].

To estimate the diodes frequency response performance, the rectified output voltage as a function of frequency for the organic diodes used in this work was measured, as shown in Fig. 2. In these measurements, the amplitude of the input ac signal was 10 V, provided by a signal generator (Keithley 3390). The diodes were connected to a discrete capacitor (47 nF) and a load resistor (1MΩ). At 13.56 MHz, A-series diodes with an approximate thickness of 500 nm were able to yield 0.6-0.7 V dc output voltages, whereas B-series diodes with an average thickness of 300 nm could provide dc voltages above 3.5 V.

Apparently, B-series diodes with thinner semiconductor

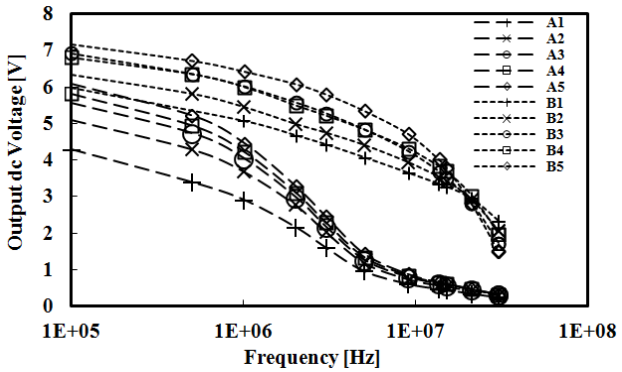

Fig 2. DC output voltage for 10 V ac input signal from signal generator as a function of frequency.

layers have better frequency response performance compared to A-series thick diodes. This result corresponds well with the theory that the frequency performance of organic diodes is dominant by the semiconductor thickness [9]. Therefore, organic diodes with thin semiconductor layers are, in general, preferable in high frequency applications. In addition, diodes with larger active area possess smaller resistance, thus resulting in higher output dc voltages. However, at high frequencies the geometric capacitance of the diode will shunt the circuit and lower the output dc voltage. Take B-series diodes for example at frequencies exceeding 18 MHz the voltage loss due to the diode capacitance surpassed the voltage loss due to the diode resistance so that the diodes with smaller active area offered higher output dc voltages.

For inductive-coupled loop antennas, the induced voltage on the antenna coil can be estimated based on Lenz's law that is the induced voltage equals to the time rate of change of the magnetic flux [19], i.e.,

$$V = -N\frac{d\Psi}{dt} \tag{2}$$

where N is number of turns in the loop antenna and Ψ is magnetic flux through each turn. The magnetic flux can be described in terms of mutual inductance and induced current and the equation becomes [19]

$$V = -M\frac{di}{dt} \tag{3}$$

where i is the induce current and M is total mutual inductance that depends on both loop geometry, such as number of turns and the area of each turn, and the spacing between the two antennas. Thus, the induced voltage is largely dependent on the mutual inductance which can be practically enhanced by increasing the turns of loop antennas.

In addition, to maximize the coupling voltage of the loop antenna, an additional capacitance is needed for tuning the loop antenna to the resonant frequency of 13.56 MHz, and the required capacitance can be estimated as

$$f_{res} = \frac{1}{2\pi\sqrt{LC}} \tag{4}$$

where f_{res} is the resonant frequency and L is the inductance of the loop antenna. The calculated tuning capacitances of the

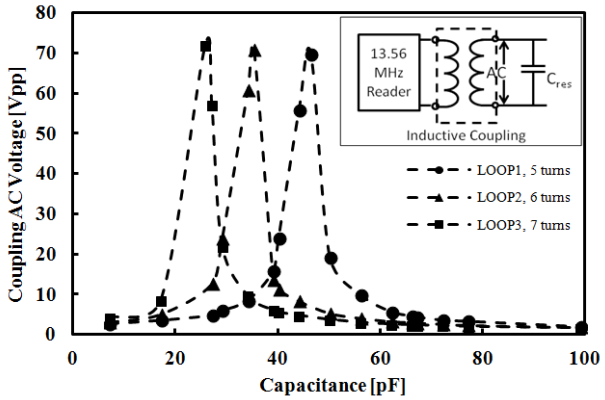

Fig. 3. Measured open-circuit coupling voltage (peak to peak) of three loop antennas as a function of resonant capacitance C_{res}. The measurement set-up schematic is presented in the inset.

loop antennas used in this work are listed in Table 2. Traditionally, a solid-state capacitor will be added to the loop antenna to realize the desired resonant frequency.

To study the effect of the tuning capacitance on the performance of the loop antenna, the coupling voltage was measured as a function of tuning capacitance (see Fig. 3). In these measurements, a set of discrete capacitors C_{res} was connected in parallel with the loop antenna. The 13.56 MHz reader antenna was placed 16.8 cm from the loop antennas, with the transmitting power of 2 W. As mentioned before, the highest coupling voltage occurs when the resonant frequency of the loop antenna is tuned to 13.56 MHz with the help of the additional capacitance. For the 7-turns loop antenna, due to its larger coil inductance, a smaller capacitance of 27 pF was required to achieve 13.56 MHz with the highest coupling voltage of 72 V. For the 6-turns and the 5-turns loop antennas, the maximum coupling voltages of 71 V and 70 V were achieved with tuning capacitances of 35 pF and 46 pF, respectively. Since the commercial reader antenna used in this work has different shape and dimension compared to the credit card size loop antennas, the mutual inductance is not optimized. Furthermore, due to the great distance between the reader antenna and the loop antennas, the mutual inductances brought by the extra turns of loop were limited. As a result, the dependence of the maximum coupling ac voltage on the number of turns of the loop antennas in this work was not as great as might be expected. In addition, due to the high conductivity of copper conductors on PCBs the loop antennas have narrow bandwidths and high quality factors (Q) of 300 to 400. In other words, the loop antennas used in this study are highly sensitive to the tuning circuit. For low-Q loop antenna, such as inkjet printed ones, the effect of the tuning circuit on the coupling voltage would be less drastic; however, tuning the whole rectenna circuit remains essential to obtain optimal performance.

To sum up, when measured separately (see Fig. 2 and Fig. 3) the thinner film diodes and the antenna with more loop turns were found to offer superior performance. Next, the organic diodes were connected to the loop antennas and dc output voltages of the rectenna circuits were investigated. To demonstrate the effect of the organic diodes, the rectified dc

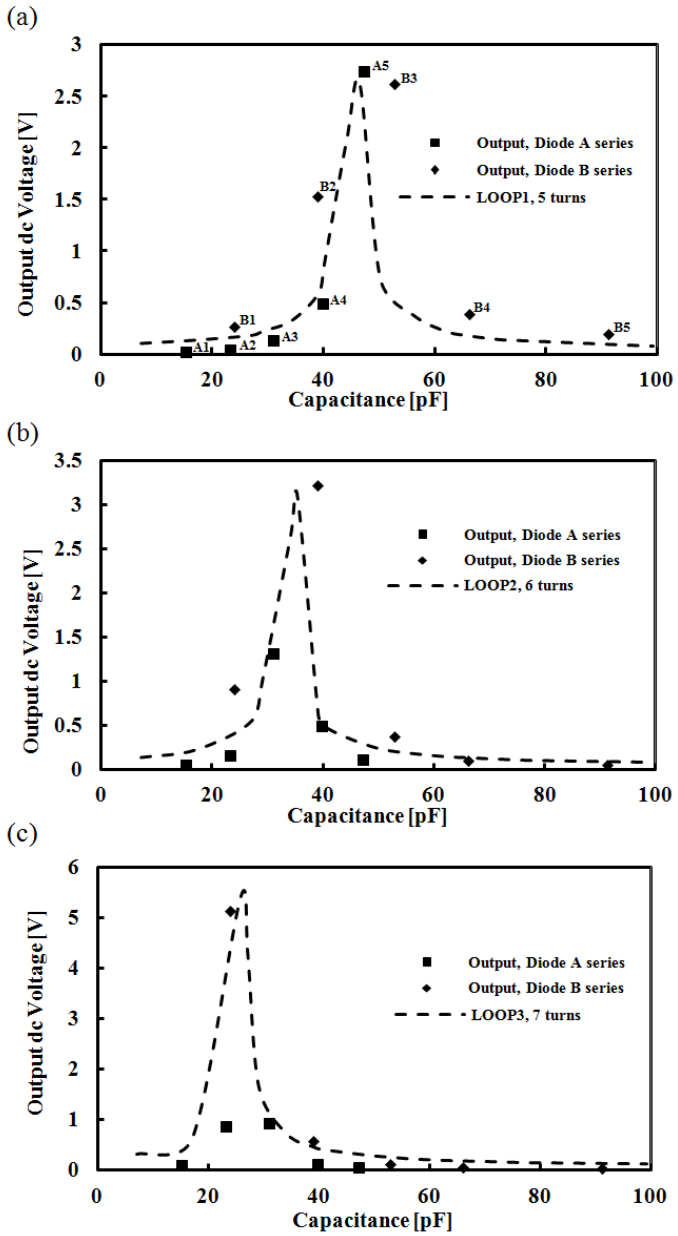

Fig. 4. Measured results of the rectennas dc output ((a) the 5-turns loop. (b) the 6-turns loop. (c) the 7-turns loop) vs. the geometric capacitance of the organic diodes, C_{diode}. Reader antenna was placed 16.8 cm from the loop antennas, with the transmitting power of 2W. The load was 1 MΩ and the filtering capacitor was 1.5 nF for the HW rectifier. Fig. 3 is inserted here as dash curves to represent the open-circuit characteristics of the loop antennas.

output voltages of all the diodes with three loop antennas of different number of turns are plotted against diodes geometric capacitance (see Fig. 4). No additional tuning capacitor C_{res} was present in this measurement. Take B-series thin diodes for example, based on the previous measured results (Fig. 2) these diodes should yield similar output dc voltages and provide higher output dc voltages compared to A-series thick diodes at 13.56 MHz. However, the results here show that when connected to the antennas their output dc voltages vary greatly from each other and are not always higher than the outputs of A-series thick diodes. Clearly, the organic diodes have an impact on the rectenna performance and thus needs further circuit analysis.

As shown in Fig. 1(c), once the organic diodes were connected to the loop antennas, the total capacitance seen from the loop antenna was the sum of diode geometric capacitance C_{diode} and the filtering capacitor $C1$. Since normally the filtering capacitor (in nF range) is decades larger than the diode capacitance (in pF range), the total capacitance can be estimated as

$$C_{total} = \frac{C_{diode} \times C1}{C_{diode} + C1} \approx C_{diode}. \quad (5)$$

For silicon-based high frequency Schottky diodes, the total diode capacitance is typically around 1 pF at MHz range. Hence an additional tuning capacitor C_{res} is required. However, in the case of organic diodes with large geometric capacitances as presented in Table 1, C_{diode} could effectively function as the tuning capacitor and thus cause dramatic changes in the resonant frequencies. In order to confirm this effect, the antenna open-circuit coupling voltages as a function of tuning capacitance (Fig.3) is inserted here as dash curves, but with arbitrary amplitudes. It can be seen that the output dc voltages of different diodes on each antenna follow the shape of the dash curves. This confirms that the geometric capacitance of the diodes functions as the tuning capacitance of the loop antennas and alters the resonant frequency of the circuit. As a result, the amplitudes of the input ac signals are not the same for each diode, which causes output dc voltage variations in Fig. 4.

As noted before, the loop antennas prepared for this study are narrow-band antennas and the coupling voltage falls rapidly as the resonant frequency varies from 13.56 MHz. This becomes critical for choosing the suitable organic diodes. For example, for the 5-turns loop antenna (see Fig. 4(a)), diode A5 (47.07 pF) provided the desired capacitance to tune the antenna at 13.56 MHz and as a result its output dc voltage was even higher compared to the outputs of B-series thin diodes. The same pattern can be found from Fig. 4 (b) and (c) as well. For example, the required capacitance for the 7-turns loop antenna is 27 pF, diode B1 with a capacitance of 23.83 pF from thin diode series B and diodes A2 (23.09 pF) and A3 (30.97 pF) from thick diode series A have the closest capacitance values. In other words, the capacitances of these three diodes could tune the circuit to resonate near 13.56 MHz for obtaining higher coupling voltages. With the higher input ac voltages, they provided the highest dc output voltages in their categories, i.e. an output voltage of 5.15 V with diode B1 and 0.88 V and 0.94 V with diode A2 and A3 respectively. Therefore, the best organic diodes obtained by using signal generator as the input source (Fig. 2) are not necessarily optimal in this case.

It should be mentioned that the presented measured values have already taken into account the additional capacitances/reactance caused by the measurement set-up, including the input impedance of the oscilloscope probe. The length of electrical traces on the customized probes and the length of the wires used to connect the components are minimized to avoid parasitic reactance. Due to the effect of the input capacitance of the oscilloscope probe on the tuning

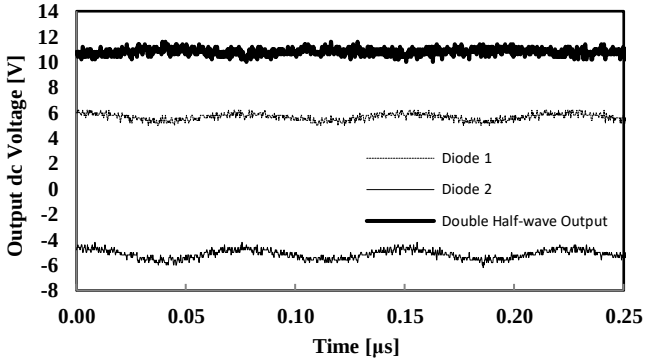

Fig. 6. Measured result of the 5-turns rectenna dc output with the double half-wave rectifier. Reader antenna was placed 16.8 cm from the loop antennas, with the transmitting power of 2W. The load was 1 MΩ and the filtering capacitors were both 1.5 nF.

frequency, the input coupling ac voltages when connected to organic diodes should not be measured simultaneously with the output dc voltage. For this reason, the exact amplitudes of the input ac signals for the rectennas are not plotted in Fig. 4. Since the resistance of the organic diodes will significantly lower the Q factor of the loop antennas, the maximum coupling ac voltages (peak to peak) for the rectenna circuit will be much lower than 70 V. Furthermore, in order to have consistent comparison between all three loop antennas, the reader antennas was placed at a great distance of 16.8 cm from the loop antennas to sustain a moderate maximum coupling ac voltage. Based on the measured output dc voltages, the maximum coupling voltages (peak to peak) for the rectenna circuits should be in the range of 20 to 30 V.

The analysis of the interaction between the loop antennas and the organic diodes provided useful information on circuit design and development. Once the inductance of the loop antenna was determined, the required tuning capacitance can be realized by selecting the suitable organic diodes. Based on the findings, a double half-wave rectifying circuit was designed (see Fig. 1(d)) with the 5-turns loop antenna to provide a higher output dc voltage. As given in Table 2, the desired tuning capacitance for the 5-turns loop antenna is 46.5 pF. This requires the combined capacitance of two diodes in the double HW rectifier to meet this value. Therefore, two B1 diodes with capacitance of 23.83 pF (Table 1) were chosen. The measured output dc voltage is shown in Fig. 5. In the circuit (Fig. 1(d)), one HW rectifier consisting of $D1$ and $C1$ rectified the positive cycles of the input ac voltage and produced an output dc voltage of 6 V, whereas the other HW rectifier including $D2$ and $C2$ rectified the negative cycles of the input voltage and provided a -5 V output dc voltage. The final output dc voltage is the combination of both HW rectifier circuits, which is about 11 V.

IV. Conclusion

In this work, the effect of the organic diodes on the performance of the rectenna circuit has been investigated. The rectanna consists of a loop antenna and a simple half-wave rectifier based on organic diodes. Unlike their silicon-base

counterparts, the geometric capacitances of organic diodes have significant values to dominate the tuning properties of the loop antennas at MHz range. The resonant frequency, and therefore the coupling ac voltage of the rectenna are heavily dependent on the geometric properties of the diodes, such as the diode area and the diode thickness. Consequently, this has a great effect on the output dc voltage of the organic diode rectifier. Based on the circuit analysis, an optimal rectenna circuit with a double half-wave rectifier was designed and measured. These results demonstrate the importance of circuit analysis in organic electronics.

REFERENCES

[1] S. Steudel, S. D. Vusser, K. Myny, M. Lenes, J. Genoe, P. Heremans, "Comparison of organic diode structures regarding high-frequency rectification behavior in radio-frequency identification tags," *J. Appl. Phys.*, vol. 99, 114519, Jun. 2006.

[2] C.-Y. Lin, C.-H. Tsai, H.-T. Lin, L.-C. Chang, Y.-H. Yeh, Z. Pei, Y.-R. Peng, C.-C. Wu, "High-frequency polymer diode rectifiers for flexible wireless power-transmission sheets," *Org. Electron.*, vol. 12, pp. 1777-1782, Jul. 2011.

[3] K. Myny, S. Steudel, P. Vicca, J. Genoe, P. Heremans, "An integrated double half-wave organic Schottky diode rectifier on foil operating at 13.56 MHz," *Appl. Phys. Lett.*, vol. 93, 093305, Sep. 2008.

[4] L. M. P. S. Heljo, D. Lupo, "Organic diodes for RF harvesting" in *Proceedings of LOPE-C 2012*, Munich, 2012.

[5] K. E. Lilja, T. G. Bäcklund, D. Lupo, T. Hassinen, T. Joutsenoja, "Gravure printed organic rectifying diodes operating at high frequencies," *Org. Electron.*, vol. 10, pp. 1011-1014, Apr. 2009.

[6] P. S. Heljo, M. Li, K. E. Lilja, H. S. Majumdar, D. Lupo, "Printed half-wave and full-wave rectifier circuits based on organic diodes" *IEEE Trans. Electron Devices*, vol. 60. no. 2, pp870-874, Feb. 2013.

[7] P. Heljo, K. E. Lilja, S. Tuukkanen, D. Lupo, "Charge Pump Circuit Using Printed Organic Diodes and Capacitors" in *Proceedings of LOPE-C 2011*, Frankfurt, 2011, pp. 53-55.

[8] P. Heljo, K. E. Lilja, H. S. Majumda, D. Lupo, "High rectifier output voltages with printed organic charge pump circuit" *Org. Electron.*, vol. 15, pp. 306-310, 2014.

[9] S. Steudel, K. Myny, V. Arkhipov, C. Deibel, S. D. Vusser, J. Genoe, P. Heremans, "50 MHz rectifier based on an organic diode," *Nat. Mater.*, vol. 4, pp. 597-600, Jul. 2005.

[10] S. Mutlu, I. Haydaroglu, A. O. Sevim, "Realization of polymer charge pump circuits using polymer semiconductors" *Org. Electron.*, vol. 12, pp. 312-321, Dec. 2011.

[11] W. Zhang, J. Smith, R. Hamilton, M. Heeney, J. Kirkpatrick, K. Song, S. E. Watkins, T. Anthopoulos, and I. McCulloch, "Systematic improvement in charge carrier mobility of air stable triarylamine copolymers", *J. Am. Chem. Soc.*, vol 131, no. 31, pp. 10814-10815, Jul. 2009

[12] C. H. Kim, O. Yaghmazadeh, Y. Bonnassieux, G. Horowitz "Modeling the low-voltage regime of organic diodes: Origin of the ideality factor" *J. Appl. Phys.* 110. 093722, 2011.

[13] A. Haldi, A. Sharma, W. J. Potscavage Jr and B. Kippelen, "Equivalent circuit model for organic single-layer diodes", *J. Appl. Phys.* 104. 064503, 2008.

[14] P. S. Davids, I. H. Campbell and D. L. Smith, "Device model for single carrier organic diodes" *J. Appl. Phys.*82. 6319, 1997.

[15] P. Kumar, S. C. Jain, V. Kumar, A. Misra, S. Chand, M. N. Kamalasanan, "Current-voltage characteristics of an organic diodes: Revisited", *Synthetic Metals*, vol. 157, 22-23. pp 905-909, Nov. 2007.

[16] A. Takshi, J. D. Madden, "Large apparent inductance in organic Schottky diodes at low frequency" J. Appl. Phys.99. 084503, 2006.

[17] K. E. Lilja, H. S. Majumdar, K. Lahtonen, P. Heljo, S. Tuukkanen, T. Joutsenoja, M. Valden, R. Österbacka, D. Lupo, "Effect of dielectric barrier on rectification, injection and transport properties of printed organic diodes" *J. Appl. Phys.* 44. 295301, 2011

[18] H. M. Greenhouse, "Design of Planar Rectangular Microelectronic Inductors", *IEEE Trans. parts, hybrids, and packaging*, Vol. PHP-10, No.2, p101-109, Jun. 1974

[19] B. Grob, Basic Electronics, 1st Metric edition, McGraw-Hill Book, 1987, pp. 286-295.

Miao Li received the M. Sc degree in Radio Frequency Electronics from Tampere University of Technology, Tampere, Finland, in 2010.

In 2011, she joined the organic electronics research group, Department of Electronics, Tampere University of Technology, as a Research Engineer. Her researcher interests are focused on printed organic devices for RF energy harvesting.

Petri S. Heljo received the B.S. and M. Sc. degrees in Biological and Chemical measurements from Tampere University of Technology, Tampere, Finland, in 2010.

Currently he is working in the organic electronics research group, Department of Electronics, Tampere University of Technology. His research interest includes gravure printing of polymer semiconductor devices and measurement systems for organic electronics.

Donald Lupo received his Ph.D. in Physical Chemistry from Indiana University. After a long industrial career in functional materials and organic electronics, he joined Tampere University of Technology in 2010, where he is professor in the Department of Electronics and Communications Engineering and director of the Laboratory for Future Electronics.

PUBLICATION III

Performance of printable supercapacitors in an RF energy harvesting circuit

S. Lehtimäki, M. Li, J. Salomaa, J. Pörhönen, A. Kalanti, S. Tuukkanen, D. Lupo

International Journal of Electrical Power and Energy Systems 58(2014) pp. 42-46
doi: 10.1016/j.ijepes.2014.01.004.

Electrical Power and Energy Systems 58 (2014) 42–46

Contents lists available at ScienceDirect

Electrical Power and Energy Systems

journal homepage: www.elsevier.com/locate/ijepes

Performance of printable supercapacitors in an RF energy harvesting circuit

Suvi Lehtimäki [a,*], Miao Li [a], Jarno Salomaa [b], Juho Pörhönen [a], Antti Kalanti [b], Sampo Tuukkanen [a], Petri Heljo [a], Kari Halonen [b], Donald Lupo [a]

[a] Tampere University of Technology, Department of Electronics and Communications Engineering, Korkeakoulunkatu 3, FI-33720 Tampere, Finland
[b] Aalto University, School of Electrical Engineering, Department of Micro- and Nanosciences, Otakaari 5 A, FI-02150 Espoo, Finland

ARTICLE INFO

Article history:
Received 2 May 2013
Received in revised form 10 December 2013
Accepted 1 January 2014

Keywords:
Supercapacitor
Ultracapacitor
Electric double layer capacitor
Energy harvesting
Autonomous power source

ABSTRACT

We report the fabrication of a supercapacitor on a plastic substrate with mass-production-compatible methods and its characterisation using galvanostatic and voltammetric methods. The supercapacitor is prepared in ambient conditions using activated carbon and an aqueous, non-acidic electrolyte. The obtained capacitances are 0.45 F and 0.21 F for device sizes of 4 cm^2 and 2 cm^2, respectively. Additionally, we demonstrate the utilisation of the supercapacitor in an autonomous energy harvesting and storage system. The RF energy harvester comprises a printed loop antenna and a half-wave organic diode rectifier operating at 13.56 MHz frequency. The harvested energy is stored in two supercapacitors connected in series to increase the maximum operating voltage. In order to power a device such as a sensor or a small indicator display, voltage regulation is needed. A voltage regulator, implemented as an application specific integrated circuit (ASIC), was designed for this purpose, and fabricated commercially. We demonstrate the ability of the harvester storage unit to power the regulator for hours with a constant regulator output voltage and power. The effect of supercapacitor charging time on the actual supercapacitor charging state is also discussed, as a slower charging rate is found to have a significant effect on the output of the supercapacitor.

1. Introduction

Energy harvesting from ambient sources such as light, electromagnetic radio frequency (RF) fields or kinetic energy provides an opportunity for building wireless, autonomous systems that can be used, for example, in ambient sensory networks or intelligent packaging [1–3]. Incorporating such "intelligence" on large areas cost-effectively calls for a new way of producing the systems needed. Printed and organic electronics offers a promising manufacturing method, where flexible, lightweight and even transparent electronic devices can be manufactured using low-cost, high-throughput processes [4–6].

An autonomous harvesting system needs a backup energy storage for periods when the primary energy source is unavailable [2], such as during the night when using solar cells, or when RF fields are not present when using RF harvesters. Supercapacitors, also called ultracapacitors or electric double layer capacitors (EDLC), are an alternative to batteries as energy storage devices, offering a higher peak power capability and a longer cycle lifetime [7].

The operation of supercapacitors is based on the electrostatic aggregation of electrolyte ions on a charged electrode surface, without significant chemical reactions. Using a high surface area electrode material, such as activated carbon, very high capacitances can be reached [7]. A limitation of supercapacitors is their operation voltage range, which is constrained by the electrochemistry of the materials. In water-based electrolytes, the voltage is limited to only about 1 V, whereas with organic electrolytes 2–3 V is attainable [8]. However, aqueous electrolytes offer smaller equivalent series resistance and higher specific capacitance than organic electrolytes [8]. They are also readily disposable and their production is less expensive, which is in many applications more advantageous than higher operation voltage. The voltage range can be increased by connecting supercapacitors in series.

Printed supercapacitors on a paperboard substrate have previously been demonstrated using disposable, non-toxic materials [9]. RF harvesters, comprising an antenna and a rectifier circuit, can also be fabricated with printing methods [10]. Combining a large-area printed harvester and energy storage device with a power management integrated circuit (IC) enables a small sensor or indicator display to operate autonomously. Many sensor and indicator functionalities, as well as the associated logic circuits, can easily be integrated directly on the IC. Furthermore, being able

* Corresponding author. Tel.: +358 408490623.
E-mail address: suvi.lehtimaki@tut.fi (S. Lehtimäki).

0142-0615/$ - see front matter © 2014 Elsevier Ltd. All rights reserved.
http://dx.doi.org/10.1016/j.ijepes.2014.01.004

to design the on-chip voltage regulator, as opposed to using a commercial IC, permits application specific optimisation of power efficiency and operating range of the regulator.

In this study, printed, aqueous supercapacitors are fabricated and connected to a printed RF harvester [10] and a voltage regulator, implemented as an application specific integrated circuit (ASIC) [11]. This harvesting circuit provides up to 10 h of stable output voltage when the RF field is not present. The capacitance of the supercapacitor can easily be tailored for the requirements of the application by selecting the supercapacitor geometrical area appropriately.

2. Experimental

Printed components were fabricated on poly(ethylene terephthalate) (PET) substrates (Melinex ST506 from Dupont Teijin Films). A commercial RFID reader was used to induce an AC voltage in a printed antenna. A printed rectifier circuit composed of an organic diode [12] and a printed capacitor rectified the input from the antenna, and charged the supercapacitor. The charged supercapacitor provided an input for the voltage regulator ASIC, which was connected to a 1 MΩ load at its output. The measurement setup is depicted in Fig. 1.

2.1. Supercapacitor fabrication

The supercapacitors were prepared by laminating two electrodes together with an electrolyte and separator in between. The structure is depicted in Fig. 2(a). The supercapacitors were fabricated in two sizes: 2 cm^2 and 4 cm^2. A 100 nm thick copper layer was vacuum evaporated onto the PET through a shadow mask. Two layers of conductive graphite ink (Electrodag PC407C from Acheson Industries Ltd.) were blade-coated on top of the copper using a plastic mask for patterning, and both layers were subsequently cured at 120 °C for 5 min, yielding a 50 μm thick layer. The width of the graphite electrodes was 2.0 cm in the larger samples and 1.4 cm in the smaller samples. As the graphite layer was needed to protect the copper layer from coming into contact with the electrolyte, the copper electrode width was slightly smaller than the graphite. A photograph of a supercapacitor sample is shown in Fig. 2(b).

The active layer was prepared from Norit DLC Super 50 activated carbon with carboxymethyl cellulose (CMC, Sigma Aldrich) as binder. The activated carbon and the polymer were dispersed in deionized water in the proportions Norit/CMC/H_2O 1.9/0.1/36 by weight. The activated carbon ink layer was blade-coated on the graphite. The active layer was dried on a hotplate at 60 °C for a few minutes until the ink appeared dried. The mass of activated

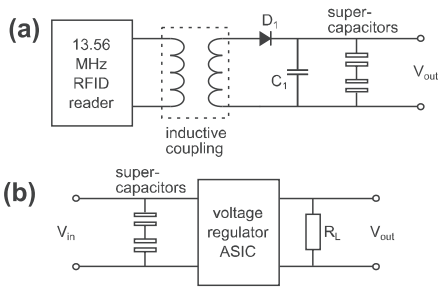

Fig. 1. Schematics of the supercapacitor (a) harvesting and (b) output measurement circuits. Diode D_1 and capacitor C_1 form the rectifier, which charges the supercapacitors. The output of the ASIC is loaded with $R_L = 1$ MΩ.

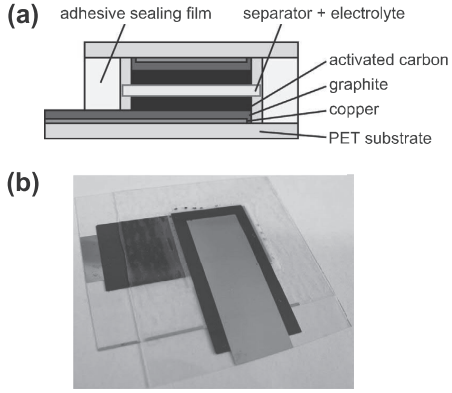

Fig. 2. (a) Structure of the assembled supercapacitor and (b) photograph of a 4 cm^2 supercapacitor sample.

carbon deposited on the electrodes was on average 2.2 mg/cm^2. The activated carbon mass was determined by weighing the substrate before and after deposition.

Supercapacitors were assembled with a TF4050 paper separator (Nippon Kodoshi Corporation) and 4.1 mol/l LiCl aqueous electrolyte. The high electrolyte concentration was selected to ensure an excess of ions such that the risk for electrolyte starvation and additional internal resistance is removed [13]. The electrodes and separator were sandwiched together with the electrolyte and sealed with an adhesive film (UPM Raflatac). The assembly was done with the electrodes at 90° angle with respect to each other, forming a square shape supercapacitor at the electrode overlap area.

2.2. Supercapacitor characterisation

The supercapacitor properties were measured using a Zennium Electrochemical Workstation (Zahner Elektrik GmbH, Germany) in the two-electrode configuration. Cyclic voltammetry from 0 V to 0.9 V was used to get a qualitative measure of the supercapacitors. The voltage sweep rate was 50 mV/s.

Galvanostatic discharging measurements were performed according to international standard IEC 62391-1:2006, Class 3 [14]. The supercapacitors were charged to 0.9 V in 1 min and held at this potential for 5 min. The capacitance was calculated from the voltage decrease rate with a 1.60 mA discharge current for the larger samples and 725 μA for the smaller samples. The equivalent series resistance (ESR) was calculated from the initial IR drop of the discharging with a 16.0 mA current for the larger samples and 7.25 mA for the smaller samples.

2.3. Harvester architecture

The all-printed harvester consisted of an antenna and a half-wave rectifier comprising an organic diode and a capacitor. The loop antenna was inkjet printed with a conductive Ag nanoparticle ink (Harima NPS-JL Silver NanoPaste) and a dielectric (SunTronic Jettable insulator U5388) for the loop cross-over. The Ag ink was sintered at 150 °C for 1 h. The dielectric strip was cured by UV light and by additional curing at 150 °C for 30 min, after which the loop cross-over was printed with the same Ag ink as the antenna. The size of the antenna was 7.5 cm by 4.2 cm.

The organic diode was fabricated on a separate substrate, where the Cu anode was evaporated and patterned using a wet-etching process on a roll-to-roll basis. The semiconductor poly(triaryl-

amine) as well as the top Ag anode were gravure printed. The process is described in more detail in [12]. The rectifier capacitor was also printed on a similar pre-patterned Cu-coated substrate. The dielectric was gravure printed poly(methyl metacrylate) (20% solution in ethyl acetate and toluene, 1:1) cured at 80 °C for 5 min. The top electrode was gravure printed using Ag flake ink (Acheson PM460A) and cured at 80 °C for 5 min. The capacitor's area was 1.5 cm^2 and its capacitance was 1.5 nF at 13.56 MHz. The diode and capacitor were integrated on the antenna substrate using the Ag flake ink.

2.4. Voltage regulator

The designed voltage regulator was fabricated in a commercial 0.18 μm CMOS process. It is based on a cross-coupled voltage doubler charge-pump, with closed-loop continuous frequency control. A similar circuit design is described in [11]. The output voltage is controlled by changing the pumping frequency, and thereby, the output impedance of the charge-pump. The regulator output can be steadily kept at 1.2 V over a wide range of input voltages (roughly down to 0.8 V), and under varying load conditions. The size of the processed ASIC is roughly 1.5 mm^2, the regulator area being less than 4% of the total ASIC area. The ASIC was packaged and wire-bonded in a 44-legged JLCC package.

2.5. Measurement setup

Two similar supercapacitors were connected in series. The supercapacitors were charged by connecting them to the harvester, after which they were immediately connected to the ASIC for the output measurement.

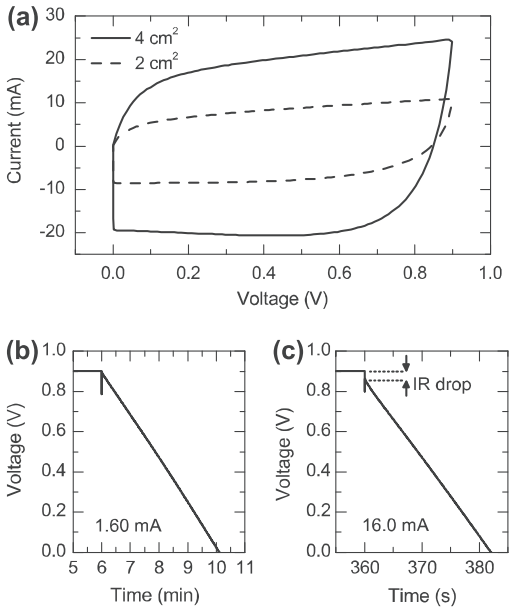

Fig. 3. (a) Cyclic voltammograms of two supercapacitors of different sizes. The sweep rate was 50 mV/s. (b) and (c) Galvanostatic discharge curves of the 4 cm^2 supercapacitor at constant discharge currents for (b) capacitance determination and (c) ESR determination. The capacitance is calculated from the slope of the voltage and the constant current, and the ESR from the initial IR drop of the discharge. The small downward spikes at the beginning of discharge are caused by parasitic capacitances in the measurement system and not related to supercapacitor behaviour.

Table 1
The supercapacitor characteristics obtained from galvanostatic measurements.

Device area	4 cm^2	4 cm^2	2 cm^2	2 cm^2
C (F)	0.45	0.46	0.21	0.22
C/area (F/cm^2)	0.11	0.11	0.10	0.11
ESR (Ω)	2.8	3.7	6.2	10

The harvester antenna was placed above a 13.56 MHz reader antenna (i-scan®HF long range reader ID ISC.LR200 from OBID) such that the two were inductively coupled [15] and the distance of the harvester was adjusted vertically between 5.5 cm and 6.0 cm. The input voltage from the antenna in the two extreme cases was measured using an oscilloscope (Tektronix DPO4104) with a 10× voltage probe when only the rectifier was connected to the antenna. The output voltage of the rectifier was measured similarly before the supercapacitor was connected to the harvester.

The series supercapacitors were charged to 1.8 V with the harvester and the charging was stopped by removing the reader antenna when the voltage over the supercapacitor reached the target value. For the discharging, the supercapacitor assembly was connected to the ASIC, and the ASIC output was loaded with a 1 MΩ resistor. The ASIC output voltage was measured through a voltage buffer, in order not to affect the ASIC operation nor loading.

The voltage over the supercapacitors as they were charged, as well as the input to the ASIC were measured with the oscilloscope through 10× voltage probes. The oscilloscope was controlled with LabVIEW software (National Instruments).

3. Results and discussion

3.1. Supercapacitor properties

Cyclic voltammograms of the supercapacitors of two sizes using a sweep rate of 50 mV/s are shown in Fig. 3(a). The rectangular shape indicates good capacitive behaviour [16]. The capacitances and ESRs were determined from the galvanostatic discharge measurements (Fig. 3(b) and (c) and they are presented in Table 1. The capacitances were approximately 0.45 F and 0.21 F in the 4 cm^2 and 2 cm^2 supercapacitors, respectively. The difference in the capacitances per geometrical area is most likely a result of dissimilar thicknesses of the activated carbon and other variations in the preparation process.

The specific capacitance of the supercapacitor was 26 F/g, when only the total activated carbon mass in the device was taken into account. This value is of similar magnitude to previous results with printed activated carbon supercapacitors [9]. The specific capacitance is, however, lower than in more traditionally assembled devices, which can reach 80 F/g for a similar material [17]. A possible reason for the difference is the pressing of the activated carbon electrode, which improves the contact between the carbon particles [17]. The particles in the printed, unpressed layer may not be fully in contact with each other or the current collector, reducing the effective amount of active electrode material.

As expected, the ESR was larger for the smaller supercapacitors, at most 10 Ω, whereas for the larger samples it was less than 4 Ω. The larger ESR can be understood as both a resistance in the current collector leads, which were narrower in the 2 cm^2 supercapacitors, as well as a smaller cross-sectional area of the electrolyte and the separator, which inhibit the movement of current-carrying ions.

3.2. Charging the supercapacitor with the harvester

At the 5.5 cm distance, the input signal to the rectifier was 20 V peak-to-peak when only the rectifier and the 10× measurement probe were connected to the antenna. At the 6.0 cm distance, the

input signal was 15 V peak-to-peak, measured similarly. The 20 V and 15 V values refer to the high and low input cases discussed below. The unloaded rectifier output DC values were 4.5 V and 3.2 V in the high and low input cases, respectively.

The charging behaviour of the series supercapacitors is shown in Fig. 4 and the charging times presented in Table 2. In the high input case, the charging was faster: 11 min and 22 min for the 2 cm^2 and 4 cm^2 supercapacitors, respectively. With the low input, the charging took 1 h 4 min for the smaller supercapacitors and 2 h 21 min for the larger supercapacitors. As expected, the charging time is proportional to the capacitance. The low input charging curve of the larger capacitors levelled off as the voltage approached 1.8 V, making the exact charging time somewhat inaccurate.

When comparing the high and low input cases, it should be noted that the rectifier output voltages are not the same as measured without the supercapacitors: when the supercapacitors are connected to the harvester, the DC voltage at the output of the rectifier is equal to the voltage of the supercapacitor assembly, and thus dependent on its charge state. The supercapacitor appears initially as nearly a short circuit [18].

Instead of a constant DC charging voltage, the output current of the diode determines the charging rate. The diode current depends exponentially on the voltage over the diode [19,20]. This accounts for the large difference between the cases where the input voltage to the diode is higher or lower. The charging profile can be explained when examining the voltage over the diode: as the supercapacitor is gradually charged, this voltage decreases. This, in turn, reduces the current and slows down the charging.

3.3. Powering the regulator circuit

The voltage over the series supercapacitors when they are discharged, as well as the output voltage of the ASIC, are presented in Fig. 5. The regulator output remains constant at 1.2 V, corresponding to an output current of 1.2 μA and output power of 1.44 μW, until the voltage over the supercapacitors reaches approximately 0.78 V. The durations of operation are summarised in Table 2.

The larger, 4 cm^2 supercapacitors can power the ASIC from 8 h to over 10 h, whereas the 2 cm^2 supercapacitors can only provide the necessary input to the ASIC for 4–5 h. In the quickly charged (high input) supercapacitors, the initial voltage drop is much more pronounced. In the slowly charged supercapacitors (low input), the overall voltage decline is more uniform even in the beginning. The difference between the voltages of the high and low input charged

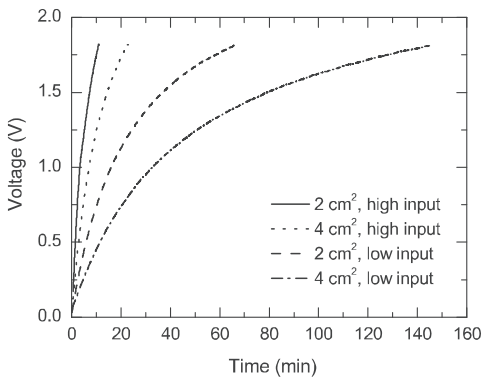

Fig. 4. Charging curves to 1.8 V for the two supercapacitors connected in series.

Table 2
The results of the harvesting measurements. High and low input refer to cases where the harvester antenna was closer to and further away from the reader antenna.

Device area	4 cm^2	2 cm^2
Charging time		
High input	22 min	11 min
Low input	2 h 21 min	1 h 4 min
Operation time		
High input	7 h 51 min	3 h 57 min
Low input	10 h 39 min	4 h 59 min

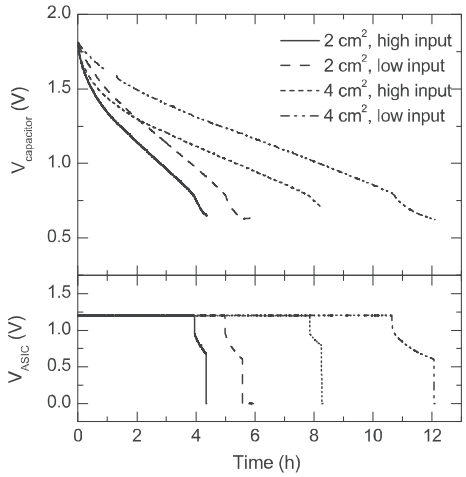

Fig. 5. Voltage over the supercapacitors (above) as it powers the regulator ASIC, and the output voltage from the ASIC (below).

supercapacitors after 1 h of discharge is approximately 0.15 V with both supercapacitor sizes.

An explanation to the observed behaviour is found in an equivalent RC circuit model [21], where the supercapacitor is represented as at least three parallel branches of a capacitor and a resistor in series, each branch with a different RC time constant, along with another leakage resistance branch. When the supercapacitor is charged quickly, only the small-time-constant branches are charged fully; as the external charging is stopped, charge redistribution from the high time constant branches to the lower ones takes place within the supercapacitor. This results in a decrease in the observed voltage over the supercapacitor. When the supercapacitor is charged slowly, however, the slower branches are also charged fully, resulting in a more steady voltage decrease as power is drawn from the supercapacitor.

In addition to the branched RC model discussed above, several other models have been proposed to describe the electrical behaviour of supercapacitors, as well as physical explanations for them [22]. One such explanation is the cumulative increase of the electrolyte resistance towards the bottom of an eletrode pore [7]. Based on this, a qualitative understanding of the charging behaviour can be described in terms of ion migration in the supercapacitor. Parts of the electrode surface, namely those deep inside the pores, are not readily accessible to the ions of the electrolyte and thus cannot initially participate in the double layer formation. However, given enough time, the ions also migrate to these surfaces. The migration can occur from the already-charged surfaces, near the pore opening, after the supercapacitor is charged externally for only a short period. This corresponds to the charge reorganization in the branched RC model.

4. Conclusions

The use of printable supercapacitors as energy storage devices in a harvester circuit using a printed RF antenna and diode rectifier along with a voltage regulator ASIC was demonstrated. The two series-connected supercapacitors can be charged to 1.8 V in a time ranging from 10 min to over 2 h, depending on the supercapacitor size and harvester antenna distance to the charging antenna. When loaded with a 1.44 μW load, the output of the voltage regulator was found to stay constant at 1.2 V for up to 5 or 10 h, depending on supercapacitor size.

The charging time, controlled by the antenna distance, was found to affect the discharge behaviour of the supercapacitor significantly. Slowly charged supercapacitors provided a more steady and long-lasting input for the regulator. The relatively rapid initial drop of the voltage in quickly charged supercapacitors is attributed to charge reorganization within the electrode pores. This important effect will need to be considered in further work aiming to develop harvester structures for different applications.

Acknowledgement

The authors would like to acknowledge the Academy of Finland for its financial support under Grant No. 139881.

References

[1] Mathuna CO, O'Donnell T, Martinez-Catala RV, Rohan J, O'Flynn B. Energy scavenging for long-term deployable wireless sensor networks. Talanta 2008;75(3):613–23.
[2] Vullers R, van Schaijk R, Doms I, Van Hoof C, Mertens R. Micropower energy harvesting. Solid State Electron 2009;53(7):684–93.
[3] Philipose M, Smith JR, Jiang B, Mamishev A, Roy S, Sundara-Rajan K. Battery-free wireless identification and sensing. IEEE Pervasive Comput 2005;4(1):37–45.
[4] Ko SH, Pan H, Grigoropoulos CP, Luscombe CK, Fréchet JM, Poulikakos D. All-inkjet-printed flexible electronics fabrication on a polymer substrate by low-temperature high-resolution selective laser sintering of metal nanoparticles. Nanotechnology 2007;18(34):345202–10.
[5] Forrest SR. The path to ubiquitous and low-cost organic electronic appliances on plastic. Nature 2004;428(6986):911–8.
[6] Cao Q, Zhu ZT, Lemaitre MG, Xia MG, Shim M, Rogers JA. Transparent flexible organic thin-film transistors that use printed single-walled carbon nanotube electrodes. Appl Phys Lett 2006;88(11):113511–3.
[7] Kötz R, Carlen M. Principles and applications of electrochemical capacitors. Electrochim Acta 2000;45(15):2483–98.
[8] Pandolfo A, Hollenkamp A. Carbon properties and their role in supercapacitors. J Power Sources 2006;157(1):11–27.
[9] Keskinen J, Sivonen E, Jussila S, Bergelin M, Johansson M, Vaari A, et al. Printed supercapacitors on paperboard substrate. Electrochim Acta 2012;85:302–6.
[10] Li M, Heljo P, Lupo D. Organic diodes for energy harvesting. Proc LOPE-C; 2010.
[11] Kalanti A, Yücetas M, Salomaa J, Aaltonen L, Halonen K. Charge-pump based frequency regulator for precision supply generation. In: Proceedings of 2010 IEEE International Symposium on Circuits and Systems (ISCAS). IEEE; 2010. p. 4077–80.
[12] Lilja KE, Bäcklund TG, Lupo D, Hassinen T, Joutsenoja T. Gravure printed organic rectifying diodes operating at high frequencies. Org Electron 2009;10(5):1011–4.
[13] Pell W, Conway B, Marincic N. Analysis of non-uniform charge/discharge and rate effects in porous carbon capacitors containing sub-optimal electrolyte concentrations. J Electroanal Chem 2000;491(1):9–21.
[14] International standard: fixed electric double layer capacitors for use in electronic equipment. IEC 62391-1; 2006.
[15] Laplante PA, editor. Comprehensive dictionary of electrical engineering. CRC Press; 2005. 10.1201/9781420037807.ch1.
[16] Conway BE. Electrochemical supercapacitors: scientific fundamentals and applications. New York: Kluwer Academic/Plenum Publishers; 1999 [chapter 2].
[17] Bonnefoi L, Simon P, Fauvarque J, Sarrazin C, Sarrau J, Lailler P. Multi electrode prismatic power prototype carbon/carbon supercapacitors. J Power Sources 1999;83(1):162–9.
[18] Simjee FI, Chou PH. Efficient charging of supercapacitors for extended lifetime of wireless sensor nodes. IEEE Trans Power Electr 2008;23(3):1526–36.
[19] Lampert MA. Simplified theory of space-charge-limited currents in an insulator with traps. Phys Rev 1956;103(6):1648–56.
[20] Jain SC, Willander M, Kumar V. Conducting organic materials and devices. Semiconduct Semimet 2007;81:1–188.
[21] Merrett GV, Weddell AS. Supercapacitor leakage in energy-harvesting sensor nodes: fact or fiction? In: Ninth International Conference on Networked Sensing Systems (INSS). IEEE; 2012. p. 1–5.
[22] Faranda R, Gallina M, Son D. A new simplified model of double-layer capacitors. In: International Conference on Clean Eelectrical Power ICCEP'07. IEEE; 2007. p. 706–10.

PUBLICATION IV

All printed Large Area E-field Antenna Utilizing Printed Organic Rectifying Diodes for RF Energy Harvesting

M. Li, G. Daniel, B. E. Kahn, L. H. Ohara, B. D. F. Casse, N. Pretorius, B. Krusor, P. Mei, G. L. Whiting, C. Tonkin, D. Lupo

In 2018 IEEE 18th International Conference on Nanotechnology (IEEE-NANO)
doi: 10.1109/NANO.2018.8626318.

All Printed Large Area E-field Antenna Utilizing Printed Organic Rectifying Diodes for RF Energy Harvesting

Miao Li[1], George Daniel[2], Bruce E. Kahn[3], Liam H. Ohara[3], Bernard D. F. Casse[2], Nathan Pretorius[3], Brent Krusor[4], Ping Mei[4], Gregory L. Whiting[5], Chip Tonkin[3] and Donald Lupo[1]
[1]Tampere University of Technology, Dept. of Electronics and Communication Engineering, Finland, email: miao.li@tut.fi
[2]Metawave Corporation, USA
[3]Clemson University, The Sonoco Institute of Packaging Design and Graphics, USA
[4]PARC- a Xerox company, USA
[5]University of Colorado Boulder, Department of Mechanical Engineering, USA

***Abstract*—**Fully printed radio frequency (RF) harvesters that operate at HF RFID and ISM frequency of 13.56 MHz are normally comprised of a small printed loop antenna. They work at short ranges using inductive coupling mechanism. In this paper, we present a novel screen printed large area E-field antenna incorporated with a printed organic diode rectifier that could provide close to 1 V dc voltage with 1 W input at a distance of a few meters. The unique high bulk capacitance of the printed organic diodes enables effective imaginary impedance matching to the antenna without an additional matching component. The results demonstrate the possibility of fully printed RF energy harvesters for long range operation at HF frequencies.

I. Introduction

Interest in harvesting and storage of ambient energy has grown strongly in the last few years. Printed electronics has been shown to be a promising way to add energy autonomy to devices, and harvesting from mechanical [1], [2], light [3], [4] and radio frequency (RF) radiation [5-9] using printed harvesters have been reported. The available energy density, especially thermal, mechanical, or RF, is usually quite low, so that a combination of large area and novel design is essential to capture as much energy as possible from the environment or dedicated source. Printing is particularly well suited to such large area devices.

RF energy harvesters typically comprise two functional units: an antenna to gather RF energy and a rectifying circuit to convert the received RF signals to dc voltages. At ultra-high frequencies (UHF), a hybrid RF harvester combining printed antennas with a rectifying circuit based on discrete surface-mount technology (SMT) components [10-12] is widely used for scavenging ambient RF radiation. At lower frequencies such as the 13.56MHz industrial, scientific and medical (ISM) or radio frequency identification (RFID) band, dedicated RF sources such as RFID readers are commonly available. At these frequencies, printed RF harvesters usually utilize small inductive loop antennas together with rectifying diodes featuring either polymer- or metal oxide- based printable semiconducting materials [8, 9, 13]. In general, these printed small inductive loop antennas, also known as inductive couplers or coils, have the size of credit cards and operate in the magnetic near field, which is typically under few tens of cm. The short operation range limits the applicability of these conventional printed 13.56 MHz RF energy harvesters. Particularly it could become impractical to power numerous sensors at such short range. By increasing the operation range of printed 13.56 MHz harvesters from centimeters to a few meters, it could finally enable advanced applications such as smart homes with IoT (internet of things) sensors, detectors and low-power devices.

For energy harvesting it is desirable to minimize losses in individual components as well as the impedance mismatching among them to optimize the efficiency of the system. This is challenging for printed antennas and even more so for printed organic diodes, whose electrical performance is affected by both the printing process and the low charge carrier mobility and density of printable organic semiconductors. Recently, there has been a great deal of efforts toward improving ink properties and printing processes. On the other hand, impedance analysis is often overlooked in reports on printed 13.56 MHz RF harvesters. Here we report the fabrication and characterization of a printed 13.56 MHz RF harvester utilizing gravure printed organic rectifying diodes and a screen printed large area antenna. The large screen printed antenna used here is capable of operating at a range of a few meters without significant performance drops. Both frequency tuning and imaginary impedance matching of the antenna were achieved simultaneously through the reactance of the printed organic diodes. The nonlinear voltage-dependent resistive behaviors of the printed diodes were investigated. With the extended operation range the present printed harvester could easily be integrated into wall papers, posters, etc., to realize, cost-effective, thin, flexible and scalable indoor energy autonomous solutions.

II. Method, Design and Characterization

A. Antenna Design and Simulations

The antenna has a double-element design with a total size of 400 by 600 mm, which was defined by the maximum printing area available on the screen printer. This design is distinctly

different from the more common small loop inductive antennas used for near field communication (NFC) that operate using the magnetic near field and are only capable of short range harvesting. Considering that the wavelength λ at 13.56 MHz is 22.12 m, this antenna is ultra-compact with an electrical size of approximately λ/40. As shown in Fig.1, the simulated S11 results for the 13.56 MHz antenna indicate that this antenna has a high inductive reactance which needs capacitive reactance to match the impedance to a 50 Ω load. The projected gain pattern of the E-field antenna (Fig.1.d) is toroidal in shape and omni-directional. This performance is predicated on achieving good conductivity and reasonable trace.

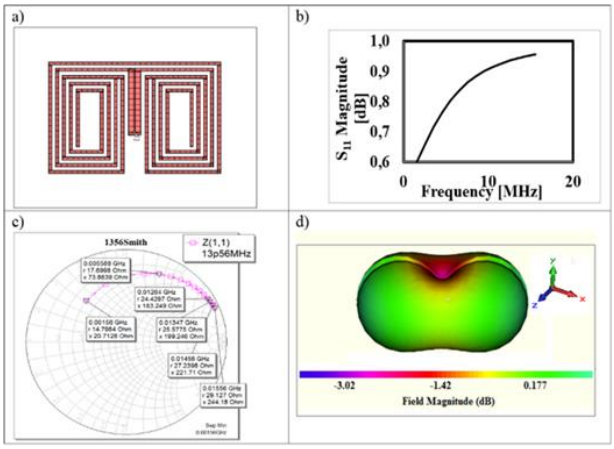

Fig 1. Simulated parameters for the antenna a) Mesh points b) S11 Magnitude vs. Frequency c) Smith plot d) Antenna pattern at 13.56MHz. S11 or S_{11} is the input reflection coefficient.

The antennas were screen printed on a Graficaindia Flextonica Nano Print Plus flat-bed press with a 100-mesh screen tensioned to 20 N using Novacentrix (PChem) ink, PSI-219. The ink was cured using a DragonAir drying tunnel at 140 ^{0}C with a dwell time of 90 seconds. Each sheet was passed through the drying tunnel twice to facilitate curing of the thick ink deposit. The final thickness of the printed antennas was about 5 um. The sheet resistance was about 30 mΩ/square.

B. Diode and Circuit Characterization

The printed organic diodes have a vertical Cu-PTAA (poly(triarylamine))-Ag sandwich structure, as reported previously [14-18]. The organic semiconducting material PTAA was chosen for its excellent stability in ambient conditions. All characterization and measurements were conducted in ambient conditions with no encapsulation. The average thickness of the semiconductor layer in the diodes was 300 nm. This thickness is calculated based on the measured geometric capacitance from the impedance measurement using a vector network analyzer. As shown in Fig.2, the forward current density of the diodes at 5 V was 0.03 A/cm^2 and the reverse leakage current density at -5 V was 0.02 mA/cm^2. The resulting rectification ratio was about 1.5x10^3.

In this work, the printed organic diodes had four different active areas: 0.004, 0.006, 0.008, and 0.01 cm^2 designated as A1, A2, A3 and A4 respectively, which were determined by the cross section of the Cu-PTAA-Ag layers. The geometric capacitance of the diodes is proportional to the size of the active area. The capacitance values of diodes A1 to A4 were about 45 pF, 60 pF, 75 pF and 90 pF respectively. The diode capacitance can be used to tune the resonant frequency, or to match the impedance of the antenna at 13.56 MHz. In addition, a smaller diode with active area of 0.002 cm^2 and corresponding capacitance of 28 pF was used. However, due to its relatively high parasitic and printing quality related to its size, it was left out of analysis and discussion.

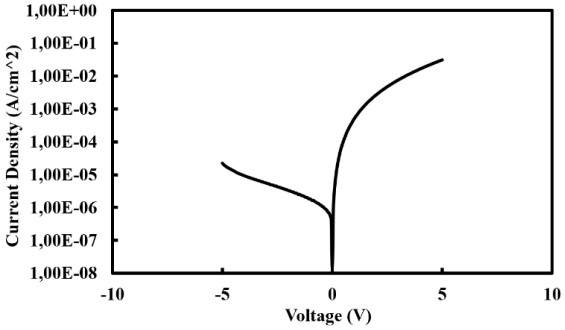

Fig.2. Printed diode Current Density-Voltage (JV) curve.

III. RESULTS AND DISCUSSION

Because of the long wavelengths of incoming signals, it often becomes impractical to utilize antennas of the physical resonant length at MHz frequencies. Instead, a small inductive loop antenna circuit is widely used in the MHz range [8, 9, 20]. These small loop antennas transfer voltage between the transmit and receive loops through magnetic/inductive coupling. However, the magnetic field strength of these small loop antennas decays rapidly with transfer distance. As a consequence, their operation range is limited to near field and short range, typically in the range of centimeters. In this work, a large area antenna with novel double-spiral design was developed to effectively increase the operation range. The unique dual-element design is composed of an outer loop structure connected to an inner double-spiral as shown in Fig. 6.a). The inner double-spiral has an overall electrical length close to 6 m, which is calculated from the feeding points to the end of each spiral. While these spirals resemble an inductive loop and its electrical length is close to a quarter of a wavelength at operating frequency of 13.56 MHz, the unique integrated outer loop structure makes the antenna an ultra-compact far-field radiating antenna. That is, with the dual element design, the antenna is no longer a spiral loop antenna with the electrical length close to λ/4 but an electrically-small antenna operating at λ/40 defined by the outer dimension of the antenna. In addition to decreasing the antenna electrical size, the duel-element design increases the radiation resistance of the antenna. Together with feeding arms, which slightly adjust the impedance of the antenna, the overall design of the antenna enables tailored complex impedance. Fig.3 shows the plot of the S21 data (forward transmission gain) of a pair of matched antennas with added discrete capacitors of 47pF and 56 pF on each antenna. These added capacitors were chosen to resemble the capacitance of the printed diodes to achieve optimal impedance matching. At 13.56 MHz, the antennas have S21

values about -4 dB to -5 dB with the antennas positioned 1 m, 2 m, 3 m and 4 m apart. The result indicates that the performance of the antennas is maintained to a distance of several meters, unlike inductive coupled loop antennas whose efficiency drops dramatically with increased distance within their operating range.

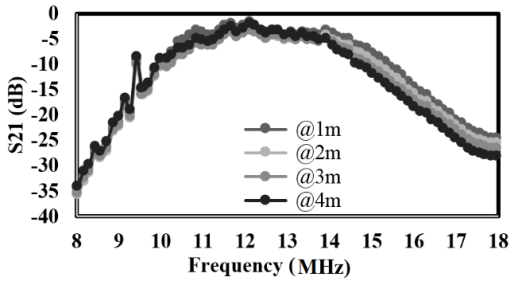

Fig.3. S21 plot of a pair of matched antennas.

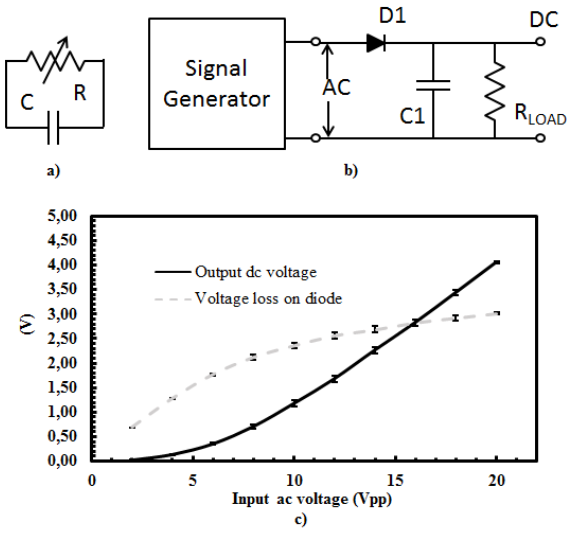

Fig.4. a) Simplified diode RC model. b) Measurement setup schematic. c) diode rectified dc output voltage and diode voltage loss vs. input ac voltage at 13.56 MHz. The load is the internal load of the oscilloscope of 1 MΩ. The error bars represent the standard deviation between diodes A1-A4.

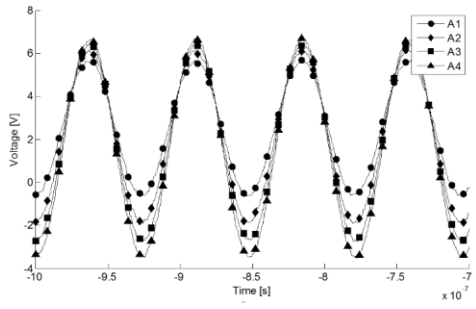

Fig.5. Diode output vs ac input of 20 V_{pp} at 13.56 MHz. No capacitor included.

In order to fully analyze the harvester system performance, especially the impedance matching, a large signal nonlinear ac model of printed diodes is essential. Previously we reported a simple RC model covering diode ac behaviors (Fig.4.a) which consisted of a voltage-dependent resistance and a diode geometric capacitance (or in other word bulk capacitance) as the equivalent circuit for the printed organic diode [17], [18]. The results indicated that the bulk capacitance of the diodes remains reasonably constant over different bias voltages and frequencies while the voltage dependent resistance is nonlinear and difficult to determine. Here, the voltage-dependent resistive behavior of the diodes was studied in more detail. Firstly, the rectified dc output of a half-wave rectifier at 13.56 MHz with a single printed PTAA diode and a filtering capacitance of 47nF was measured as a function of input ac voltage. As shown by the size of the error bars in Fig.4, at 13.56 MHz the diode voltage outputs are very similar despite the variation of active area from 0.004 to 0.01 cm^2 (A1-A4). With an input ac signal of 10 V_{pp} (peak to peak), the average dc output of all diodes was 1.18 V. The input root mean square (rms) voltage was 3.54 V, which results in a voltage loss across the diode of about 2.36 V. When input voltages increased to 16 and 20 V_{pp}, the corresponding voltage losses were about 2.83 and 3.01 V, respectively. Therefore, in contrast to conventional inorganic diodes, the voltage losses across organic diodes are not constant but increase with the input ac voltages as shown in Fig.4.c). Since it has been demonstrated before [17] that the bulk capacitance of the diode is fairly independent of the bias voltages, the increment in diode voltage loss is likely owing to the nonlinear voltage-dependent resistance of the diode.

Since the small signal impedance measurement cannot adequately represent the large signal nonlinear behavior of the diodes, we measure directly the output voltage of the diodes with ac input voltages of 20 V_{pp} at 13.56 MHz, but without the presence of the 47 nF filtering capacitor C_1 in Fig.4.b). Based on the measured waveforms in Fig.5, one can calculate the rms voltage of diode output and the equivalent impedance of diodes for both positive and negative cycles using the equation below

$$\frac{V_{rms.out}}{Z_{load}} = \frac{V_{rms.in} - V_{rms.out}}{Z_{diode}} \quad (1)$$

where $V_{rms.out}$ is the rms voltage of the diode output, $V_{rms.in}$ is the rms voltage of the input ac signal, Z_{load} is the internal impedance of the measurement device. Due to the parasitic reactance of the measurement setup, the load impedance Z_{load} became a complex impedance which makes the calculation in (1) extremely difficult. However, if we neglect the parasitic reactance of the measurement setup as well as the geometric capacitance of the diode, the Z_{diode} in equation (1) becomes purely resistive with roughly a few hundred kΩ during the positive cycles and few MΩ during the negative cycles. These values by no means represent in-depth behaviors of the voltage-dependent resistor in the diode model, however, they indicate that the printed organic diode has a significantly large forward resistance and a relatively small reverse resistance compared to conventional Schottky diodes. To sum it up, though the exact values of the nonlinear voltage-dependent resistor are difficult to obtain, the resistance of the organic diodes are determined to be in the range of hundreds of kΩ to few MΩ for positive and negative cycles based on the large-signal measurements at

13.56 MHz. To be clear, the impedance values obtained using the vector network analyzer is the diode small-signal impedance, which ranges from 3.5 kΩ to 1.7 kΩ. These values, as mentioned before, cannot represent the nonlinear large-signal behaviors of the printed diodes.

As mentioned above, one of the special properties of printed organic diodes is their relatively high geometric capacitance; the capacitance of organic diodes A1 to A4 was about 45 pF, 60 pF, 75 pF and 90 pF respectively. These values are in the range of the exact capacitance required for 13.56 MHz customized tag antennas [20]. In other words, the printed organic diodes can be effectively incorporated in the 13.56 MHz RF harvester to tune the resonant frequency and rectify the input ac signal simultaneously. In this work, the measured impedance of the antenna was about (56.5+j279) Ω at 13.56 MHz. To ensure good antenna matching, the imaginary part of the antenna impedance needs to be reduced to as close to zero through organic diode with the most suitable capacitance. Therefore, the diode with capacitance of 45 pF and a corresponding reactance of –j260.8 Ω was the closest. Unfortunately, due to the high resistance of the organic diode, the overall impedance matching between the diodes and the antennas are not perfect.

To boost the dc output voltage, a double half-wave rectifier was fabricated. This configuration delivered approximately twice the dc output voltage of that shown Fig.4. In addition, the ripples from each half-wave rectifier are in the opposite directions and cancel each other out somewhat, which enables the use of a smaller filtering capacitor. It should be pointed out that the total capacitance of a double half-wave rectifier is the combination of two diodes at each branch. Therefore, to have a 56 pF matching capacitance two smaller diodes (A5) with capacitance of 28 pF were used. In the double half-wave circuit, two 1.5 nF capacitors were used; this capacitance can be printed in a size of 1.3 cm^2 area, as previously demonstrated [19]. However in this work two surface mounted capacitors were used due to time constraints. Fig.6 shows the antenna layout including a multipurpose connector to accommodate the matching double half-wave rectifier. An image of the portion of the antenna with the attached rectifier is shown in Fig.6.b).

To demonstrate the 13.56 MHz energy harvesting system, two screen printed antennas were used as a transmitter and a receiver. The transmit antenna was fitted with a matched capacitor of 56 pF. The 13.56 MHz harvesting antenna was placed 1 m, 2 m, 3 m and 4 m from the transmit antenna in a typical office environment. In addition to the harvester (series1) with the optimal matching provided by the two A5 diodes with capacitance of 28pF from each diode, a second harvester (series2) with two A1 diodes with 45pF from each diode was fabricated for comparison. The input power was provided by a signal generator. The dc output voltage of the harvester as a function of distance is shown in Fig. 7. It can be seen that above 800 mV dc output from the harvester with two A5 diodes (series1) was obtained using an input power of (1W) from the signal generator fed to the transmit antenna. The output dc voltage declined slightly with distance in this case. On one hand, the impedance mismatch on the harvesting antenna end, specifically the huge diode resistance, played a huge role to limit the performance of the harvester. That is, the nonlinear resistance of the printed PTAA diodes, in the range from kΩ to MΩ depending on the input signal amplitude, makes the impedance matching between the antenna and the rectifier circuit very challenging. On the other hand, the capacitance of the printed PTAA diodes has an effect on the imaginary impedance (reactance) matching which, when done correctly, could improve the performance of the harvester significantly. As shown in Fig. 7, the harvester with better reactance matching (series1) yielded much higher output dc voltage compared to the harvester (series2) with non-optimal matching. It clearly shows that the operating range of this fully printable large area antenna harvesting system is in the range of a few meters with reasonable dc output voltages to enable low-power IoT sensors.

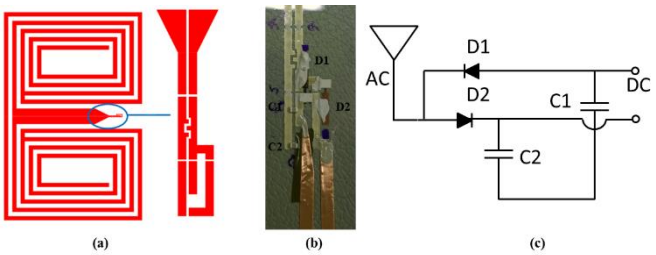

Fig.6.a) 13.56 MHz antenna design with the multipurpose connector. b) zoomed in image of the rectifier circuit. c) circuit schematic.

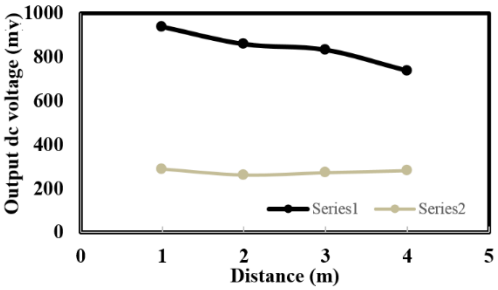

Fig.7. DC output voltage vs. input power of 13.56MHz printed harvesting system.

IV. Conclusions

An entirely printable RF energy harvesting system comprising a screen printed large area E-field antenna and a printed organic diode double half-wave rectifier was demonstrated. At 13.56 MHz, the organic diodes were carefully selected based on their geometric capacitance to match the impedance of the antenna. With 1W transmitted power the printed harvester could generate close to 1V dc output at a distance of a few meters from the source. This operating range is significantly greater than near field small loop antenna harvesters and indicates the possibility of long-range energy harvesting.

Acknowledgment

This work was supported in part by Tekes (project PAUL 40146/14) and in part by Flextech Alliance (RFP12-169_Clemson).

References

[1] Juho Pörhönen, Satu Rajala (Née Kärki), Suvi Lehtimäki, and Sampo Tuukkanen, "Flexible piezoelectric energy harvesting circuit with printable supercapacitor and diode," *IEEE Transactions On Electron Devices*, vol. 61, no. 9, pp. 3303-3308. Sep. 2014.

[2] Moazzam Ali, Deep Prakash, Tino Zillger, Pradeep Kumar Singh, and Arved Cral Hübler, "Printed piezoelectric energy harvesting device," *Adv. Energy Mater*, vol. 4, 1300427, Jan. 2014.

[3] Sampo Tuukkanen, Marja Välimäki, Suvi Lehtimäki, Tiina Vuorinen, and Donald Lupo, "Behaviour of one-step spray-coated carbon nanotube supercapacitor in ambient light harvester circuit with printed organic solar cell and electrochromic display," *Scientific Reports*, 6:22967, DOI: 10.1038/srep22967, Mar. 2016.

[4] Pälvi Apilo, Jussi Hiltunen, Marja Välimaäki, Santtu Heinilehto and Rafal Sliz, "Roll-to-roll gravure printing of organic photovoltaic modules-insulation of processing defects by an interfacial layer," *Prog. Photovoltaics*, 23, pp.918–928, 2015.

[5] Suvi Lehtimäki, Miao Li, Jarno Salomaa, Juho Pörhönen, Antti Kalanti, Sampo Tuukkanen, Petri Heljo, Kari Halonen, and Donald Lupo, "Performance of printable supercapacitors in an RF energy harvesting circuit," *International Journal of Electrical Power and Energy Systems*, vol. 58, pp.42–46, Jun. 2014.

[6] Juha-Veikko Voutilainen, Tuomas Happonen, Juha Hakkinen, and Tapio Fabritius, "All silk-screen printed polymer-based remotely readable temperature sensor," *IEEE Sensors Journal*, vol.15, no.2, pp.723–733, Feb. 2015.

[7] Namsoo Lim, Jaeyoung Kim, Soojin Lee, Namyoung Kim, and Gyoujin Cho, "Screen printed resonant tags for electronic article surveillance tags," *IEEE Transactions on Advanced Packaging*, vol. 32, no.1, pp.72–76, Feb. 2009.

[8] Hwiwon Kang, Hyejin Park, Yongsu Park, Minhoon Jung, Byung Chul Kim, Gordon Wallace, and Gyoujin Cho, "Fully Roll-to-Roll Gravure Printable Wireless (13.56 MHz) Sensor-Signage Tags for Smart Packaging," *Scientific Report*, 4:5387, DOI: 10.1038/srep05387 23, Jun. 2014.

[9] Younsu Jung, Hyejin Park, Jin-Ah Park, Jinsoo Noh, Yunchang Choi, Minhoon Jung, Kyunghwan Jung, Myungho Pyo, Kevin Chen, Ali Javey, and Gyoujin Cho, "Fully printed flexible and disposable wireless cyclic voltammetry tag," *Scientific Report*, 5:8105, DOI: 10.1038/srep08105, Jan. 2015.

[10] Rushi Vyas, Vasileios Lakafosis, Manos Tentzeris, Hiroshi Nishimoto, and Yoshihiro Kawahara, "A battery-less wireless mote for scavenging wireless power at UHF (470–570 MHz) frequencies," in *Proc. IEEE Int. Symp. Antennas Propag.*, WA, USA, pp. 1069–1072, Jul. 2011.

[11] John Kimionis, Apostolos Georgiadist, Michael Isakov, Hang J. Qi, and Manos M, "Tentzeris. 3D Inkjet-printed Origami Antennas for Multi-direction RF Harvesting," *IEEE MTT-S International Microwave Symposium*, 978-1-4799-8275-2/15, May. 2015.

[12] Sangkil Kim, Rushi Vyas, Apostolos Georgiadis, Ana Collado, and Manos M. Tentzeris, "Inkjet-printed RF Energy Harvesting and Wireless Power Trasmission Devices on Paper Substrate," in *Proceedings of the 43rd European Microwave Conference*, 978-2-87487-031-6 EuMA, Nuremberg, Germany, 2013.

[13] Kris Myny, Soeren Steudel, Peter Vicca, Jan Genoe, and Paul Heremansb, "An integrated double half-wave organic Schottky diode rectifier on foil operating at 13.56 MHz," *Applied Physics Letters*, 93, 093305, 2008.

[14] Kaisa E. Lilja, Tomas G. Bäcklund, Donald Lupo, Tomi Hassinen, and Timo Joutsenoja, "Gravure printed organic rectifying diodes operating at high frequencie," *Organic Electronics*, vol. 10, pp.1011-1014, Aug. 2009.

[15] Kaisa E. Lilja, Himadri. S. Majumdar, Kimmo Lahtonen, Petri Heljo, Sampo Tuukkanen, Timo Joutsenoja, Mika Valden, R. Österbacka, and Donald Lupo, "Effect of dielectric barrier on rectification, injection and transport properties of printed organic diodes," *Journal of Applied Physics*, 44, 295301, 2011.

[16] Petri Heljo, Miao Li, Kaisa E. Lilja, Himadri S. Majumdar, and Donald Lupo, "Printed half-wave and full-wave rectifier circuits based on organic diodes," *IEEE Transactions on Electron Devices*, vol. 60. no. 2, pp870-874, Feb. 2013.

[17] Petri Heljo, Kaisa. E. Lilja, Himadri S. Majumda, and Donald Lupo, "High rectifier output voltages with printed organic charge pump circuit," *Organic Electronics*, vol.15, pp.306-310, 2014.

[18] Miao Li, Petri Heljo, and Donald Lupo, "Organic rectifying diode and circuit for wireless power harvesting at 13.56 MHz," *IEEE Transactions on Electron Devices*, vol.61, no.6, pp.2164-2169, Jun. 2014.

[19] Miao Li, Petri Heljo, and Donald Lupo, "Organic diodes for RF harvesting," in Proc. LOPE-C, Munich, Jun. 2012.

[20] *How to design a 13.56 MHz customized tag antenna*, ST, AN2866 Application

PUBLICATION V

0.7 GHz Solution-Processed Indium Oxide Rectifying Diodes

M. Li, M. Honkanen, X.J. Liu, C. Rokaya, A. Schramm, M. Fahlman, P. R. Berger, D. Lupo

IEEE Transactions on Electron Devices, 67(2020)1, pp. 360-364
doi: 10.1109/TED.2019.2954167

0.7 GHz Solution-Processed Indium Oxide Rectifying Diodes

Miao Li, Mari Honkanen, Xianjie Liu, Chakra Rokaya, Andreas Schramm, Mats Fahlman, Paul R. Berger, and Donald Lupo

***Abstract*— Solution-based deposition, with its simplicity and possibility for upscaling through printing, is a promising process for low-cost electronics. Metal oxide semiconductor devices, especially indium oxide with its excellent electrical properties, offer high performance comparable to amorphous Si-based rivals, and with a form factor conducive to flexible and wearable electronics. Here rectifying diodes based on amorphous spin-coated indium oxide are fabricated for high-speed applications.**

We report a solution-processed diode approaching the UHF range, based on indium oxide, with aluminum and gold as the electrodes. The device was spin-coated from a precursor material and configured into a half-wave rectifier. The J-V and frequency behavior of the diodes were studied, and the material composition of the diode was investigated with x-ray photoemission spectroscopy (XPS). The 3dB point was found to be over 700 MHz. The results are promising for development of autonomously-powered wireless Internet-of-Things systems based on scalable, low-cost processes.

***Index Terms*—metal oxide semiconductors, high frequency rectifying diodes, solution processed indium oxide.**

I. Introduction

TRANSPARENT metal oxide semiconductor based devices have attracted considerable interest for their applications in thin film electronics, especially solution processed pathways for large area electronics. For many years, they found their applications in optoelectronics as transparent conducting oxide [1-5]; the most known oxide is Sn-doped indium oxide, also better known as indium-tin-oxide (ITO). Due to their high carrier mobility and carrier concentration resulting in high drive current, the performance of oxide semiconductor based devices such as thin film transistors (TFT) has matched that of amorphous Si-based counterparts and exceeded that of typical organic semiconductors [6]. Among metal oxides, indium oxide is a promising n-type semiconductor thanks to its high carrier mobility and wide bandgap [7]. High quality indium oxide grown from molecular beam epitaxy (MBE), or by sputtering, have been thoroughly studied from a semiconductor physics perspective [8-13], which provides a better understanding of contact properties and carrier transport properties of the devices. However, such processes can be a major obstacle to cost-effective device manufacturing. Solution-processed deposition such as spin coating and various printing technologies offers the advantages of simplicity, low-cost, large-area and scale-up capability. There has been remarkable progress in high-performance devices based on solution processed indium oxide semiconductor in recent years [14-17].

Rectifying diodes and circuits are vital in modern electronics with their widespread applications in radio frequency identification (RFID) tags and wireless power harvesting systems for the Internet-of-Things (IoT). The main function of a rectifying diode circuit is to convert ac signals at a given frequency range to dc voltages. Rectifying diodes with high speed are therefore highly desirable and essential for utilizing (ultra-) high frequency applications. Various solution-processed diodes based on metal-oxide semiconductor [18-19], organic semiconductors [20-22] and conventional semiconductors [23-25] have been reported to date. Solution-based organic diodes offer flexibility and low temperature processing, but have the lowest operating frequency range, typically limited at tens of MHz. Nanoparticle semiconductor inks are also a common way to realize solution processed conventional semiconductors. Although they can potentially reach GHz range, the major technical challenge is the complexity of making the nanoparticle composites that normally involve time-consuming process [25]. Solution processed metal oxide semiconductor devices are mostly reported in the context of TFTs, although a high-speed diode without quantification of rectification efficiency was reported in a nanogap configuration based on zinc oxide [19]. In addition, the current voltage and impedance analysis of a solution processed indium oxide/p-type Si Schottky diode has been report in [18], but the frequency behaviors of the diodes were not present.

Manuscipt received on 18 September 2019. This work was supported by Tekes (Project PAUL 40146/14) and Austrian Research Foundation (Project Self-PoSH 856940).

Miao Li (Corresponding author), Chakra Rokaya, Andreas Schramm (was), Paul R. Berger and Donald Lupo are with Electronics and Communication Engineering, Tampere University, FI-33014, Tampere, Finland (e-mail: miao.li@tuni.fi).

Mari Honkanen is with Tampere Microscopy Center, Tampere University, FI-33014 Tampere, Finland

Xianjie Liu and Mats Fahlman are with Laboratory of Organic Electronics, Department of Science and Technology, Linköping University, SE-60174, Norrköping, Sweden.

Paul R. Berger is also with Electrical and Computer Engineering, The Ohio State University, Columbus, OH 43210, USA

Here we report a rectifying diode based upon spin coated indium oxide that operates up to at least the 0.7 GHz range. Indium oxide is the n-type semiconductor, and Au and Al were determined as Ohmic injecting anode contact and non-ohmic rectifying cathode contact, respectively. The device parameters were investigated using current density-voltage (J-V) characteristics and the material composition was studied by XPS. High frequency measurements demonstrate that these solution processed indium oxide diodes operate up to the GHz range with a 3-dB cutoff frequency over 700MHz.

II. Experiments

The indium oxide diodes were fabricated on a SiO_2 coated Si wafer. A 25 nm thick patterned Al electrode was first evaporated on the wafer through a mask, followed by three iterative layers of spin coated indium oxide precursor to prevent short circuits in the diode structure. The precursor, with a molar concentration 0.2 mol/L, was made by mixing indium nitrate hydrate with 2-methoxyethanol (both from Sigma Aldrich). This precursor formula was first published by Technical Research Centre of Finland (VTT) [26]. The first two layers were cured at 300 ^{o}C in an oven under atmosphere for 5 minutes and the last layer was cured for 30 minutes at the same temperature. Finally, a 100 nm patterned Au electrode was evaporated. To improve the wetting of the indium oxide precursor, the Al electrode was subjected to UV-ozone treatment for 15 minutes immediately before the deposition of indium oxides.

The I(J)-V characteristics were determined using a Keysight B1500A semiconductor design analyzer. A Keithley 3390 50 MHz arbitrary waveform generator and a Hewlett Packard ESG-DS300A 250 kHz to 3000 MHz digital signal generator were used to provide input signal for frequency dependent rectifying measurement. At higher frequencies, the power of the input signal was boosted with a ZHL-2-12 high dynamic range amplifier 10 MHz to 1.2 GHz from Mini-circuits. The rectifier dc output was measured with a Tektronix DPO4104 digital phosphor oscilloscope. All the fabrication steps and the measurements were carried out in ambient environments except for electrode evaporation.

The cross-section of the diode was studied with a focused ion beam scanning electron microscope (FIB-SEM, Zeiss, Crossbeam 540) equipped with an energy dispersive spectrometer (EDS, Oxford Instruments, MaxN) for elemental analysis. The cross-sections were prepared with FIB-SEM by depositing a Pt protection layer on the region of interest and using Ga ions to mill the cross-section under the Pt covering layer. Prior to FIB-SEM studies, the diode was carbon-coated to avoid the sample charging during the milling process.

XPS experiments were carried out using a Scienta ESCA 200 spectrometer with a monochromatic Al Kα x-ray source (hv=1486.6 eV) in ultrahigh vacuum with a base pressure of $1x10^{-10}$ mbar. The XPS experimental condition was set so that the full width at half maximum of the clean Au $4f_{7/2}$ line at 84.00 eV was 0.65 eV. All spectra were collected at room temperature with a photoelectron takeoff angle of 0°, i.e., normal emission.

III. Results and Discussion

Indium oxide is an undoped semiconductor; when sandwiching between two metal electrodes, a metal-insulator-metal (MIM) diode structure is formed. For this type of diode, two metals with different work functions act as an Ohmic contact and a non-Ohmic contact, respectively. The non-Ohmic contact is sometimes referred to as a Schottky or rectifying contact if the resulting diodes show rectifying behavior. Some preliminary tests were conducted to determine the suitable Ohmic and non-Ohmic contacts for indium oxide in this work. Candidate metal electrodes such as Ag (4.64eV), Al (4.2eV), Au (5.47eV), Cu (5.1 eV) and Cr (4.5eV) and Pd (5.6eV) [27], have been fabricated to observe the contact effects. The test devices include a spin coated indium oxide layer and a top metal layer with a lateral gap structure fabricated on a glass substrate as shown in Fig. 1. The I-V characteristics were measured to briefly determine each candidate contact's Ohmic behavior. Among the low work function metal electrodes, as shown in Fig. 1, Al contacts showed the highest current indicating the formation of reasonable Ohmic contacts. We attempted to measure contact resistance of indium oxide and different contacts using the transfer length (TLM) method [28], however, as the minimum gap on steel shadow mask was limited to 40-60 um, the TLM results were not accurate. For Cr and Ag, initial results showed lower current levels, likely due to high contact resistance at the metal-semiconductor interface, perhaps fromthe work function mismatching, within the measured voltage range, therefore these metals were not considered further as Ohmic contacts in this work. On the other hand, between high work function metals Pd and Au , Au was chosen here for the subsequent diodes, because of its overall reduced chemical reaction to the indium oxide precursor and better wetting properties. To sum up, the preliminary tests indicated that Au and Al were suitable anode and cathode, respectively, for the indium oxide diodes in this work. Due to poor adhesions of Au on glass or on SiO_2 substrates, Al was deposited as the bottom electrode and Au was on top to minimize fabrication steps.

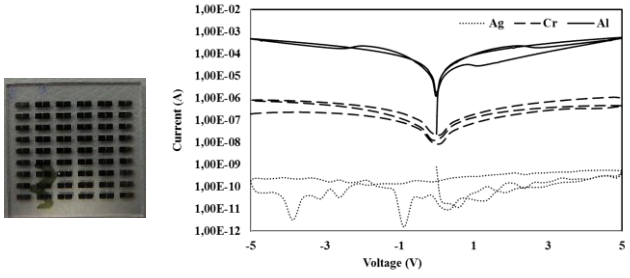

Fig.1 A photo of the device and I-V plot of indium oxide with various metal electrodes on top.

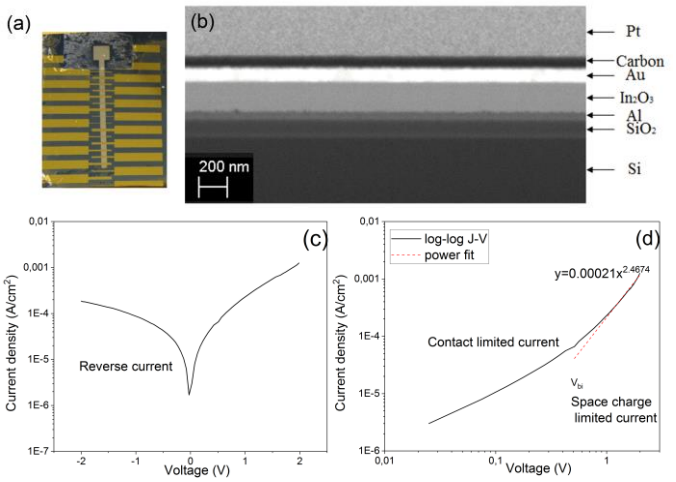

Fig. 2. (a) A photo of Al/In2O3/Au diodes. (b) FIB-SEM cross section image of the diode. (c) J-V characteristics of the diode. (d) Log-log plot the diode J-V characteristics at forward bias.

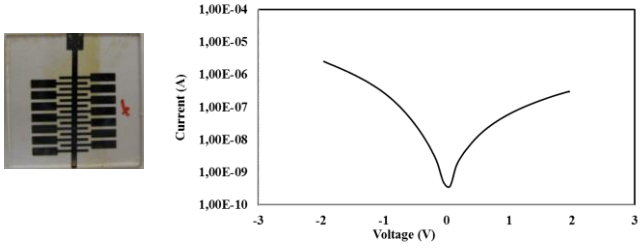

Fig. 3. A photo of $Al/In_2O_3/Al$ on glass and I-V curves of $Al/In_2O_3/Al$ diode.

As shown in Fig. 2a, the diode active area was varied from 0.002 to 0.01 cm^2. The cross section of the diode was studied by FIB-SEM as shown in Fig. 2b. Different layers were defined by SEM-EDS. The SiO_2 layer was determined to be around 100 nm. The layer thickness of three indium oxide film was around 200 nm. Al and Au layers appeared to be uniformly deposited. J-V characteristics of the $Al/In_2O_3/Au$ diodes are shown in Fig. 2c. It is clear that the diodes demonstrate modest rectifying behavior, i.e., different current levels for forward/reverse voltages. The forward current of the diodes is higher than the reverse current. However, since the measured input was at the Al electrode, the J-V curve indicates that the Al-In_2O_3 contact acted as the anode, i.e., a rectifying contact, whereas the In_2O_3-Au contact became Ohmic-like.

One of the interesting properties of indium oxide is the surface electron accumulation layer (SEAL) on MBE-grown indium oxide single crystalline thin films, as reported in [8] and fully reviewed in [7]. The immediate consequence of the SEAL is to prevent the formation of rectifying Schottky contacts, but instead causes the formation of Ohmic contacts despite using high work function metals such as Pt. The J-V characteristics of solution-based indium oxide clearly present similar surface behavior, i.e., instead of forming Schottky contacts, high work function metal Au acted as Ohmic contacts on top of indium oxide. This result is in agreement with literature reports for MBE-grown indium oxide layers. To further investigate the rectifying behavior of the bottom Al-In_2O_3 contact, we fabricated diodes with a Al-In_2O_3-Al (on glass) structure, as shown in Fig. 3. Here, the measured input was at top Al electrode. The evaporated bottom Al electrodes forms a thin aluminum oxide coating layer in ambient air conditions before the deposition of the indium oxide precursor atop. This native oxide interlayer changes the contact properties between the bottom Al and the indium oxide, which results in the formation of rectifying contacts as shown in Fig. 3. To sum up, for the Al-In_2O_3-Au diodes fabricated in this work, the bottom Al electrode with a thin native oxide layer atop forms rectifying contacts, whereas the top Au electrode establishes Ohmic-like contacts to indium oxide as a result of behaviors similar to SEAL in MBE-grown indium oxide. These unexpected contact behaviors lead to non-optimal dc rectification and poor ideality factor of the diodes.

For MIM diodes, the current characteristics can be divided into three regimes, reverse current region ($V<0$), diffusion and contact limited current region ($0<V<V_{bi}$) and space charge limited current (SCLC) region ($V>V_{bi}$), where the built in voltage V_{bi} is defined as work function difference of the metal electrodes [29]. In this work, V_{bi} was determined to be about 0.52 V based on the log-log plot of J-V characteristics of the diode. In reverse bias, the current level is normally low due to the junction barrier. The diffusion and contact limited current can be determined by assuming an ideal Ohmic contact and using a conventional thermionic emission model [29]. However, the ideality factor in this model which is based on recombination of charge carriers at junctions is usually inapplicable to MIM diodes. In addition, both Al-In_2O_3 and In_2O_3-Au contacts are not perfect Schottky and Ohmic contacts, respectively. Consequently, the value of bulk resistance and the ideality factor of the indium oxide diode is calculated to be 1.76 MOhm and 8.93, respectively, when using Cheung's function [29].

The significantly high ideality factor witnessed here indicates that the contacts do not fit well to a classic Schottky contact model. When taking band bending at the interfaces and the effect of a barrier at the cathode-semiconductor interface into consideration, the diffusion limited current in MIM devices becomes much more complicated [30]. At voltages higher than the V_{bi} of the diode, the current is no longer diffusion and injection limited and follows SCLC assuming the semiconductor is trap-free [31]:

$$J = \frac{9\varepsilon_r\varepsilon_o\mu(V-V_{bi})^2}{8L^3} \quad (1)$$

where the SCLC is proportional to the square of the applied voltage, i.e., ($I \propto V^2$). However, due to the non-ideal interfaces and trap states within the indium oxide semiconductor the proportion becomes the form of $I \propto V^m$, where $m>2$ [32]. The value extracted here was around 2.47 as shown in Fig. 2d.

To understand the chemical composition of the diode, XPS analysis was performed on diodes with a structure of Al-In_2O_3 on SiO_2 substrate. Fig. 4a shows the Al2p spectrum, which has two peaks corresponding to neutral (Al^0) and oxidized (Al^+) components when fabricated on SiO_2 substrate. After the deposition of indium oxide layer on top, the Al signal

disappeared. This is indicative of a pinhole-free, homogenous coverage of indium oxide on top of the Al. Fig. 4b displays the In3d core level spectrum of the In_2O_3 layer. Two peaks located at 445 eV and 452.6 eV are clearly identified, which are attributed to $In3d_{5/2}$ and $In3d_{3/2}$, respectively. This indicates that the indium valence is mainly In^{3+} in the lattice structure. Fig. 4c shows the corresponding O1s peak which was deconvoluted into three components (colored curves). The peak at the highest binding energy can be assigned to the absorbed oxygen residence on In_2O_3 surface. The peak at 530.2 eV comes from the oxygen bond of In-O-In, and the peak at 531.9 eV originates from the oxygen defects in the metal oxide [33] [34]. The vacancy states of the oxygen have a huge effect on electrical performance of the device [33] [34], and therefore to affect the J-V characteristics of the diodes and contribute to imperfections, i.e., m>2 in SCLC regions.

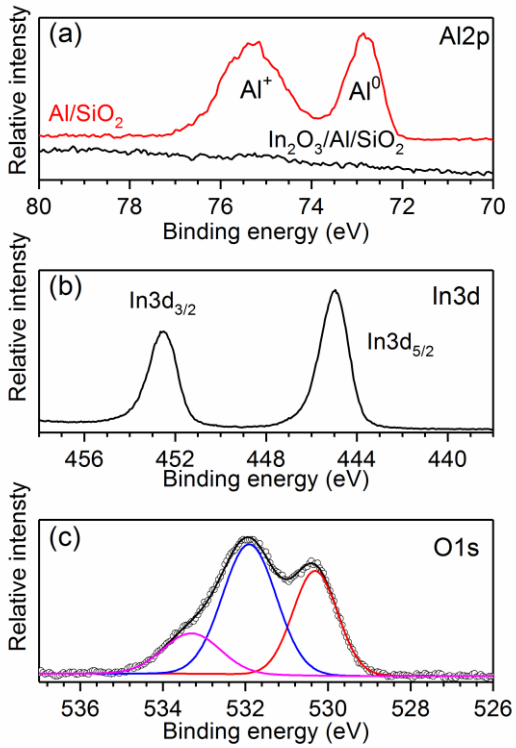

Fig. 4 (a) Al2p spectra of Al deposited on SiO_2 and In_2O_3 deposited on Al/SiO_2. (b) In3d spectra of In_2O_3 deposited on Al/SiO_2. (c) O1s spectra of In2O3 deposited on Al/SiO_2 and curving fitting of three peaks.

The frequency performance of the indium oxide diodes was next investigated in a half-wave (HW) rectifying circuit. First, for comparison reasons the HW rectifier was tested with a standard signal generator and an oscilloscope without any matching network circuit as shown in Fig. 5a. This set-up has been commonly used in the past for measuring printed organic diodes operating in the high frequency range, typically around the HF standard of 13.56 MHz [20-23]. The output amplitude of the signal generator was 10V with the maximum frequency up to 50MHz. The load was a 1 MOhm internal load of the oscilloscope instrument. The filtering capacitor of the rectifier is 47 nF. For comparison, a Si-based rectifying diode (1N4001) was also included in the measurements.

The diode high frequency behavior depends mainly on the semiconductor properties, electrode interfaces and parasitic impedances of the devices. A simplified equation to determine the diode maximum operation frequency, assuming perfect electrode interface properties, can be found as [35],

$$f_{max} = \frac{\mu(V_{in}-V_{dc})}{L^2} \quad (2)$$

where V_{in} is input ac voltage amplitude, V_{dc} is output dc voltage. Although the maximum frequency calculated with this equation

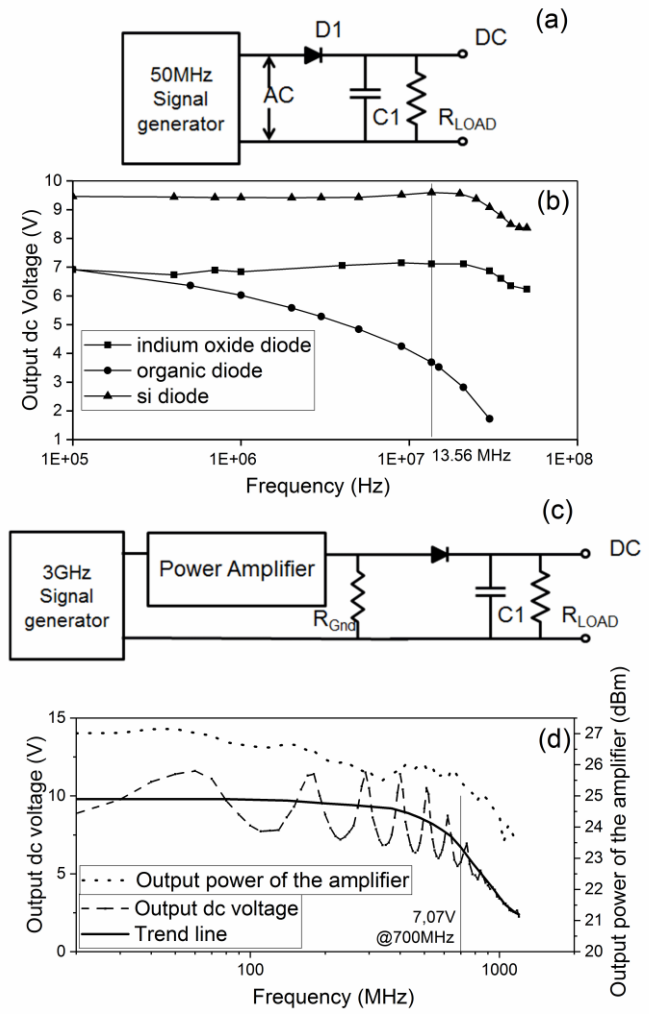

Figure 5. (a) The circuit diagram of the measurement and (b) frequency response of the Al/In2O3/Au rectifier with a comprising to typical organic diode and Si-diode rectifier up to 50MHz. (c) The circuit diagram of the measurement and (d) frequency response of the Al/In2O3/Au rectifier up to GHz range. The measured power after the power amplifier and its relative loss vs frequency, with the diode circuit.

is overestimated, it indicates that a higher mobility and thinner semiconducting layer thickness increase the maximum frequency significantly. As shown in Fig. 5b, the rectifier with

the indium oxide diode exhibited similar rectified dc output at low frequencies to that of an organic diode rectifier [20]. However, whereas the rectified dc output of the organic diode rectifier started to decrease rapidly with increased frequency, the output of the indium oxide diode rectifier remained constant and only dropped slightly beyond 35 MHz. This voltage drop, which also present in the commercial Si-based diode rectifiers, was caused by the parasitic reactance within the measurement set-up. Compared to commercial Si-based rectifiers, the indium oxide diode rectifiers had a bigger voltage loss due to high contact resistances and to trap states in the semiconductor as witnessed from the J-V and XPS results.

In order to investigate the frequency performance beyond 50 MHz and to find the cutoff frequency of the rectifier, a 3 GHz RF signal generator together with a power amplifier were used to replace the standard signal generator as the power source. No additional impedance matching circuits were included. The filtering capacitor and load impedance was the same as that of the previous 50 MHz measurement. The input power was 0 dB from the RF generator. The power gain of the amplifier is 24-29 dB from 10 MHz to 1.2 GHz based on the datasheet. The actual output power of the amplifier as a function of frequency, measured by a spectrum analyzer, is shown in Fig. 5d. The output power of the amplifier started at 27 dBm at 10 MHz and slowly dropped to below 24 dBm at GHz range.

Fig. 5c and 5d shows the rectified dc output of the rectifier with the frequency swept from 20 MHz up to 1.2 GHz. The waveform of the output dc voltage indicated that there were standing waves between the diode and the power amplifier causing by impedance mismatching. The solid line functioned as a trend line of the measured data to help interpret the data due to the standing waves. The cutoff frequency was determined to be around 700 MHz when the voltage dropped from 10 V to 7.07 V. Due to the significantly lower output power of the amplifier at higher frequencies as present in Fig. 5d, the exact cutoff frequency of the rectifier is higher than 700 MHz.

IV. Conclusion

We have fabricated solution-processed indium oxide diode with a structure of Al-In_2O_3-Au on SiO_2 wafer. The J-V characteristics of the diode are studied at voltage up to 2 V. The material composition of the diode is analyzed with XPS demonstrating oxide defects. The suboptimal Ohmic and rectifying contacts together with imperfections and the oxide defects in indium oxide caused voltage losses when converting ac signals to dc voltages regardless of the frequency band. Thanks to the thin and pinhole free indium oxide layer, the cut-off frequency of the diode was beyond 700 MHz given the power losses caused by the cables.

Acknowledgment

This work was financially supported by Tekes (Project PAUL 40146/14) and Austrian Research Foundation (Project Self-PoSH 856940). We thank J. Leppäniemi and A. Alastalo of VTT for support in formulation and processing of indium oxide.

References

[1] C. G. Granqvist and A. Hulaker, "Transparent and conducting ITO films: new developments and applications," *Thin Solid Films,* vol. 411, no. 1, pp. 1-5, Apr. 2002.

[2] A. Porch, D. V. Morgan, R. M. Perks, M. O. Jones and P. P. Edwards, "Transparent current spreading layers for optoelectronic devices," *J. Appl. Phys.,* vol. 96, no. 8, pp. 4211-4218, Oct. 2004.

[3] G. S. Chae, "A modified transparent conducting oxide for flat panel displays only," *Japanese Journal of Applied Physics,* vol. 40, no. 1, pp. 1282-1286, Mar. 2001.

[4] A. N. Tiwari, G. Khrypunov, F. Kurdzesau, D. L. Batzner, A. Romeo and H. Zogg, "CdTe solar cell in a novel configuration," *Prog. Photovoltaics: Research and Applications,* vol. 12, pp. 33-38, Jan. 2004.

[5] M. T. Hardy, C. O. Holder, D. F. Feezell, S. Nakamura, J. S. Speck, D. A. Cohen and S. P. DenBaars, "Indium-tin-oxide clad blue and pure green semipolar InGaN/GaN laser diodes," *Appl. Phys. Lett.,* vol. 103, no. 8, p. 081103, Aug. 2013.

[6] M. Lorenz, M. S. Ramachandra Rao, T. Venkatesan, E. Fortunato, P. Barquinha, R. Branquinho, D. Salgueiro, R. Martins, E. Carlos, A. Liu, F. K. Shan, M. Grundmann, H. Boschker, J. Mukherjee, M. Priyadarshini, N. DasGupta, D. J. Rogers, F. H. Teherani, E. V. Sandana, P. Bove, K. Rietwyk, A. Zaban, A. Veziridis, A. Weidenkaff, M. Muralidhar, M. Murakami, S. Abel, J. Fompeyrine, J. Zuniga-Perez, R. Ramesh, N. A. Spaldin, S. Ostanin, V. Borisov, I. Mertig, V. Lazenka, G. Srinivasan, W. Prellier, M. Uchida, M. Kawasaki, R. Pentcheva, P. Gegenwart, F. Miletto Granozio, J. Fontcuberta and N. Pryds, "The 2016 oxide electronic materials and oxide interfaces roadmap," *J. Phys. D: Appl. Phys.,* vol. 49, no. 433001, Oct. 2016.

[7] O. Bierwagen, "Indium oxide-a transparent, wide-band gap semiconductor for (opto)electronic applications," *Semicond. Sci. Technol.,* vol. 30, no. 024001, Jan. 2015.

[8] O. Bierwagen and J. S. Speck, "High electron mobility In2O3(001) and (111) thin films with nondegenerate electron concentration," *Appl. Phys. Lett.,* vol. 97, no. 072103, Aug. 2010.

[9] N. Preissler, O. Bierwagen, A. T. Ramu and J. S. Speck, "Electrical transport, electrothermal transport, and effective electron mass in single-crystalline In2o3," *Phys. Rev. B.,* vol. 88, no. 085305, Aug. 2013.

[10] H. von Wenckstern, D. Splith, F. Schmidt, M. Grundmann, O. Bierwagen and J. S. Speck, "Schottky contacts to In2O3," *APL Materials,* vol. 2, no. 046104, Apr. 2014.

[11] P. D. King, T. D. Veal, D. J. Payne, A. Bourlange, R. G. Egdell and C. F. McConville, "Surface Electron Accumulation and the Charge Neutrality Level in In2o3," *Phys. Rev. Lett.,* vol. 101, no. 116808, Sep. 2008.

[12] O. Bierwagen, M. E. White, M.-Y. Tsai, T. Nagata and J. S. Speck, "Non-Alloyed Schottky and Ohmic Contacts to As-Grown and Oxygen-Plasma Treated n-Type SnO2 (110) and (101) Thin Films," *Appl. Phys. Express.,* vol. 2, no. 106502, Oct. 2009.

[13] T. Nagata, O. Bierwagen, M. E. White, M.-Y. Tsai and J. S. Speck, "Study of the Au Schottky contact formation on oxygen plasma treated n-type SnO2 (101) thin films," *J. Appl. Phys.,* vol. 107, no. 033707, Feb. 2010.

[14] L. Zhu, G. He, J. Lv, E. Fortunato and R. Martins, "Fully solution-induced high performance indium oxide thin film transistors with ZrOx high-k gate dielectrics," *RSC Advances,* vol. 8, pp. 16788-16799, May 2018.

[15] J. Leppäniemi, K. Eiroma, H. Majumdar and A. Alastalo, *"*Far-UV Annealed Inkjet-Printed In2O3 Semiconductor Layers for Thin-Film Transistors on a Flexible Polyethylene Naphthalate Substrate*," ACS Appl. Mater. Interfaces,* vol. 9, no.10, pp. 8774-8782, Mar 2017.

[16] A. kyndiah, A. Ablat, S. Guyot-Reeb, T. Schultz, F.Zu, N. Koch, P. Amsalem, S. Chiodini, T. Y. Alic, Y. Topal, M. Kus, L. Hirsch, S. Fasquel and M. Abbas, "A Multifunctional Interlayer for Solution Processed High Performance Indium Oxide Transistors," *Sci. Rep,* vol. 8, no. 10946, July 2018.

[17] E. Fortunato, P. Barquinha and R. Martins, "Oxide semiconductor thin-film transistors: a review of recent advances," *Adv. Mater.,* vol. 24, pp. 2945-2986, May 2012.

[18] R. K. Gupta and F. Yakuphanoglu, "Analysisof device parameters of Al/In2O3/p-Si Schottky diode," *Microelectron. Eng.,* vol. 105, pp. 13-17, May 2013.

[19] J. Semple, S. Rossbauer, C. H. Burgess, K. Zhao and L. K. Jagadamma, “Radio Frequency Coplanar ZnO Schottky Nanodiodes Processed from Solution on Plastic Substrates,” *Small*, vol. 12, no. 15, pp. 1993-2000, Feb. 2016.
[20] M. Li, P. S. Heljo and D. Lupo, “Organic rectifying diode and circuit for wireless power harvesting at 13.56MHz,” *IEEE Trans. Electron Device*, vol. 61, no. 6, pp. 2164-2169, Jun. 2014.
[21] C.-Y. Lin, C.-H. Tsai, H.-T. Lin, L.-C. Chang, Y.-H. Yeh, Z. Pei, Y.-R. Peng and C.-C. Wu, “High-frequency polymer diode rectifiers for flexible wireless power-transmission sheets,” *Org. Electron.,* vol. 12, no. 11, pp. 1777-1782, Nov. 2011.
[22] S. Steudel, S. D. Vusser, K. Myny, M. Lenes, J. Genoe and P. Heremans, “Comparison of organic diode structures regarding high-frequency rectification behavior in radio-frequency identification tags,” *J. Appl. Phys.*, vol. 99, no. 114519, Jun. 2006.
[23] H. Park, H. Kang, Y. Lee, Y. Park, J. Noh and G. Cho, “Fully roll-to-roll gravure printed rectenna on plastic foils forwireless power transmission at 13.56 MHz,” *Nanotechnology*, vol. 23, no. 344006, Aug. 2012.
[24] C. Johansson, X. Wang and M. Robertsson, “Printable rectifying device using Si composite,” *Electron. Lett.,* vol. 44, no. 1, Jan. 2008.
[25] N. Sani, M. Robertsson, P. Cooper, X. Wang, M. Svensson, P. A. Ersman, P. Norberg, M. Nilsson, D. Nilsson, X. Liu, H. Hesselbom, L. Akesso, M. Fahlman, X. Crispin, I. Engquist, M. Berggren and G. Gustafsson, “All-printed diode operating at 1.6 GHz,” *Proc. Natl. Acad. Sci. U. S. A.,* vol. 111, no. 33, pp. 11943-11948, Aug. 2014.
[26] J. Leppaniemi, O-H. Huttunen, H. Majumdar and A. Alastalo, “Flexography-Printed In2O3 Semiconductor Layers for High-Mobility Thin-Film Transistors on Flexible Plastic Substrate,” *Adv. Mater.,* vol. 27, no. 44, Oct. 2015.
[27] J. Holzl and F. K. Schult, *Soild Surface Physics, 1979.*
[28] D. K. Schroder, *Semiconductor Material and Device Characterization, 2006*
[29] S. K. Cheung and N. W. Cheung, “Extraction of Schottky diode parameters form forward current-voltage characteristics,” *Appl. Phys. Lett., vol. 49, no. 2, pp. 85-87, Jul. 1986.*
[30] P. de Bruyn, A. van Rest, G. Wetzelaer, D. de Leeuw and P. Blom, “Diffusion-limited current in organic metal-insulator-metal diodes,” *Phys. Rev. Lett.,* vol. 111, no.18, 2013.
[31] A. Rose, “Space-charge-limited currents in soilds,” *Phys. Rev*, vol. 97, no. 6, 1955.
[32] M.A. Lampert, “Simplified theory of space-charge-limited currents in an insulator with traps,” *Phys. Rev*, vol. 103, no. 6, 1956.
[33] J. Gan, X. Lu, J. Wu, S. Xie, T. Zhai, M. Yu, Z. Zhang, Y. Mao, S. C. Wang, Y. Shen and Y. Tong, “Oxygen vacancies promoting photoelectrochemical performance of In2O3 nanocubes,” *Sci. Rep.,* 3 : 1021, Jan. 2013.
[34] T.B. Daunis and D. Barrera, “Solution-processed oxide thin film transistors on shape memory polymer enable by photochemical self-patterning,” *J. Mater. Res.,* vol. 33, no.17, Sep. 2018.
[35] S. Steudel, K. Myny, V. Arkipov, C. Deibel, S. de Vusser, J. Genoe and P. Heremans, “50 MHz rectifier based on an organic diode,” *Nat. Mater*, vol. 4, no. 8, pp597-600, September 2005.